

PDF hosted at the Radboud Repository of the Radboud University Nijmegen

The following full text is a publisher's version.

For additional information about this publication click this link.

<http://hdl.handle.net/2066/145312>

Please be advised that this information was generated on 2017-12-05 and may be subject to change.

Femoral fracture risk prediction in metastatic bone disease

Loes Derikx



Femoral fracture risk prediction
in metastatic bone disease

Loes Derikx

© **Loes Derikx. Nijmegen, 2015.**

All rights reserved. No part of this thesis may be reproduced in any form without written permission of the author.

Cover design:

Loek Janssen

Layout:

Loes Derikx

Printing:

GVO drukkers & vormgevers B.V.

ISBN:

978-90-6464-928-8

The work presented in this thesis was carried out within the Radboud Institute for Health Sciences and funded by Orthopaedic Research UK, Fonds NutsOhra and the Dutch Cancer Society.

Financial support for printing of this thesis by Annafonds|NOREF is greatly acknowledged.

Femoral fracture risk prediction in metastatic bone disease

Proefschrift

ter verkrijging van de graad van doctor
aan de Radboud Universiteit Nijmegen
op gezag van de rector magnificus prof. dr. Th. L. M. Engelen,
volgens besluit van het college van decanen

en ter verkrijging van de graad van doctor
aan de Katholieke Universiteit Leuven
op gezag van de rector magnificus prof. dr. R. Torfs,

in het openbaar te verdedigen
op donderdag 19 november 2015
om 12.30 uur precies

door

Loes Catharina Elisabeth Maria Derikx

geboren op 12 april 1984
te Neer

Promotoren

Prof. dr. ir. N. Verdonschot

Prof. dr. I. Jonkers (KU Leuven)

Copromotoren

Dr. E. Tanck

Dr. Y.M. van der Linden (LUMC)

Manuscriptcommissie

Prof. dr. ir. N. Karssemeijer

Prof. dr. J.H.A.M. Kaanders

Prof. dr. ir. G.H. van Lenthe (KU Leuven)

Contents

Chapter 1	7	General introduction and outline
Chapter 2	25	The assessment of the risk of fracture in femora with metastatic lesions: Comparing case-specific finite element analyses with predictions by clinical experts
Chapter 3	45	Implementation of asymmetric yielding in case-specific finite element models improves the prediction of femoral fractures
Chapter 4	65	Finite element analysis and CT-based structural rigidity analysis to assess failure load in bones with simulated lytic defects
Chapter 5	85	Can patient-specific finite element models better predict fractures in metastatic bone disease than experienced clinicians? Towards introducing computational modelling into daily clinical practice
Chapter 6	103	Muscle optimisation techniques impact the magnitude of calculated hip joint contact forces
Chapter 7	127	Physiological load cases combined with plasticity in patient-specific finite element models in metastatic bone disease: does it affect fracture predictions?
Chapter 8	147	General discussion and future perspectives
Chapter 9	161	Summary
Chapter 10	169	Samenvatting
Chapter 11	179	Dankwoord
	183	Curriculum Vitae
	186	PhD Portfolio

I

General introduction and outline

Parts of this chapter have been published in *Loes C. Derikx, Nico Verdonschot, Esther Tanck. Towards clinical application of biomechanical tools for the prediction of fracture risk in metastatic bone disease. J Biomech 2015; 48(5), 761-766.*



Cancer and cancer-related complications in bone

One in every three people in the Netherlands will suffer from cancer during their lives (Signaleringscommissie Kanker van KWF Kankerbestrijding, 2007). Currently, over 100,000 Dutch inhabitants are diagnosed with cancer yearly (Figure 1) and this number is expected to increase to 123,000 in 2020 (Signaleringscommissie Kanker van KWF Kankerbestrijding, 2011). This rise can mainly be attributed to ageing, which is a major determinant for the development of cancer: both the total number of Dutch elderly and their life expectancy are sharply increasing. At the same time, cancer treatments have become increasingly effective, as reflected in a more or less stable mortality rate over the last decades (Figure 1). When living longer with cancer, patients have more time to develop severe complications after surgery, chemotherapy or radiotherapy, such as pain, fatigue, emotional distress, pulmonary or sexual dysfunction or cardiotoxicity (Siegel et al., 2012). Consequently, the treatment of these severe complications forms an integral part of the care of cancer patients.

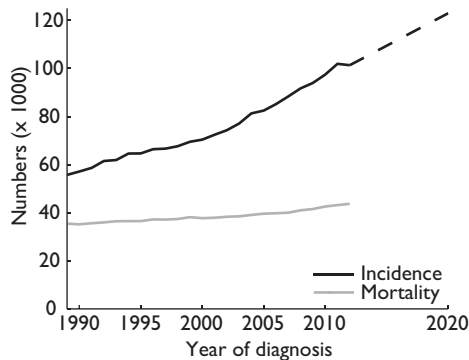


Figure 1. Cancer incidence and mortality in the Netherlands between 1989 and 2012. The dashed line represents expected incidence as projected by the Dutch Cancer Society. Source: the Netherlands Cancer Registry, managed by IKNL © December 2014.

The treatment of the primary cancer often affects the bone tissue (Gralow et al., 2013; Rizzoli et al., 2013). In breast and prostate cancer, for example, hormonal therapy is a common treatment option. The suppression of gonadal hormones is effective in the primary treatment of these cancers, but, as a side-effect, can induce osteoporosis (Rizzoli et al., 2013) by disturbing the bone remodelling process and compromising the bone mass. Such treatment-related bone quality compromise can be devastating (Gralow et al., 2013), especially in patients at risk of age-related or postmenopausal osteoporosis, as it may induce pathological fractures.

Due to better cancer survival rates, patients have more time to develop complications caused

by the primary tumour or its treatment. In addition, they have higher chances to reach more progressive disease states, in which the development of metastases plays an important role. The diagnosis of metastases flags a dramatic tipping point for the patient, as the aim of the treatment then shifts from curative to palliative (Laitinen et al., 2012). In progressive disease states, primary tumour cells may spread through the body and seed distantly. Following Paget's seed and soil theory (1889), different tumour cell types have specific tissues of preference for distant seeding. Bone appears to be a fertile soil for primary tumour cells in breast, prostate, lung, kidney and thyroid cancer (Coleman, 1997; Coleman, 2006; Laitinen et al., 2012; Gralow et al., 2013), some of which are among the most common cancer types. Hence, the incidence and disease burden of bone metastases in patients in the palliative phase of their disease is high.

Bone metastases

Skeletal parts that are highly vascularised or contain bone marrow are prone to tumour cell invasion. Consequently, the skull, ribs, spine, pelvis and long bones of the axial skeleton are commonly affected (Johnson et al., 2008; Laitinen et al., 2012; Mavrogenis et al., 2012). Bone metastases can have lytic, blastic or mixed radiographic appearances (Figure 2). Depending on the tumour type, malignant cells can excrete substances that induce either osteoclast or osteoblast activity, or both (Rizzoli et al., 2013). In breast, lung, thyroid, renal, gastrointestinal cancer, and in multiple myeloma and melanoma (Coleman, 1997), tumour cells activate osteoclasts, resulting in local bone resorption. The resulting lesion has a lytic appearance, as depicted in Figure 2A. In contrast, in, amongst others, prostate, breast and lung cancer, or carcinoid and medullablastoma cancer (Coleman, 1997), the release of cytokines is strongly increased. These cytokines induce osteoblast activation (Rizzoli et al., 2013), which results in bone formation and the subsequent development of blastic lesions (Figure 2B). Some of the tumours mentioned above can induce both osteoblast and osteoclast activity, which may result in bone tissue extensively affected by lesions with a mixed blastic and lytic appearance (Figure 2C).

Metastatic bone disease: clinical practice

Metastatic bone disease is clinically flagged by severe pain flares, hypercalcaemia, impending or actual fractures (Coleman, 1997; Laitinen et al., 2012), and, in case of vertebral lesions, spinal cord injuries. Approximately ten percent of the lesions develop in the femur (van der Linden et al., 2004b), which may cause actual or impending pathological fractures that severely threaten the quality of life of patients. In fact, sustaining a pathological fracture signifi-

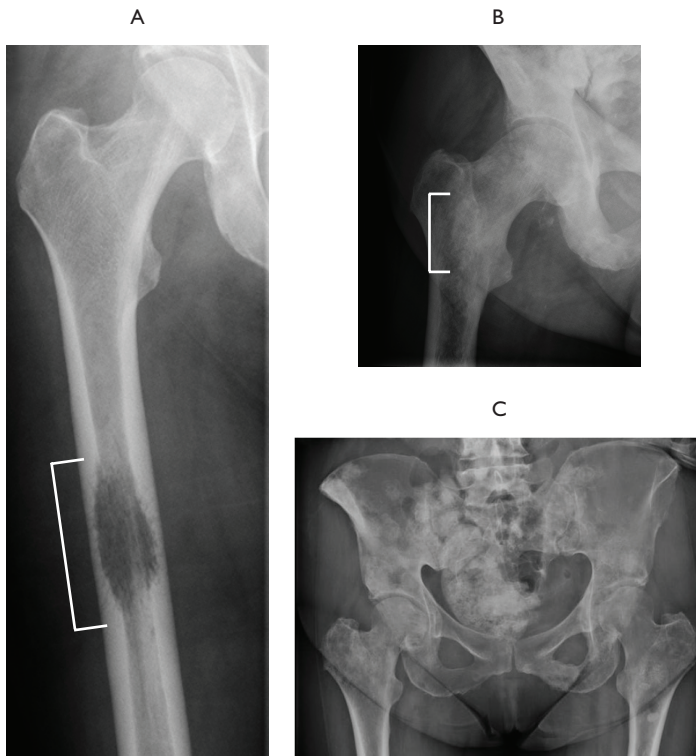


Figure 2. Three radiographic appearances of bone metastases; A) lytic, B) blastic and C) mixed. In figures A and B, lesions are indicated with brackets.

cantly decreases patient survival (Laitinen et al., 2012; Mavrogenis et al., 2012; Ratasvuori et al., 2013), as these patients fully lose their mobility and are at risk of developing comorbidities such as deep vein thrombosis or pulmonary embolism, not to mention the psychological impact of fracturing one's leg. Furthermore, the release of bone marrow may lead to further spread of the tumour cells throughout the body (Ruggieri et al., 2010; Mavrogenis et al., 2012). In addition, pathological fractures require surgical treatment such as osteosynthesis or total hip replacement, which are complex procedures that lay a burden on the patient.

In order to prevent pathological fractures, metastatic lesions identified with an impending fracture are treated with preventive surgery. This treatment is far less complex and has better survival rates than surgical treatment of actual pathological fractures (Laitinen et al., 2012; Mavrogenis et al., 2012; Ratasvuori et al., 2013). Lesions that do not jeopardise the mechanical integrity of the bone are treated conservatively with the aim to relieve pain, with (a combination of) radiotherapy, analgesics, chemotherapy, hormonal therapy or bisphosphonates (van der Linden, 2005). In order to decide upon the optimal treatment for the patient (conservative

treatment or preventive surgery), a thorough fracture risk assessment must be performed. Surgeons have to weigh the impact of the operation and rehabilitation against the patient's physical status after treatment of the primary malignancy and remaining life expectancy (Attar et al., 2012).

Current clinical methods for fracture risk assessment in metastatic bone disease

Finding an objective measure for fracture risk assessment of bones with metastases has been under study for several decades. The size of the lesion (Snell et al., 1964; Beals et al., 1971; Harrington et al., 1976; Zickel et al., 1976; Cheng et al., 1980; Miller et al., 1984; Keene et al., 1986; van der Linden et al., 2004a), the extent to which cortical bone is disrupted by the lesion (van der Linden et al., 2004a) and the radiographic appearance of the lesion (Snell et al., 1964; Beals et al., 1971; Zickel et al., 1976; Miller et al., 1984; Bunting et al., 1985; Keene et al., 1986; Mirels, 1989; Yazawa et al., 1990; van der Linden et al., 2004a) have been analysed as potential predictors of fracture risk, mainly by evaluating retrospective x-rays of patients who sustained a pathological fracture in the femur. In many of these studies, pain has been included as well (Parrish et al., 1970; Beals et al., 1971; Fidler, 1973; Harrington et al., 1976; Keene et al., 1986; Mirels, 1989; van der Linden et al., 2004a), as pain was hypothesised to be a measure for loss of mechanical strength (Mirels, 1989), or an indicator of excessive deformation (Fidler, 1973). Unfortunately, these studies did not unequivocally identify a powerful predictor for the fracture risk.

The most recent prospective clinical study on this topic was performed by Van der Linden et al. (2004a). They compared, amongst others, two guidelines: Mirels' scoring system and a threshold for cortical disruption (van der Linden et al., 2004a). Mirels' system scores the location of the lesion, pain and the appearance and size of the lesion. Patients with high scores need immediate surgery, while patients with low scores can be treated conservatively. Had Mirels' scoring system been applied to the 102 patients in the study of Van der Linden et al., who were treated with non-invasive radiotherapy, and in whom 9 developed an actual fracture during follow-up, none of the impending fractures would have been missed but a large number of patients would have undergone unnecessary surgery (sensitivity = 1.0, specificity = 0.13). Alternatively, a threshold of 3 cm cortical disruption was proposed to identify impending pathological fractures (van der Linden et al., 2003). Had this method been applied to the patients in Van der Linden's work, some of the impending fractures would have been missed (sensitivity = 0.86), but the power to identify non-fracture patients would have increased (specificity = 0.58). Thus, the new guideline using the 3 cm threshold improved upon Mirels' scoring system, but difficulties in preventing unnecessary surgeries persisted.

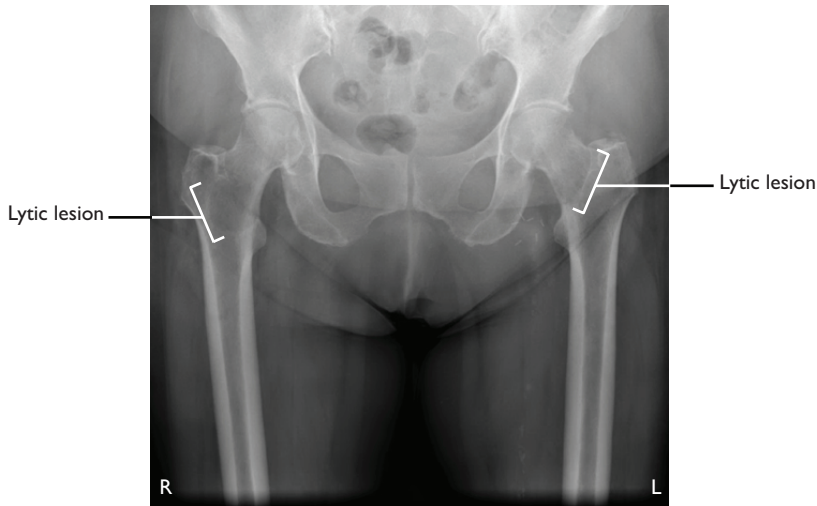


Figure 3. Preoperative X-ray of the patient. Based on this image it was decided to treat the lytic lesion in the right femur surgically. After surgery, both femurs were irradiated.

A clinical case to illustrate the challenges in current fracture risk assessment.

To illustrate the challenges in current fracture risk assessment, a recent clinical case is presented here. A 66 year old woman with recently diagnosed widespread metastatic lung cancer was referred for palliative local treatment of painful metastases in both femurs, before the start of a systemic treatment. An anterior-posterior radiograph revealed an extensive lytic lesion in the right femur and a smaller lesion in the left femur (Figure 3).

Following current clinical guidelines, the right femur had a high fracture risk and the left femur a low risk. After vigilant consideration of the patient's physical status, it was decided to treat the patient's right femur with elective stabilizing surgery and to subsequently irradiate both femurs. The left femur was to receive a single fraction of 8 Gy to relieve pain, and the right operated femur was to receive 20 Gy in 5 fractions for stabilization of the prosthesis. The day after the first fraction of radiotherapy, the patient sustained a pathological fracture of the left femur (Figure 4), and the treatment was ended. In retrospect, cortical destruction of the left femur was already present on the computed tomography (CT) simulation scan made for the planning of the radiotherapy (Figure 5).

Elective osteosynthesis of the left femur could have prevented the occurrence of the pathological fracture. The left femur was operated on (Figure 6) and the patient regained the ability to walk with a walking aid. She was then treated with postoperative radiotherapy to both femora (20 Gy). The patient sadly died two weeks after the end of the irradiation due to an unexpected deteriorating condition.

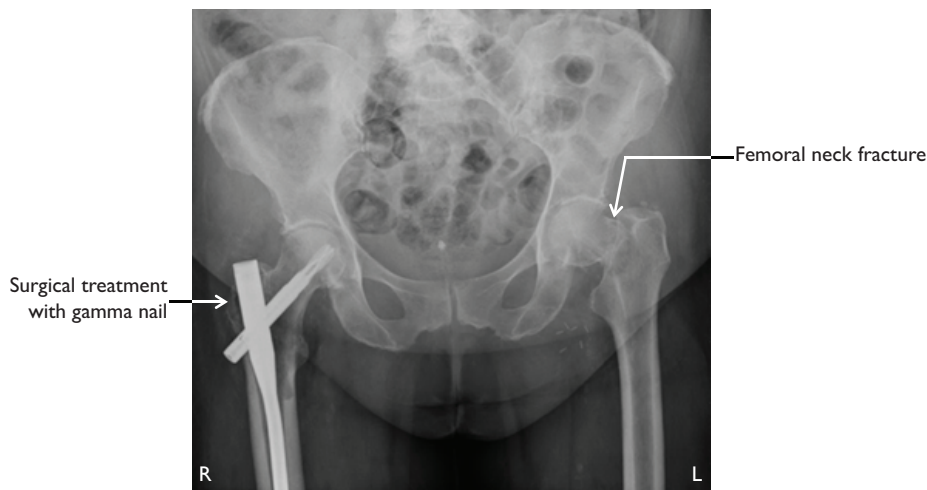


Figure 4. Postoperative X-ray of the patient, one day after the first fraction of radiotherapy. The right femur has been surgically treated with a gamma nail. The patient has now sustained a fracture in the left femur.

This case exemplifies the difficulties in fracture risk assessments in clinical practice. So far, clinical studies have mainly focussed on lesion characteristics and pain, while the original bone strength of the femur was largely ignored. In order to estimate the fracture risk, however, it is important to assess the reduction in bone strength caused by the lesion relative to the original bone strength. This is extremely difficult; even for experienced clinicians (as shown by the abovementioned case). This was also demonstrated in a study by Hipp et al. (1995), who asked

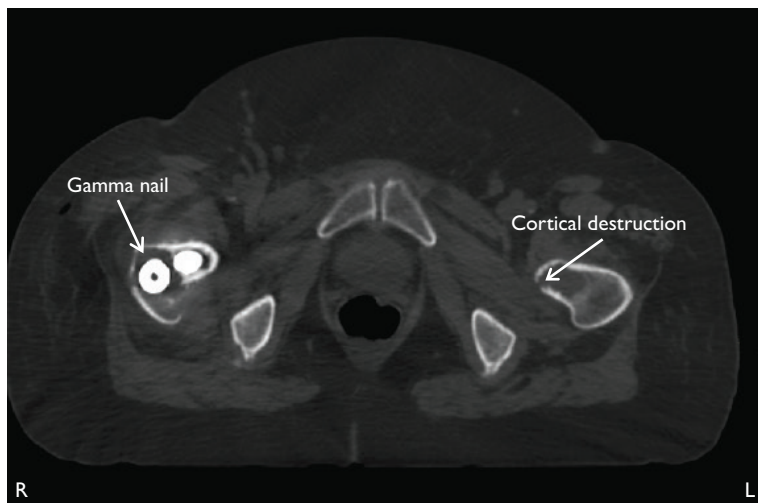


Figure 5. CT scan for planning radiotherapy. The right femur has been surgically stabilised by a gamma nail. In the left femur, the metastatic lesion has caused cortical destruction.



Figure 6. The fracture in the left femur was surgically treated with total hip arthroplasty.

three orthopaedic surgeons to report the lesion size, the femoral failure load and the strength reduction in paired cadaver femurs with simulated lesions using CT-scans and radiographs. Even in this simplified condition, the surgeons only moderately agreed on defining the lesion size (mean difference 11%, range 2%-47%). In addition, there was no relationship between the failure load estimated by the surgeons and the actual failure load of the cadaver femurs. Hence, these results again demonstrate that a more objective and quantitative measure of bone strength in patients with metastatic bone disease is urgently needed.

Finite element models to assess femoral fracture risk

A promising tool for the assessment of femoral fracture risk in metastatic bone disease is subject-specific finite element (FE) analysis. Although this method is widely studied to calculate fracture risk in osteoporosis (for example (Bessho et al., 2009; Orwoll et al., 2009; Keyak et al., 2013; Kopperdahl et al., 2014)), few groups have used it to assess failure load in metastatic bone disease in the femur (Cheal et al., 1993; Keyak et al., 2005a; Spruijt et al., 2006; Keyak et al., 2007). Cheal et al. (1993) were one of the first to use FE modelling for this purpose. Unfortunately, they found large differences between the calculated failure loads and the failure loads measured in their experiments. These inferior results may be explained by the fact that they used a femoral FE model based on average anatomy and material behaviour data (Cheal et al., 1993), and therefore did not capture the relevant biomechanical differences that exist amongst

bones of different subjects. Some years later, Keyak and co-workers developed and extensively validated a full workflow for subject-specific FE modelling based on quantitative CT (QCT) images. They empirically established relationships between CT intensities and bone material properties (Keyak et al., 1996). Subsequently, in a mechanical test setup they loaded intact cadaver femurs until failure and found good agreement between the experiments and the FE simulations (Keyak, 2001; Keyak et al., 2005b). Additionally, they applied this workflow to femurs with simulated and actual metastatic lesions (Keyak et al., 2005a; Keyak et al., 2007) and were able to accurately predict bone strength ($r=0.97$, $r=0.98$ and $r=0.94$, for intact femurs, and femurs with simulated and actual lesions, respectively) (Keyak et al., 2005a). Although these studies were performed on cadaver femurs, the results show great potential to improve fracture risk predictions in clinical practice.

Therefore, within the context of this thesis, a workflow for generating subject-specific finite element models was developed and validated. In short, this technique is based on the use of QCT images (Figure 7). Using the contrast in CT intensities, the femoral bone tissue is segmented in every CT image. By means of interpolation, this 2D geometrical information is converted into a 3D volume, representing the femoral anatomy of the subject.

In addition, information on the bone density of the femur can be derived from the CT intensities. A calibration phantom, containing four different known calcium hydroxyapatite concentrations, is scanned along with the cadaver bone (*in vitro*) or the actual patient (*in vivo*). By relating the CT intensities measured in the phantom tubes to the according calcium equivalent densities, a calibration line can be fitted. Using this calibration line, the local CT intensities measured in the bone tissue of the subject can be converted to calcium equivalent values. In previous empirical research (Keyak et al., 2005b), calcium equivalent values have been related to ash densities and mechanical properties of bone, respectively. Hence, using these empirical relationships, CT intensities can be converted to non-linear elastic-plastic material behaviour at the element level. In this way, the FE model accounts for the patient-specific geometry as well as bone density and material behaviour. Finally, the boundary conditions for the FE model have to be defined, in order to determine the subject-specific failure load of the bone as a construct. When developing an FE model, the initial loading regime should be simple so that mechanical experiments can be reliably mimicked in the FE simulations. For *in vivo* simulations, however, a more sophisticated loading regime may be required since it has been demonstrated that the association between FE bone strength and osteoporotic fractures increases when modelling multiple loading conditions (Falcinelli et al., 2014). The variations in loading regime applied in these studies mainly concerned different lines of action for hip contact forces (resembling stance loading and fall loading), but did not incorporate muscle

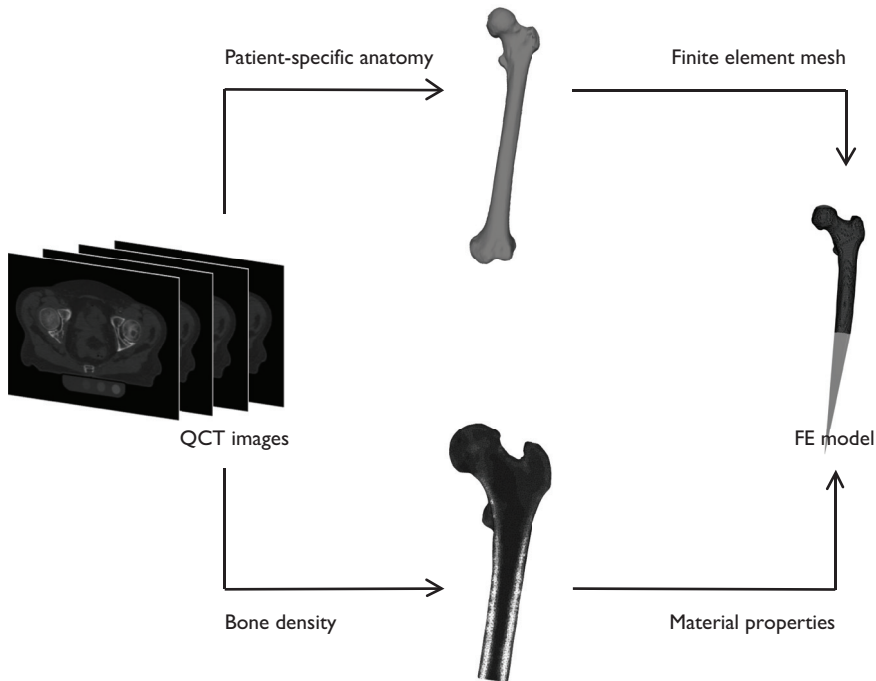


Figure 7. Workflow for generating patient-specific finite element models.

forces. In metastatic bone disease, however, the bone quality is locally affected. Hence, it may be important to study the local balance between applied load and load bearing capacity. This requires applying a physiological loading pattern that includes hip contact forces as well as muscle forces, which can be determined using musculoskeletal modelling.

In short, musculoskeletal modelling uses 3D marker trajectories and ground reaction forces measured during an instrumented gait analysis of the subject, in combination with a musculoskeletal model to calculate joint moments using inverse dynamics principles. In a next step, muscle forces are determined using optimisation techniques and, subsequently, the joint contact forces are calculated based on the muscle force distribution at each time frame of the motion under study. As such, the load imposed on the femur during daily activities, such as walking or rising from a chair, can be determined. This sophisticated loading regime can then be applied to the patient-specific FE models.

Aim and outline of this thesis

The goal of this thesis was to develop and validate a patient-specific finite element model to assess the femoral fracture risk in patients with metastatic bone disease. More specifically,

the work aimed to validate the model predictions against mechanical experiments as well as prospective clinical follow-up data in actual patients, using both simple and more physiological loading conditions. In addition, the prediction accuracy of the FE model was compared to an alternative state-of-the-art biomechanical tool implementing composite beam theory for fracture risk assessment. The following outline describes the different aspects of the thesis in more detail.

Validation of a subject-specific finite element model against mechanical experiments

The aim of Chapter 2 was to verify if the failure loads calculated using FE models were in agreement with the experimentally measured failure loads. For that purpose, mechanical axial loading experiments were performed on cadaveric femurs with and without artificial lesions, which were subsequently mimicked in finite element simulations. In addition, the clinical relevance of these models was determined by comparing fracture risk assessments of clinical experts to the FE predictions. Chapter 3 aimed to implement more realistic material behaviour. A parametric study was performed, in which the effect of an asymmetric yield criterion on the simulated failure loads and failure locations was investigated.

Comparing the performance of FE models and an alternative state of the art biomechanical tool

Chapter 4 describes a collaborative study with the group of Prof. Snyder at the Center for Advanced Orthopaedic Studies, Beth Israel Deaconess Medical Center at Harvard University in Boston. In addition to FE modelling, computed tomography based rigidity analysis (CTRA) (Windhagen et al., 1997; Snyder et al., 2006; Snyder et al., 2009; Leong et al., 2010) constitutes another promising tool to improve fracture risk assessments. This method was developed and validated by the Harvard group. In short, this method uses composite beam theory to calculate axial, bending and torsional rigidities, which are used to distinguish high-risk lesions from low-risk lesions. The aim of this study was to directly compare the prediction accuracy of FE models and CTRA analyses on the basis of the cadaveric experiments described in Chapter 2.

In vivo validation of finite element models

Chapter 5 describes a prospective patient study that was conducted as a next step in the validation process. The goal of this study was to investigate whether the FE models were able to identify the patients with an impending fracture. For that purpose, patients with painful femoral metastases were prospectively followed during and after treatment with radiotherapy. Some of the patients in this study sustained an unexpected fracture in the femur during follow-up. Using FE models with boundary conditions as defined in Chapter 2, the failure load

was calculated for the treated femurs of all patients. Subsequently, it was validated whether the FE models were able to classify patients with an impending fracture. In addition, these predictions were directly compared to clinical assessments by two radiation oncologists and two orthopaedic surgeons who were all experienced at assessing femoral fracture risks.

Implementation of physiological loading conditions

The *in vivo* FE simulations in Chapter 5 may need a more sophisticated loading regime to predict femoral failure, in order to capture a local decrease in bone strength caused by a metastatic lesion. Such a sophisticated loading regime can be developed using musculoskeletal modelling. This modelling technique comprises complex biomechanical analyses and is elaborately studied by the Human Movement Biomechanics Research Group at the Katholieke Universiteit Leuven in Belgium (Ilse Jonkers, PhD). In collaboration with this group, physiological loading conditions comprising muscle forces and hip contact forces were developed, in order to study the local balance between applied load and load bearing capacity. For that purpose, two studies were conducted. The aim of the first study (Chapter 6) was to investigate the effect of four different optimisation techniques on muscle force distribution and the subsequent hip joint contact force. The results that best resembled hip contact forces measured *in vivo* (Bergmann et al., 2001), were selected to develop sophisticated loading conditions for the FE models. The ultimate goal of this work is to improve the sensitivity and specificity of fracture predictions in the femurs of patients with metastatic bone disease. As a first step, in Chapter 7, muscle forces and hip contact forces were applied to the FE models of two typical patients who sustained a fracture in the prospective study. We assessed whether modelling physiological load cases majorly affects failure predictions, in terms of volume of failure and failure location. In addition, we investigated whether the inclusion of non-linear elastic-plastic material properties is required to capture these effects.

Discussion and future perspectives of FE modelling for fracture risk assessment in metastatic bone disease

To conclude, Chapter 8 reflects on the outcomes of this thesis. It reviews the potential of current FE models to predict femoral fracture risk in metastatic bone disease, and describes the challenges that have to be tackled before clinical implementation of these models is safe and viable. Moreover, it discusses future perspectives of FE modelling in metastatic bone disease by summarizing potential applications of biomechanical models in the daily care for these patients with metastatic bone disease.

References

- Attar S, Steffner RJ, Avedian R, Hussain WM. 2012. Surgical intervention of nonvertebral osseous metastasis. *Cancer Control* 19(2): 113-121.
- Beals RK, Lawton GD, Snell WE. 1971. Prophylactic internal fixation of the femur in metastatic breast cancer. *Cancer* 28(5): 1350-1354.
- Bergmann G, Deuretzbacher G, Heller M, Graichen F, Rohlmann A, Strauss J, Duda GN. 2001. Hip contact forces and gait patterns from routine activities. *J Biomech* 34(7): 859-871.
- Bessho M, Ohnishi I, Matsumoto T, Ohashi S, Matsuyama J, Tobita K, Kaneko M, Nakamura K. 2009. Prediction of proximal femur strength using a CT-based nonlinear finite element method: Differences in predicted fracture load and site with changing load and boundary conditions. *Bone* 45(2): 226-231.
- Bunting R, Lamont-Havers W, Schweon D, Kliman A. 1985. Pathologic fracture risk in rehabilitation of patients with bony metastases. *Clin Orthop Relat Res* 192: 222-227.
- Cheal EJ, Hipp JA, Hayes WC. 1993. Evaluation of Finite-Element Analysis for Prediction of the Strength Reduction Due to Metastatic Lesions in the Femoral-Neck. *J Biomech* 26(3): 251-264.
- Cheng DS, Seitz CB, Eyre HJ. 1980. Nonoperative management of femoral, humeral, and acetabular metastases in patients with breast carcinoma. *Cancer* 45(7): 1533-1537.
- Coleman RE. 1997. Skeletal complications of malignancy. *Cancer* 80(8 Suppl): 1588-1594.
- Coleman RE. 2006. Clinical features of metastatic bone disease and risk of skeletal morbidity. *Clin Cancer Res* 12(20 Pt 2): 6243s-6249s.
- Falcinelli C, Schileo E, Balistreri L, Baruffaldi F, Bordini B, Viceconti M, Albinetti U, Ceccarelli F, Milandri L, Toni A, Taddei F. 2014. Multiple loading conditions analysis can improve the association between finite element bone strength estimates and proximal femur fractures: a preliminary study in elderly women. *Bone* 67: 71-80.
- Fidler M. 1973. Prophylactic internal fixation of secondary neoplastic deposits in long bones. *Br Med J* 1(5849): 341-343.
- Gralow JR, Biermann JS, Farooki A, Fornier MN, Gagel RF, Kumar R, Litsas G, McKay R, Podoloff DA, Srinivas S, Van Poznak CH. 2013. NCCN Task Force Report: Bone Health In Cancer Care. *J Natl Compr Canc Netw* 11 Suppl 3: S1-S50; quiz S51.
- Harrington KD, Sim FH, Enis JE, Johnston JO, Diok HM, Gristina AG. 1976. Methylmethacrylate as an adjunct in internal fixation of pathological fractures. Experience with three hundred and seventy-five cases. *J Bone Joint Surg Am* 58(8): 1047-1055.
- Hipp JA, Springfield DS, Hayes WC. 1995. Predicting pathologic fracture risk in the management of metastatic bone defects. *Clin Orthop Relat Res* 312: 120-135.
- Johnson SK, Knobf MT. 2008. Surgical interventions for cancer patients with impending or actual pathologic fractures. *Orthop Nurs* 27(3): 160-171; quiz 172-173.
- Signaleringscommissie Kanker van KWF Kankerbestrijding. *Kanker in Nederland tot 2020. Trends en prognoses.* Amsterdam: KWF Kankerbestrijding, 2011.
- Keene JS, Sellinger DS, McBeath AA, Engber WD. 1986. Metastatic breast cancer in the femur. A search for the lesion at risk of fracture. *Clin Orthop Relat Res* 203: 282-288.
- Keyak JH. 2001. Improved prediction of proximal femoral fracture load using nonlinear finite element models. *Med Eng Phys* 23(3): 165-173.
- Keyak JH, Kaneko TS, Rossi SA, Pejic MR, Tehranzadeh J, Skinner HB. 2005a. Predicting the strength of femoral shafts with and without metastatic lesions. *Clin Orthop Relat Res* 439: 161-170.
- Keyak JH, Kaneko TS, Skinner HB, Hoang BH. 2007. The effect of simulated metastatic lytic lesions on proximal femoral strength. *Clin Orthop Relat Res* 459: 139-145.
- Keyak JH, Kaneko TS, Tehranzadeh J, Skinner HB. 2005b. Predicting proximal femoral strength using structural engineering models. *Clin Orthop Relat Res* 437: 219-228.
- Keyak JH, Lee IY, Nath DS, Skinner HB. 1996. Postfailure compressive behavior of tibial trabecular bone in three anatomic directions. *J Biomed Mater Res* 31(3): 373-378.

- Keyak JH, Sigurdsson S, Karlsdottir GS, Oskarsdottir D, Sigmarsdottir A, Kornak J, Harris TB, Sigurdsson G, Jonsson BY, Siggeirsdottir K, Eiriksdottir G, Gudnason V, Lang TF. 2013. Effect of finite element model loading condition on fracture risk assessment in men and women: the AGES-Reykjavik study. *Bone* 57(1): 18-29.
- Kopperdahl DL, Aspelund T, Hoffmann PF, Sigurdsson S, Siggeirsdottir K, Harris TB, Gudnason V, Keaveny TM. 2014. Assessment of incident spine and hip fractures in women and men using finite element analysis of CT scans. *J Bone Miner Res* 29(3): 570-580.
- Laitinen M, Ratasvuori M, Pakarinen TK. 2012. The multi-model approach to metastatic disease, in: *European Instructional Lectures*. Springer Berlin Heidelberg, Berlin, pp. 35-44.
- Leong NL, Anderson ME, Gebhardt MC, Snyder BD. 2010. Computed tomography-based structural analysis for predicting fracture risk in children with benign skeletal neoplasms: comparison of specificity with that of plain radiographs. *J Bone Joint Surg Am* 92(9): 1827-1833.
- Mavrogenis AF, Pala E, Romagnoli C, Romantini M, Calabro T, Ruggieri P. 2012. Survival analysis of patients with femoral metastases. *J Surg Oncol* 105(2): 135-141.
- Miller F, Whitehill R. 1984. Carcinoma of the breast metastatic to the skeleton. *Clin Orthop Relat Res* 184: 121-127.
- Mirels H. 1989. Metastatic disease in long bones. A proposed scoring system for diagnosing impending pathologic fractures. *Clin Orthop Relat Res* 249: 256-264.
- Orwoll ES, Marshall LM, Nielson CM, Cummings SR, Lapidus J, Cauley JA, Ensrud K, Lane N, Hoffmann PR, Kopperdahl DL, Keaveny TM, Osteoporotic Fractures in Men Study G. 2009. Finite element analysis of the proximal femur and hip fracture risk in older men. *J Bone Miner Res* 24(3): 475-483.
- Paget S. 1889. The Distribution of Secondary Growths in Cancer of the Breast. *The Lancet* 133(3421): 571-573.
- Parrish FF, Murray JA. 1970. Surgical treatment for secondary neoplastic fractures. A retrospective study of ninety-six patients. *J Bone Joint Surg Am* 52(4): 665-686.
- Ratasvuori M, Wedin R, Keller J, Nottrott M, Zaikova O, Bergh P, Kalen A, Nilsson J, Jonsson H, Laitinen M. 2013. Insight opinion to surgically treated metastatic bone disease: Scandinavian Sarcoma Group Skeletal Metastasis Registry report of 1195 operated skeletal metastasis. *Surg Oncol* 22(2): 132-138.
- Rizzoli R, Body JJ, Brandi ML, Cannata-Andia J, Chappard D, El Maghraoui A, Gluer CC, Kendler D, Napoli N, Papaioannou A, Pierroz DD, Rahme M, Van Poznak CH, de Villiers TJ, El Hajj Fuleihan G, International Osteoporosis Foundation Committee of Scientific Advisors Working Group on Cancer-Induced Bone D. 2013. Cancer-associated bone disease. *Osteoporos Int* 24(12): 2929-2953.
- Ruggieri P, Mavrogenis AF, Casadei R, Errani C, Angelini A, Calabro T, Pala E, Mercuri M. 2010. Protocol of surgical treatment of long bone pathological fractures. *Injury-International Journal of the Care of the Injured* 41(11): 1161-1167.
- Siegel R, DeSantis C, Virgo K, Stein K, Mariotto A, Smith T, Cooper D, Gansler T, Lerro C, Fedewa S, Lin C, Leach C, Cannady RS, Cho H, Scoppa S, Hachey M, Kirsh R, Jemal A, Ward E. 2012. Cancer treatment and survivorship statistics, 2012. *CA Cancer J Clin* 62(4): 220-241.
- Signaleringscommissie Kanker van KWF Kankerbestrijding. Signaleringsrapport 'De kans op kanker. Bewerking van cijfers NKR en CBS 1999-2003'. Amsterdam: KWF Kankerbestrijding, 2007.
- Snell W, Beals RK. 1964. Femoral Metastases and Fractures from Breast Cancer. *Surg Gynecol Obstet* 119: 22-24.
- Snyder BD, Cordio MA, Nazarian A, Kwak SD, Chang DJ, Entezari V, Zurakowski D, Parker LM. 2009. Noninvasive Prediction of Fracture Risk in Patients with Metastatic Cancer to the Spine. *Clin Cancer Res* 15(24): 7676-7683.
- Snyder BD, Hauser-Kara DA, Hipp JA, Zurakowski D, Hecht AC, Gebhardt MC. 2006. Predicting fracture through benign skeletal lesions with quantitative computed tomography. *Journal of Bone and Joint Surgery Am* 88A(1): 55-70.
- Spruijt S, van der Linden JC, Dijkstra PDS, Wiggers T, Oudkerk M, Snijders CJ, van Keulen F, Verhaar JAN, Weinans H, Swierstra BA. 2006. Prediction of torsional failure in 22 cadaver femora with and without simulated subtrochanteric metastatic defects - A CT scan-based finite element analysis. *Acta Orthopaedica* 77(3): 474-481.
- van der Linden YM. 2005. Radiotherapy in bone metastases. The Dutch Bone Metastasis Study. Thesis. University of Leiden, Leiden, The Netherlands.
- van der Linden YM, Dijkstra PD, Kroon HM, Lok JJ, Noordijk EM, Leer JW, Marijnen CA. 2004a. Comparative analysis of risk factors for pathological fracture with femoral metastases. *J Bone Joint Surg Br* 86(4): 566-573.
- van der Linden YM, Kroon HM, Dijkstra SP, Lok JJ, Noordijk EM, Leer JW, Marijnen CA, Dutch Bone Metastasis

- Study G. 2003. Simple radiographic parameter predicts fracturing in metastatic femoral bone lesions: results from a randomised trial. *Radiother Oncol* 69(1): 21-31.
- van der Linden YM, Lok JJ, Steenland E, Martijn H, van Houwelingen H, Marijnen CA, Leer JW, Dutch Bone Metastasis Study G. 2004b. Single fraction radiotherapy is efficacious: a further analysis of the Dutch Bone Metastasis Study controlling for the influence of retreatment. *Int J Radiat Oncol Biol Phys* 59(2): 528-537.
- Windhagen HJ, Hipp JA, Silva MJ, Lipson SJ, Hayes WC. 1997. Predicting failure of thoracic vertebrae with simulated and actual metastatic defects. *Clin Orthop Relat Res* 344: 313-319.
- Yazawa Y, Frassica FJ, Chao EY, Pritchard DJ, Sim FH, Shives TC. 1990. Metastatic bone disease. A study of the surgical treatment of 166 pathologic humeral and femoral fractures. *Clin Orthop Relat Res* 251: 213-219.
- Zickel RE, Mouradian WH. 1976. Intramedullary fixation of pathological fractures and lesions of the subtrochanteric region of the femur. *J Bone Joint Surg Am* 58(8): 1061-1066.



2

The assessment of the risk of fracture in femora with metastatic lesions: Comparing case-specific finite element analyses with predictions by clinical experts

*Loes C. Derikx, Jantien B. van Aken, Dennis Janssen, An Snyers,
Yvette M. van der Linden, Nico Verdonschot, Esther Tanck.
J Bone Joint Surg Br 2012; 94(8), 1135-1142.*



Introduction

Patients with metastatic disease in the femur are at risk of pathological fracture. In some the risk is low, and pain can be managed with radio- (Hoskin, 2003) or systemic chemotherapy (Harvey, 1997), hormonal therapy (Harvey, 1997) and/or bisphosphonates (Body, 2003; Hoskin, 2003) for widespread disease. If the predicted risk of fracture is high, the bone is mechanically stabilised (Body, 2003; Wedin et al., 2005); however, assessing the risk of fracture can be difficult. Among the predictive factors are the plain radiological features or those on CT scan, which are prone to error (Hipp et al., 1995). Overall there are no indicators which reliably predict impending pathological fractures (Mirels, 1989; Hipp et al., 1995; Dijkstra et al., 1997; van der Linden et al., 2003; van der Linden et al., 2004).

Additional aspects that play an important role in the assessment of the risk of fracture are the initial strength of the bone and the daily activity pattern of the patient (Hipp et al., 1995). These aspects can be analysed using patient-specific finite element (FE) models (Keyak et al., 1998; Cody et al., 1999; Keyak, 2001; Bessho et al., 2004; Spruijt et al., 2006; Taddei et al., 2006; Bessho et al., 2007), which are based on quantitative CT (QCT) scans, from which the bone geometry and quality is retrieved (Lenaerts et al., 2009). Mechanical properties are calculated from the distribution of the bone mineral density (BMD) and are then assigned to the FE model (Keyak et al., 2005; Tanck et al., 2009). A loading pattern is applied and the load at which the femur fails is calculated. Although essentially an *in vitro* method of predicting the load at which the femur will fail, this method could have an important clinical application.

In a previous pilot study (Tanck et al., 2009), we ranked five paired femora with and without artificial metastases according to their load to failure. The data were retrieved from mechanical experiments, and compared with rankings predicted by the FE model and by clinical experts, respectively. Predictions using the FE model were considerably better than those made by the experts. However, due to the limited variety in the characteristics of the lesions in the femur we could not establish which determinants accounted for the differences in the accuracy of prediction. Moreover, in the pilot study we used FE-models that provided numerical stability problems in about 20% of the simulations, meaning that in those cases the results were not fully reliable. Obviously, if this model is to be used to analyse femoral fracture risks in patients, numerical problems to this extent are not acceptable.

The aim of this study was to assess whether case-specific non-linear FE models could improve the prediction of the load at which the femur would fail as compared with the predictions of experienced physicians, using improved FE models with a non-voxel based element type and modelling an increased variety in lesion characteristics. We defined the following research questions: 1) is the current FE model able to predict case-specific fracture risks under uniaxi-

al loading in terms of load to failure and location of the failure? 2) is this FE model better at predicting the risk of fracture than clinical experts when a large set of metastatic and control femora are tested? 3) which characteristics of the lesion, such as size or location, are important in predicting the risk of fracture, and how are these scored by clinical experts?

Materials and Methods

Ten paired fresh-frozen human cadaveric femora aged between 63 and 96 years, (mean 81.7 years), seven male and three female, were mechanically tested to failure. Five of these pairs were tested previously (Tanck et al., 2009). The specimens were obtained from the Department of Anatomy with institutional approval. After removing the soft-tissues, one of each pair of femora was left intact and assigned to the control group. In the contralateral femur, one or more artificial lytic metastases were created by drilling holes through one cortex only. The location, size and number of these lesions varied between the specimens and resembled the clinical appearance of metastases in bone, as previously discussed with orthopaedic oncologists (Table 1, Figure 1). All femora were embedded distally in polymethylmethacrylate (PMMA). Before starting the experiments, anterior-posterior and mediolateral radiographs were taken.

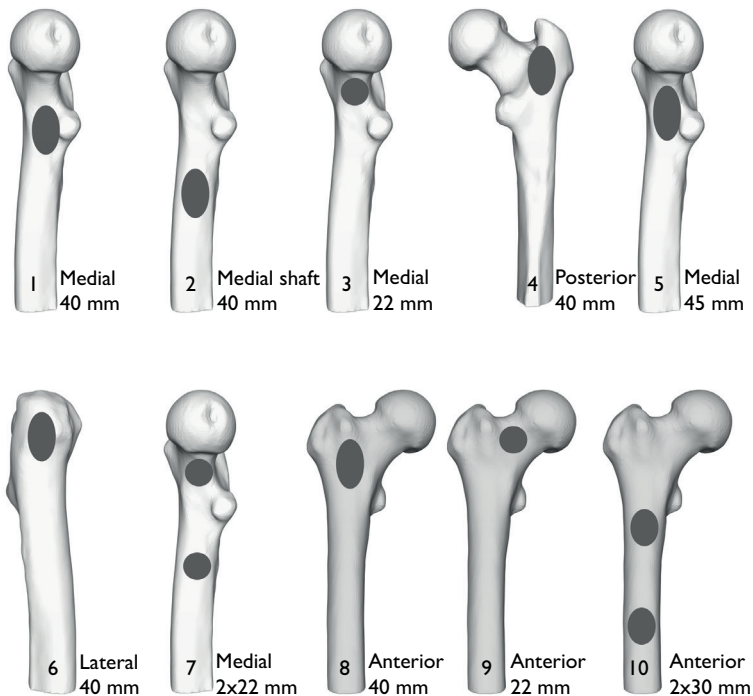


Figure 1. Diagrams showing the varying size and location of the artificial lytic lesions created in the ten femora.

For alignment purposes, the femora were subsequently equipped with 28 tantalum markers, which were glued along the femoral cortex in the sagittal and frontal plane. QCT images (ACQSim/Brilliance Big Bore; Philips, Eindhoven, The Netherlands) with the following settings were acquired: 120 kVp, 220 mAs, slice thickness 3 mm, pitch 1.5, spiral and standard reconstruction, in-plane resolution 0.9375 mm. The femora were scanned in a water basin, positioned on top of a solid calibration phantom containing four tubes with 0, 50, 100 and 200 mg/ml calcium hydroxyapatite (Image Analysis, Columbia, Kentucky), respectively. A stereo radiograph was then taken of the femora in order to calculate the three-dimensional (3D) position of the tantalum markers.

Table 1. Lesion characteristics and experimental results of the 20 femora in this study.

Subject	Lesion site	Lesion size (mm)	Failure load of control femur (N)	Failure load of metastatic femur (N)	Reduction in failure load
1	medial, proximal	40	4141	1237	70 %
2	medial, shaft	40	5007	1853	63 %
3	medial, proximal	22	5031	2181	57 %
4	posterior, proximal	40	4728	2806	41 %
5	medial, proximal	45	7852	3002	62 %
6	lateral, proximal	40	4660	3960	15 %
7	medial, proximal & shaft	2 x 22	11034	3980	64 %
8	anterior, proximal	40	7970	5985	25 %
9	anterior, proximal	22	6821	6547	4 %
10	anterior, proximal & shaft	2 x 30	10470	8815	16 %

Mechanical experiments

In line with our pilot study (Tanck et al., 2009), the femora were fixed using a distal ball-bearing and a sliding hinge, allowing only rotation around the dorsoventral axis (Figure 2). Using a hydraulic MTS machine, an axial load was applied on the femoral head, via a plastic cup (diameter 30 mm, polyoxymethylene, Delrin) with 10 N/s from 0 N until failure. During these load controlled experiments the force and displacement of the plunger were registered. The course of failure of each femur was recorded with a conventional digital camera.

Finite element model

Geometric information for the FE models was retrieved by segmenting the QCT images and converting them to a solid mesh consisting of four-noded tetrahedral elements (mean edge length approximately 2 mm). Calibration of the CT data and material property assignment was performed using software developed in our lab. Subsequently, we adopted non-linear isotropic material behaviour according to Keyak et al. (2005). The position of the tantalum

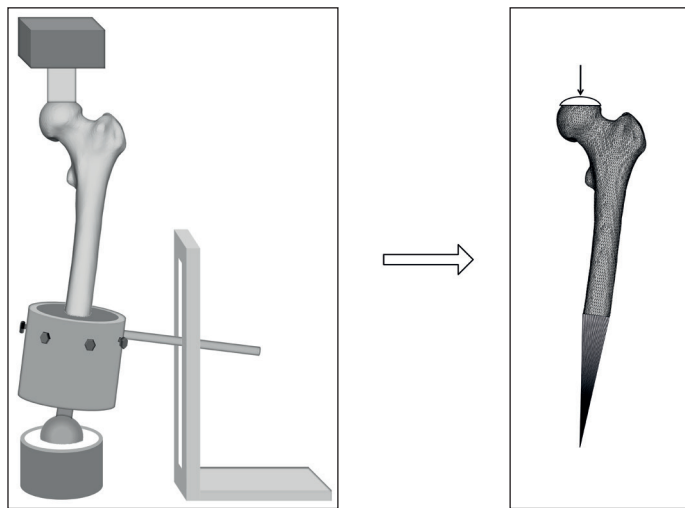


Figure 2. Diagrams showing the experimental set-up (left) and the same conditions mimicked in the finite element model (right).

markers in the stereo radiographs and in the CT scans was used to orient the FE model in the experimental configuration. The experimental boundary conditions were exactly mimicked in the FE simulations (Figure 2); the distal fixation of the femora was accomplished by adding two bundles of high-stiffness springs (Tanck et al., 2009).

In the FE simulations we used a displacement-controlled loading condition. Loads were applied via a cup (diameter 30 mm) that displaced with 0.1 mm per increment. In order to prevent artefacts as a result of the loading configuration, post-yield material behaviour (Keyak et al., 2005) was not implemented in the surface elements underneath the cup. The FE simulations were performed with MSC Marc (MSC.MARC2007r1; MSC Software Corporation, Santa Ana, California). The total time expenditure for generating a case-specific FE model and running the simulation was approximately eight hours. The incremental displacement was registered via a reference node underneath the cup. The total reaction force in the loading direction was defined as the sum of the contact normal forces of all the nodes in the model. Structural fracture was assumed to occur when the maximum total reaction force was reached. The location of the failure was defined by elements that plastically deformed when the maximal total reaction force was reached (Keyak et al., 2005).

Clinical assessment

Clinicians often rely on conventional radiographs when assessing the risk of femoral fracture due to metastases (Mirels, 1989; van der Linden et al., 2004). Moreover, current clinical guide-

lines such as Mirels' score (Mirels, 1989) or the degree of cortical destruction (van der Linden et al., 2004) are based on radiological assessment. Furthermore, it has been shown by Hipp et al. (1995) that the estimation by clinical experts of the femoral load to failure does not improve when they are provided with CT scans in addition to conventional radiographs. Therefore, six experts (three orthopaedic surgeons, two radiation oncologists and one radiologist) were provided with the baseline anterior-posterior (AP) and mediolateral (ML) radiographs of the femora and information on gender, age and experimental set-up. The radiographs of one of the controls were missing; this femur was therefore excluded from the clinical assessment. The clinicians ranked the 19 remaining femora on load to failure, starting with the weakest femur. We did not prescribe any rules or guidelines for ranking, as it appeared from clinical practice that clinicians use a combination of techniques, depending on their professional background. Subsequently, a short survey was conducted among them in which they reported their strategies for assessing the load to failure. They indicated the five most relevant factors they used to predict the load to failure. Five points were assigned to the most important factor, while the least important factor received one point and the redundant factors zero points. The scores per factor were then summed for all clinicians.

Analysis of data

The accuracy of the FE predictions was determined by regressing the predicted load to failure on the experimental failure load. Furthermore, we ranked the femora on experimental load to failure and on the failure load predicted by the FE model. These rankings were then compared using the Kendall rank correlation coefficient (τ), which defines the degree of similarity between two rankings (Abdi, 2007). In the same vein, the rankings by the clinicians were compared to the experimental ranking, to the ranking by the FE model, and to the rankings by the other clinicians, respectively. Studying consistencies and inconsistencies in the predictions among the clinicians could reveal which characteristics they did (or did not) take into account when ranking the femora with metastases. Finally, the reduction in load to failure as a result of the artificial metastatic lesions was defined as the difference in failure load between a pair of femora. We compared the reduction in load to failure measured in the experiments to the reductions predicted by the FE model.

Statistical analysis

Statistical analyses were performed in SPSS v16.02 (SPSS Inc., Chicago, Illinois). The fracture locations in the experiments were qualitatively compared to the fracture lines predicted by the FE model. Results were considered statistically significant if $p < 0.05$.

Results

In all femoral loading experiments, the artificial lesions decreased the load to failure of the femora with metastases compared to the controls (Table 1). The experiments were all simulated by the FE models, without numerical problems.

In the control group, the fracture lines predicted by the FE model only moderately agreed with the experimental results. In most of the controls an intertrochanteric fracture was seen, yet the FE models mainly predicted subcapital fractures. However, in most of the metastatic femora, the model correctly predicted a fracture through the metastatic lesions, comparable to the experimental fracture lines (Figure 3). The FE model accurately predicted the load to failure as measured in the experiments, both for intact femora ($R^2 = 0.90$, $p < 0.001$; slope = 1.0, $p < 0.001$; intercept = -0.50 kN, $p = 0.576$) and for metastatic femora ($R^2 = 0.93$, $p < 0.001$; slope = 0.95, $p < 0.001$; intercept = 0.72 kN, $p = 0.119$) (Figure 4). There were no significant differences between the regression lines in the two groups.

In the metastatic subset, the FE ranking of load to failure corresponded very well with the actual experimental ranking ($\tau = 0.87$; $p < 0.001$), whereas none of the clinical experts ranked the femora in agreement with the experimental results ($0.11 < \tau < 0.42$, $p \geq 0.089$) (Table 2). Kendall tau rank correlations between clinicians and the FE model were not significant and ranged from 0.16 to 0.47 (Table 2). The Kendall tau rank correlations among clinicians were quite variable and ranged from moderate ($\tau = 0.33$, $p = 0.180$) to good ($\tau = 0.96$, $p < 0.001$; Table 2). Remarkably, the load to failure of the bone with the 40 mm posterior lesion in the proximal femur (Figure 1) was largely overestimated by the FE model and by five of six

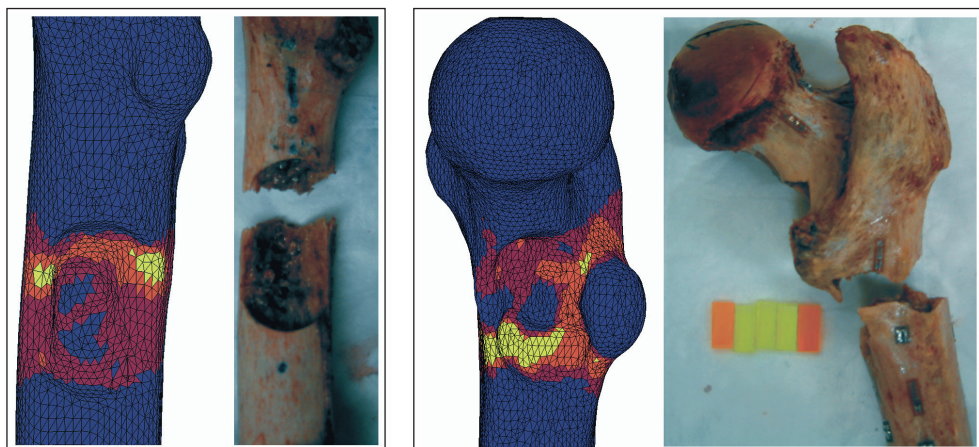


Figure 3. Finite element images predicting two representative fracture locations, showing areas of plastic deformity (indicated in red/orange/yellow), with experimental photographs showing fracture sites corresponding to those predicted by the FE model.

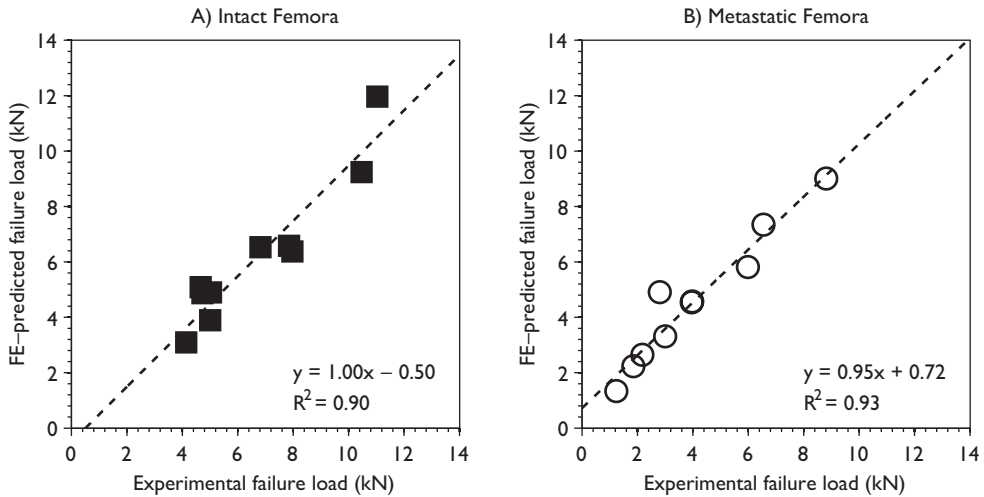


Figure 4. Graphs of the experimental load to failure versus the load to failure predicted by the finite element (FE) model for A) intact and B) metastatic femora showed a strong correlation for both ($R^2 = 0.90$ and 0.93 , respectively).

clinical experts. Therefore, an outlier analysis was performed, but none of the femora could significantly be defined as such (Cook's distance ≤ 0.83 (Kleinbaum et al., 1998)).

A more detailed analysis of the clinicians' predictions of load to failure revealed the following: the experimental results showed that three femora with lesions were stronger than five of the intact femora (Table 1) and the FE model correctly ranked these three metastatic femora among the strongest femora (Figure 4). However, five clinicians predicted that all metastatic femora were weaker than all the control bones, thus clearly penalising the presence of lesions in the bones, irrespective of the initial strength of the femur. Furthermore, the load to failure of the femur with a 22 mm medial lesion (number 3) was overestimated by all clinicians, but not by the model. The femur with a 45 mm medial lesion and the femur with a double lesion (30 mm) on the anterior side, respectively, were stronger than estimated by five clinicians (numbers 5 and 10). Two femora, with a 40 mm medial lesion and a 22 mm anterior lesion in the proximal femur, respectively, were correctly ranked by the model and all clinicians (numbers 1 and 9).

In the experiments, the relative reduction in failure load was largest ($> 50\%$) for medial lesions, regardless of their size (Table 1). Anterior lesions had a smaller effect on failure load ($\leq 25\%$). The FE model adequately predicted the reduction in load to failure caused by the metastatic lesions ($R^2 = 0.92$, $p < 0.001$) (Figure 5). In the survey the clinicians indicated that the extent of cortical destruction is considered to be most important for the prediction of the risk of fracture, followed by the size of the lesion and their location (Figure 6). The distribu-

Table 2. Kendall rank correlations between experimental and predicted rankings on failure load for metastatic femora. The asterisk indicates that the correlation is significant at the 0.05 level (2-tailed).

	Experiment	FE	Clinician 1	Clinician 2	Clinician 3	Clinician 4	Clinician 5	Clinician 6
Experiment	-							
FE	0.87*	-						
Clinician 1	0.33	0.47	-					
Clinician 2	0.24	0.29	0.64*	-				
Clinician 3	0.42	0.47	0.38	0.47	-			
Clinician 4	0.20	0.33	0.78*	0.60*	0.33	-		
Clinician 5	0.11	0.16	0.60*	0.60*	0.51*	0.56*	-	
Clinician 6	0.24	0.38	0.73*	0.64*	0.38	0.96*	0.51*	-

tion of the BMD and the femoral geometry were considered by them to be of less importance in predicting the strength of the bone. Furthermore, they reported that their strategy in this study differed from clinical practice in that they normally also take into consideration the appearance of the lesion (lytic, blastic or mixed type) and the expected pattern of daily activity of the patient.

Discussion

Current clinical practice lacks an accurate predictor of the expected risk of fracture in patients with metastatic lesions in the femur. Yet, patient-specific FE models have been shown to be very promising in this field. In this study, we reassessed the robustness of our FE model and tried to link its predictions to clinical practice by focussing on the question as to why clinicians have difficulties in predicting load to failure of femora containing metastases.

As we found a moderate to good agreement in the predictions among our clinicians, we concluded that they more or less rely on the same determinants. However, their predictions neither corresponded to the experiments, nor to the FE predictions. On the contrary, there was a good correlation between the FE predictions and the experiments, from which we conclude that clinicians focussed on determinants that attributed less to the load to failure than those implemented by the FE model.

The FE model was shown to be sensitive to several characteristics of the lesions. Thus, the predicted fracture line often corresponded to the actual fracture line through the metastasis, suggesting that the model can incorporate cortical destruction. Furthermore, the FE models correctly predicted the relative reductions in load to failure, suggesting that they allow for the location of the metastasis. Most importantly, the FE models incorporated the initial bone strength, as they correctly ranked three metastatic femora among the strongest femora. In contrast, the clinicians could not incorporate the bone strength, but clearly focussed on the

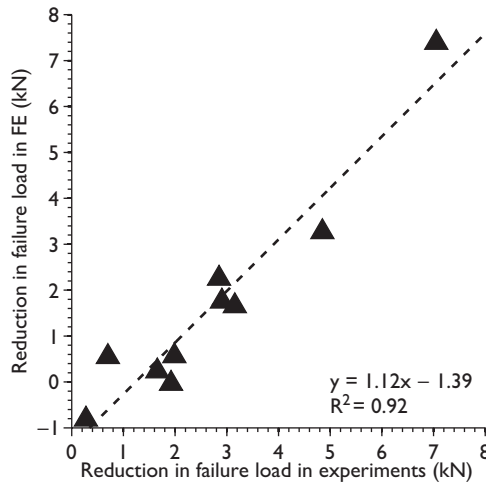


Figure 5. Graph of the failure load reduction found in experiments versus that predicted by the finite element (FE) model, showing a strong correlation between the two ($R^2 = 0.92$).

characteristics of the lesions as shown by the ranking results and the survey.

The relevance of accounting for initial bone strength or bone quality when assessing the femoral load capacity has previously been demonstrated, both by FE models and other methods. Michaeli et al. (1999) showed that the total bone mineral content and the BMD were both predictive of the load to failure of femora with artificial lytic metastases whilst climbing stairs and in external rotation. However, the total bone mineral content is not sensitive to the location of the lesion and potentially less predictive in the presence of blastic metastases. Another method of assessing the loading capacity of femora is to calculate structural rigidities on the basis of bone material properties retrieved from QCT scans. In this way, Lee et al. (2007) found that the load to failure calculated on the basis of bending and axial rigidity was predictive for the experimental load to failure, whereas the characteristics of the lesions such as the size or relative width of the defect were not. The same conclusion was drawn by Snyder et al. (2006), who studied the accuracy of predicting fractures in patients with benign skeletal lesions. They showed that the sensitivity and specificity determined on the basis of bending and torsional rigidity were much higher than the sensitivity and specificity of any lesion characteristic. These results all emphasise that the initial strength and the biomechanical effect of metastatic lesions are very important for the assessment of the loading capacity of bone.

An important limitation that is often mentioned in this type of study is that these complex and comprehensive methods are not ready for clinical implementation, as specific technical knowledge is needed in order to perform such simulations or calculations. Furthermore, in order to prove the clinical relevance of implementing such complicated methods to predict



Figure 6. Chart showing the results of a small survey into clinicians' strategies for assessing the load capacity of the femora. Five points were assigned to the most important factor, while the least important factor received one point and the redundant factors zero points. The scores per factor were then summed for all clinicians.

the risk of fracture, prospective studies should be performed. In this way, the true predictive value of these methods can be shown, and it will then become clearer how their output can be translated into a concrete advice for clinicians when planning treatment. Griffith and Genant (2011) recently reported that imaging modalities such as FE models gradually make their way into clinical practice. For example, they refer to the work of Keaveny et al. (Keaveny et al., 2008; Orwoll et al., 2009; Keaveny et al., 2010; Christiansen et al., 2011) who have extensively used FE modelling to study osteoporosis in a clinical setting. In one of the first prospective case-cohort studies, they studied 250 men over 65 years of age and showed that the femoral strength calculated by FE models was more strongly associated with femoral fracture than the bone mineral density (Orwoll et al., 2009). Such prospective studies with this number of participants which are analysed using patient-specific FE techniques indicate that clinical implementation of FE modelling will become possible in the near future.

This study has some limitations. Although the accuracy of our FE model was in line with other studies (Keyak et al., 2005; Bessho et al., 2007), the case-specific under- or overestimation of the load to failure could still be quite large. Obviously, these aberrant predictions need to be improved in order to predict patient-specific fracture risks on which diagnoses and treatments can be based.

Although the location of the fracture was correctly predicted in the femora with metastatic lesions, in intact femora there was a difference between the predicted and actual location of the fractures. In line with previous studies (Cody et al., 1999; Keyak, 2001; Keyak et al., 2005;

Bessho et al., 2007; Tanck et al., 2009), our FE model mainly predicted subcapital fractures in intact femora under axial loading, whereas in the experiments mostly intertrochanteric femoral fractures were seen. This discrepancy may be reduced by using parameters describing more realistic behaviour of bone such as an asymmetric yield criterion (Kopperdahl et al., 1998; Bayraktar et al., 2004; Bessho et al., 2007; Mullins et al., 2009) or mechanical anisotropy (Lenaerts et al., 2009).

Moreover, the simplified laboratory conditions and the artificial lytic metastases might have been quite different from those seen in clinical practice. However, the loading configuration was simple and clearly explained to the clinicians. The geometrical appearance of the lesions was simplified as compared to bone metastases in patients with cancer. If these simplified conditions were difficult for the clinicians to imagine, they would have had even more difficulty in predicting the risk of fracture *in vivo*. Additionally, bone metastases often have an osteoblastic component, which cannot be mimicked in healthy femora. Incorporating blastic metastases in FE models is challenging, since it has not been definitively determined how best to represent the structural contribution of this radio-dense but potentially weak mineralised tissue.

Finally, the axial loading condition in this study eliminated torsional components that are important for predicting the risk of femoral fracture. However, in this validation stage, the essence is that the loading condition from the experiment is copied in the FE simulations, and that the FE results agree with the experimental results. After implementing a more complex and more realistic loading scenario, the load cases will have closer agreement with the patterns of daily activity of the patients and clinicians therefore may be better at assessing the risk of fracture in these situations. As a result, they might come closer to the FE results. On the other hand, the loading condition is more complex, and therefore more difficult to comprehend which might lead to even worse predictions by the clinicians.

In this study, we validated an improved, numerically stable, case-specific non-linear FE model against experiments. The superior predictions of the FE model relative to the predictions of clinicians enabled us to disentangle determinants that are important for achieving more accurate predictions of load to failure. We showed that the FE model was sensitive for cortical destruction, the location of the lesions and the initial strength of the femur. It appeared that clinicians relied heavily on the cortical destruction, the size and location of the lesion, but not on the initial bone strength.

We conclude that the assessment of initial bone strength is essential for the accurate clinical prediction of the risk of fracture in patients with femoral metastases. Obviously, for clinicians it is hard to glean this information from conventional imaging data, and to combine it with

detailed characteristics of the lesion and the patients' medical history. In this study, we showed that FE models can accommodate these multi-factorial aspects. We therefore feel that FE models should be further developed into a clinical tool to clinicians to assess the risk of pathological fracture in patients with metastatic bone disease.

Acknowledgements

The authors would like to thank the clinical experts who were involved in the clinical assessment of the femora. Furthermore, we thank MSc students Joke Kalisvaart and Hub van den Boomen, technical staff of the Orthopaedic Research Laboratory and the Department of Anatomy for their assistance. No benefits in any form have been received or will be received from a commercial party related directly or indirectly to the subject of this article.

Supplementary material

Figures showing the Kendall rank correlations between experimental and finite element (FE)-predicted rankings on load to failure for metastatic femora and for the total sets of metastatic and intact femora.

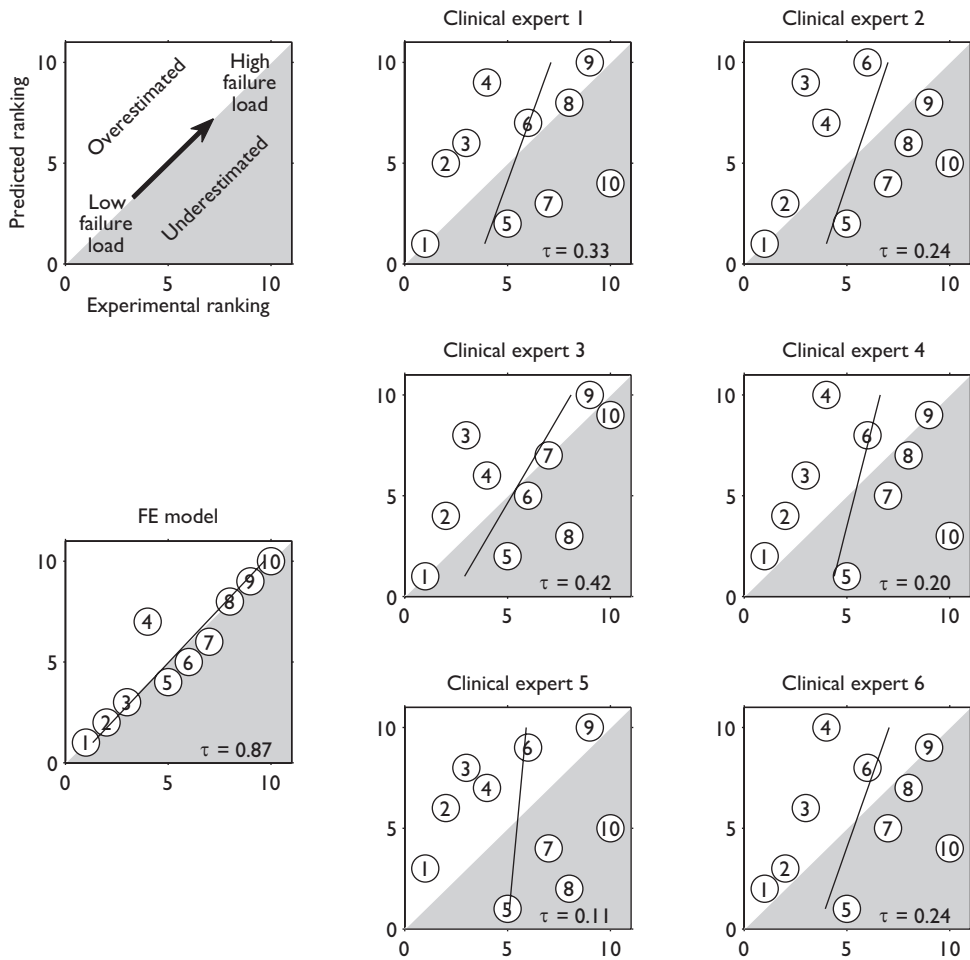


Figure S1. Kendall rank correlations between experimental and finite element (FE)-predicted rankings on load to failure for metastatic femora. The subplots show the correlations between experimental rankings and rankings predicted by either the FE model (left) or the six clinicians (right). The femora were ranked from weak (0) to strong (10).

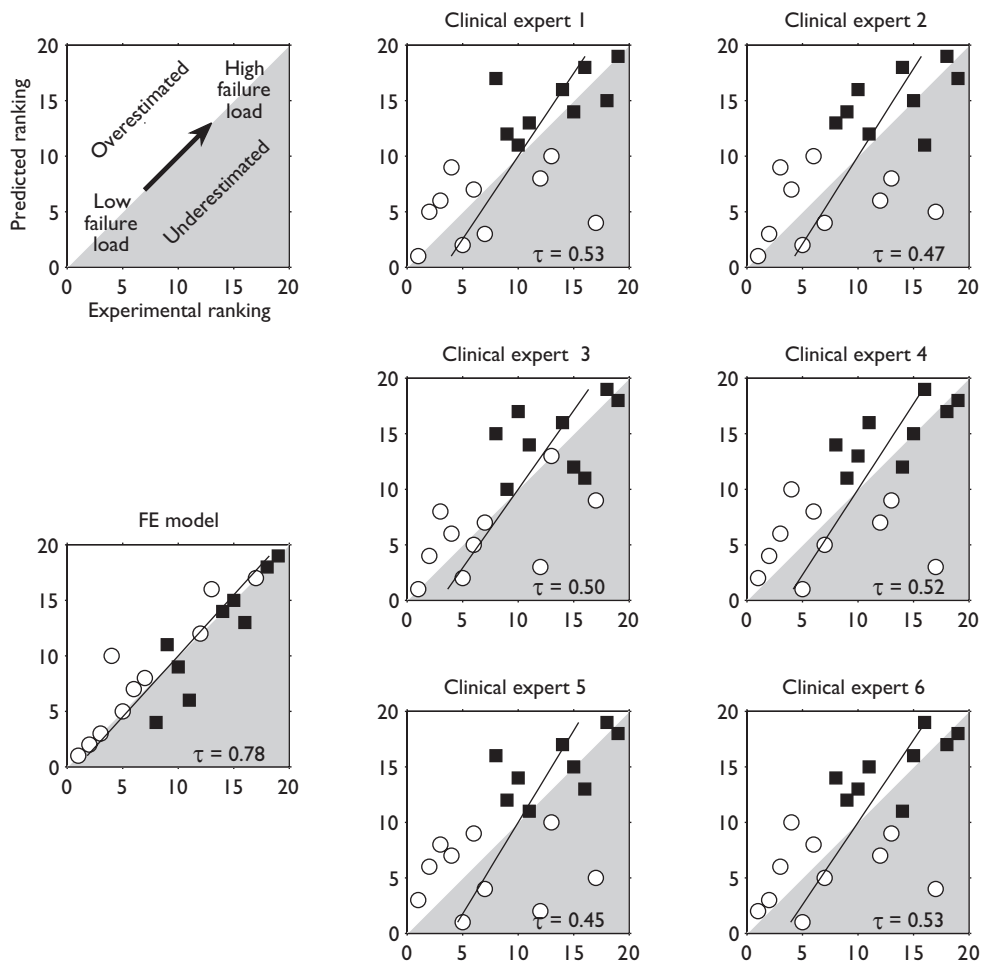


Figure S2. Kendall rank correlations between experimental and finite element (FE)-predicted rankings on load to failure for the total set of metastatic femora (circles) and intact femora (squares). The subplots show the correlations between experimental rankings and rankings predicted by either the FE model (left) or the six clinicians (right). The femora were ranked from weak (0) to strong (19).

References

- Abdi H. 2007. Kendall rank correlation, in: *Encyclopedia of Measurement and Statistics*. 1 ed. Sage, Thousand Oaks, pp. 508-510.
- Bayraktar HH, Morgan EF, Niebur GL, Morris GE, Wong EK, Keaveny TM. 2004. Comparison of the elastic and yield properties of human femoral trabecular and cortical bone tissue. *J Biomech* 37(1): 27-35.
- Bessho M, Ohnishi I, Matsuyama J, Matsumoto T, Imai K, Nakamura K. 2007. Prediction of strength and strain of the proximal femur by a CT-based finite element method. *J Biomech* 40(8): 1745-1753.
- Bessho M, Ohnishi I, Okazaki H, Sato W, Kominami H, Matsunaga S, Nakamura K. 2004. Prediction of the strength and fracture location of the femoral neck by CT-based finite-element method: a preliminary study on patients with hip fracture. *J Orthop Sci* 9(6): 545-550.
- Body JJ. 2003. Rationale for the use of bisphosphonates in osteoblastic and osteolytic bone lesions. *Breast* 12: S37-S44.
- Christiansen BA, Kopperdahl DL, Kiel DP, Keaveny TM, Bouxsein ML. 2011. Mechanical contributions of the cortical and trabecular compartments contribute to differences in age-related changes in vertebral body strength in men and women assessed by QCT-based finite element analysis. *J Bone Miner Res* 26(5): 974-983.
- Cody DD, Gross GJ, Hou FJ, Spencer HJ, Goldstein SA, Fyhrie DP. 1999. Femoral strength is better predicted by finite element models than QCT and DXA. *J Biomech* 32(10): 1013-1020.
- Dijkstra PDS, Oudkerk M, Wiggers T. 1997. Prediction of pathological subtrochanteric fractures due to metastatic lesions. *Arch Orthop Trauma Surg* 116(4): 221-224.
- Griffith JF, Genant HK. 2011. New imaging modalities in bone. *Curr Rheumatol Rep* 13(3): 241-250.
- Harvey HA. 1997. Issues concerning the role of chemotherapy and hormonal therapy of bone metastases from breast carcinoma. *Cancer* 80(8 Suppl): 1646-1651.
- Hipp JA, Springfield DS, Hayes WC. 1995. Predicting pathologic fracture risk in the management of metastatic bone defects. *Clin Orthop Relat Res* 312: 120-135.
- Hoskin PJ. 2003. Bisphosphonates and radiation therapy for palliation of metastatic bone disease. *Cancer Treat Rev* 29(4): 321-327.
- Keaveny TM, Hoffmann PF, Singh M, Palermo L, Bilezikian JP, Greenspan SL, Black DM. 2008. Femoral Bone Strength and Its Relation to Cortical and Trabecular Changes After Treatment With PTH, Alendronate, and Their Combination as Assessed by Finite Element Analysis of Quantitative CT Scans. *J Bone Miner Res* 23(12): 1974-1982.
- Keaveny TM, Kopperdahl DL, Melton LJ, 3rd, Hoffmann PF, Amin S, Riggs BL, Khosla S. 2010. Age-dependence of femoral strength in white women and men. *J Bone Miner Res* 25(5): 994-1001.
- Keyak JH. 2001. Improved prediction of proximal femoral fracture load using nonlinear finite element models. *Med Eng Phys* 23(3): 165-173.
- Keyak JH, Kaneko TS, Tehranzadeh J, Skinner HB. 2005. Predicting proximal femoral strength using structural engineering models. *Clin Orthop Relat Res* 437: 219-228.
- Keyak JH, Rossi SA, Jones KA, Skinner HB. 1998. Prediction of femoral fracture load using automated finite element modeling. *J Biomech* 31(2): 125-133.
- Kleinbaum DG, Kupper LL, Muller KE, Nizam A. 1998. *Regression Diagnostics*, in: *Applied regression analysis and multivariate methods*. 3rd ed. Books/Cole Publishing Company, Pacific Grove, pp. 212-280.
- Kopperdahl DL, Keaveny TM. 1998. Yield strain behavior of trabecular bone. *J Biomech* 31(7): 601-608.
- Lee T. 2007. Predicting failure load of the femur with simulated osteolytic defects using noninvasive imaging technique in a simplified load case. *Ann Biomed Eng* 35(4): 642-650.
- Lenaerts L, van Lenthe GH. 2009. Multi-level patient-specific modelling of the proximal femur. A promising tool to quantify the effect of osteoporosis treatment. *Philos Trans A Math Phys Eng Sci* 367(1895): 2079-2093.
- Michaeli DA, Inoue K, Hayes WC, Hipp JA. 1999. Density predicts the activity-dependent failure load of proximal femora with defects. *Skeletal Radiol* 28(2): 90-95.
- Mirels H. 1989. Metastatic disease in long bones. A proposed scoring system for diagnosing impending pathologic

- fractures. *Clin Orthop Relat Res* 249: 256-264.
- Mullins LP, Bruzzi MS, McHugh PE. 2009. Calibration of a constitutive model for the post-yield behaviour of cortical bone. *J Mech Behav Biomed Mater* 2(5): 460-470.
- Orwoll ES, Marshall LM, Nielson CM, Cummings SR, Lapidus J, Cauley JA, Ensrud K, Lane N, Hoffmann PR, Koppenhagen DL, Keaveny TM, Osteoporotic Fractures in Men Study G. 2009. Finite element analysis of the proximal femur and hip fracture risk in older men. *J Bone Miner Res* 24(3): 475-483.
- Snyder BD, Hauser-Kara DA, Hipp JA, Zurakowski D, Hecht AC, Gebhardt MC. 2006. Predicting fracture through benign skeletal lesions with quantitative computed tomography. *Journal of Bone and Joint Surgery Am* 88A(1): 55-70.
- Spruijt S, van der Linden JC, Dijkstra PDS, Wiggers T, Oudkerk M, Snijders CJ, van Keulen F, Verhaar JAN, Wejnans H, Swierstra BA. 2006. Prediction of torsional failure in 22 cadaver femora with and without simulated subtrochanteric metastatic defects - A CT scan-based finite element analysis. *Acta Orthopaedica* 77(3): 474-481.
- Taddei F, Cristofolini L, Martelli S, Gill HS, Viceconti M. 2006. Subject-specific finite element models of long bones: An in vitro evaluation of the overall accuracy. *J Biomech* 39(13): 2457-2467.
- Tanck E, van Aken JB, van der Linden YM, Schreuder HWB, Binkowski M, Huizenga H, Verdonschot N. 2009. Pathological fracture prediction in patients with metastatic lesions can be improved with quantitative computed tomography based computer models. *Bone* 45(4): 777-783.
- van der Linden YM, Dijkstra PD, Kroon HM, Lok JJ, Noordijk EM, Leer JW, Marijnen CA. 2004. Comparative analysis of risk factors for pathological fracture with femoral metastases. *J Bone Joint Surg Br* 86(4): 566-573.
- van der Linden YM, Kroon HM, Dijkstra SP, Lok JJ, Noordijk EM, Leer JW, Marijnen CA, Dutch Bone Metastasis Study G. 2003. Simple radiographic parameter predicts fracturing in metastatic femoral bone lesions: results from a randomised trial. *Radiother Oncol* 69(1): 21-31.
- Wedin R, Bauer HC. 2005. Surgical treatment of skeletal metastatic lesions of the proximal femur: endoprosthesis or reconstruction nail? *J Bone Joint Surg Br* 87(12): 1653-1657.

3

Implementation of asymmetric yielding in case-specific finite element models improves the prediction of femoral fractures

*Loes C. Derikx, Roeland Vis, Timo Meinders, Nico Verdonschot, Esther Tanck.
Comput Methods Biomech Biomed Engin 2011; 14 (2), 183-193.*



Introduction

The pathological fracture risk is one of the most impeding complications for patients suffering metastatic bone disease in weight bearing long bones (van der Linden et al., 2003). The metastatic lesion weakens the bone locally, and has often a dominant effect on the risk of fracture. Lesions with an expected low fracture risk are treated conservatively with radiotherapy for pain (Hoskin, 2003), or, if widespread disease is present, with systemic chemotherapy (Harvey, 1997), hormonal therapy (Harvey, 1997) and/or bisphosphonates (Body, 2003; Hoskin, 2003), whereas high-risk lesions are treated surgically in order to stabilise the bone surrounding the lesion. In the case of femoral metastases, the surgical procedures can have a significant impact on the quality of life of cancer patients, since they are associated with high morbidity and mortality rates and an intensive period of rehabilitation. Therefore surgeons are critical in their judgement towards the risk of fracture and the health of the patient before they choose to operate on the patient. In the event that it is decided not to operate on a patient with a high risk lesion, a pathological fracture may occur spontaneously which dramatically reduces the quality of life of the patient. Thus, the reliable prediction of the femoral fracture risk is important for the treatment of cancer patients with bone metastases. The currently available clinical methods to determine the femoral fracture risk have shown to be unable to clearly discern the two risk categories. These methods are mainly based on lesion characteristics derived from conventional X-rays, and poorly estimate the fracture risk of low risk lesions. In addition, they greatly over-predict the number of high risk lesions, resulting in large numbers of surgical overtreatment (Mirels, 1989; Hipp et al., 1995; Body, 2003; van der Linden et al., 2004). Therefore, there is an urgent need for a better predictor of the femoral fracture risk in cancer patients suffering from bone metastases.

Case-specific non-linear finite element (FE) models have shown to be promising in the prediction of the individual fracture risk both in intact and in affected femora (Keyak, 2001; Keyak et al., 2005a; Keyak et al., 2005b; Bessho et al., 2007; Keyak et al., 2007; Lenaerts et al., 2009; Orwoll et al., 2009; Tanck et al., 2009). In contrast to the currently available clinical methods, these models account for the individual bone strength and allow for the application of specific loading patterns, which has considerably improved the accuracy of the femoral fracture risk prediction as compared to predictions by clinical experts (Tanck et al., 2009).

Previous non-linear finite element models adopted post-yield material behaviour, using the Von Mises yield criterion (VMYC) (Keyak, 2001; Keyak et al., 2005b; Tanck et al., 2009). This yield criterion assumes that the ultimate bone strength under tension equals the ultimate strength under compression. However, it is commonly known from studies on bone material that compressive yield strength ($\sigma_{y,c}$) is higher than the tensile yield strength ($\sigma_{y,t}$) (Keaveny

et al., 1994; Kopperdahl et al., 1998; Morgan et al., 2001; Kaneko et al., 2003; Bayraktar et al., 2004b). Asymmetric yielding can be captured by using the pressure dependent Drucker-Prager yield criterion (DPYC), as already utilised in bone specimens on the micro scale level (Mullins et al., 2009).

To our knowledge, asymmetric yielding using the DPYC has been applied in a few macro scale femur FE studies before (Bessho et al., 2007; Bessho et al., 2009), in which the parameters defining the DPYC were based on limited experimental data. For example, an ultimate yield stress ratio of 80% was implemented, as found in one study on trabecular bone (Keaveny et al., 1994) and one on cortical bone (Kaneko et al., 2003). However, the literature shows very variable data in terms of the degree of yield asymmetry. Ratios of tensile to compressive yield stress range from 54% (Kaneko et al., 2003) to 91% (Kopperdahl et al., 1998). Hence, implementing yield asymmetry to predict the fracture risk of metastatic bones requires a sensitivity analysis of the FE predictions to these variable degrees of asymmetrical failure.

Therefore, the aim of the study presented in this paper was twofold. First, it was verified that asymmetric yielding in bone could be captured by the DPYC and can provide better results than the commonly used VMYC. Second, a sensitivity analysis was performed, in which we focused on variations in the parameters defining asymmetric yielding, based on ranges reported in literature, and the subsequent effect on bone failure, in terms of failure force and failure location. On the basis of these results, we defined the best parameter settings for using the DPYC in the prediction of the femoral bone strength by case-specific non-linear finite element models.

Methods

Mechanical experiments

Two pairs and two single fresh-frozen cadaveric human femora (age 63 to 81; 2 women, 2 men; institutional approval obtained) were cleaned from soft tissue. The two single femora were kept intact. In the paired femora, one was kept intact, whereas in the other femur artificial metastatic lesions were created by drilling holes through the cortex of the femora. The location and size of these lesions were discussed with experienced physicians in order to resemble clinical appearance of bone metastases in cancer patients. In one bone, we created a 40 mm lesion in the medial shaft of the femur, whereas in the other femur we drilled two 30 mm holes in the anterior shaft, located at the level of the lesser trochanter, and in the distal shaft of the femur, respectively.

All femora were mechanically loaded to failure. For a detailed description of the setup of the mechanical experiments, the reader is referred to Tanck et al. (2009). All femora were

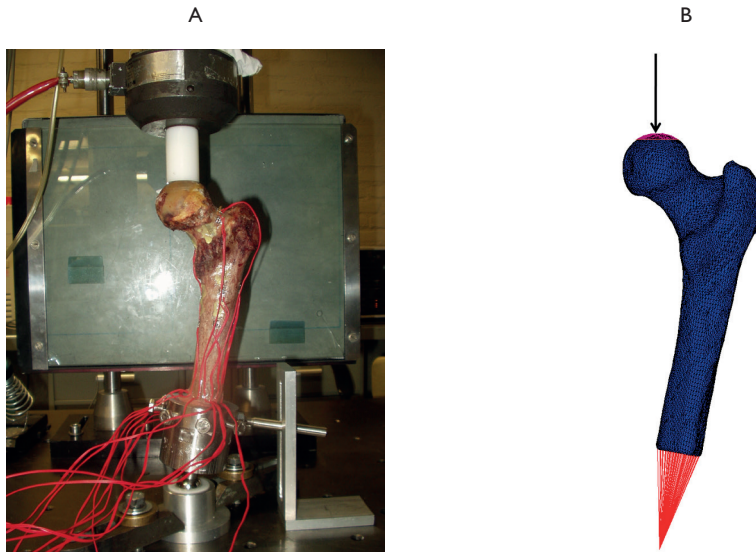


Figure 1. The methodological setup in this study. A) In the mechanical experiments, the femora were placed in a hydraulic MTS machine and loaded until failure. Movement of the femur was restricted to rotation around the dorsoventral axis by means of a distal bearing ball and a sliding hinge. B) The FE model exactly mimicked the boundary conditions of the experimental setup.

embedded in polymethylmethacrylate bone cement (PMMA) for adequate fixation in the experimental setup. The FE models were exactly aligned with the experimental setup, in order to identically apply the load in the two setups. For that purpose, a Roentgen Stereophotogrammetric Analysis (RSA) was performed. All femora were equipped with 24 tantalum RSA pellets. Subsequently, imaging data were collected. First, quantitative CT (QCT) images were acquired (ACQSim/Brilliance Big Bore, Philips, Eindhoven, The Netherlands). The following settings were used: 120 kVp, 220 mAs, slice thickness 3 mm, pitch 1.5, spiral and standard reconstruction, in-plane resolution 0.9375 mm. As the ultimate goal of this study is to enable true case-specific bone strength predictions in patients suffering bone metastases, we used a rather coarse resolution for the QCT-scans, common to current clinical practice in radiotherapeutic departments. The specimens were scanned in a water basin which was positioned atop a solid calibration phantom containing tubes with 0, 50, 100, and 200 mg/ml calcium hydroxyapatite (Image Analysis, Columbia, KY, USA). Hounsfield Units (HUs) found in the tubes of the calibration phantom were related to their known calcium equivalent values (ρ_{QCT}). On the basis of these relations, grey values in the CT scans were converted to calcium equivalent densities. Second, for the purpose of RSA analysis, a stereo X-ray was taken from the femora while positioned in their experimental setup (Figure 1A). Movement

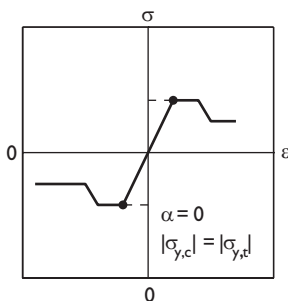
of the femora was restricted to rotation around the dorsoventral axis by using a distal bearing ball and a sliding hinge. A single-limb stance-type loading pattern was applied by means of a hydraulic MTS machine, using a plastic cup (\varnothing 30 mm, polyoxymethylene, Delrin®). The femora were loaded from 0 N until failure, with a load rate of 10 N/s. During the experiments failure forces and displacements were recorded.

FE model

The QCT images served as a basis for the geometrical and mechanical properties of the FE model. By segmenting the CT images (Mimics 11.0, Materialise, Leuven, Belgium) the 3D surface geometry of the model was retrieved, which in turn was converted into a solid mesh (Patran 2005 r2, MSC Software Corporation, Santa Ana, CA, USA) using four-noded tetrahedral elements (mean edge length \sim 2 mm). Using the phantom's calibration data, HUs in the CT scan were automatically converted to ρ_{QCT} values using the Dicom Toolkit software package, developed in-house. Subsequently, these element specific ρ_{QCT} values were converted into ash densities (ρ_{ash}) and bone material properties, respectively (Keyak et al., 2005b). Next, a non-linear isotropic post yield material behaviour was adopted, according to Keyak et al. (2005b).

The orientation of the model was based on the RSA analysis. The RSA pellet positions in the FE model, retrieved from the CT scans, were projected onto the positions of the RSA pellets in the X-rays. The resulting transformation matrix was applied to the FE model. In this way,

Von Mises Yield Criterion (VMYC)



Drucker-Prager Yield Criterion (DPYC)

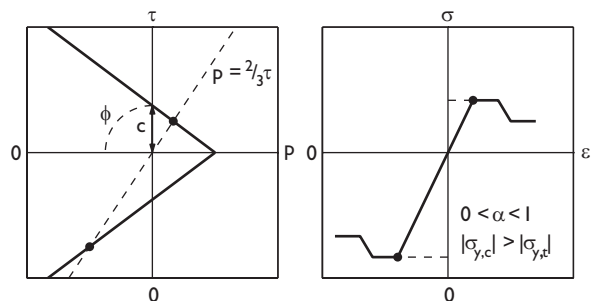


Figure 2. Schematic overview of post yield material behaviour. A) The Von Mises yield criterion, using post yield material behaviour according to Keyak et al. (2005b). This criterion assumes equal bone strength under tension and compression. B) A 2D representation of the Drucker-Prager yield envelope. The intersection points of the yield envelope and the dashed line indicate the yield points in uniaxial tension (upper right) and uniaxial compression (lower left). The yield points in this figure correspond to the yield points in the right panel. C) The Drucker-Prager yield criterion, which accounts for yield asymmetry, i.e. the absolute value of the tensile yield stress is smaller than the compressive yield stress.

the FE model was oriented exactly in the experimental position. The distal PMMA fixation and the distal ball bearing in the experiments were simulated by means of two bundles of high stiffness springs, only allowing rotation around the dorsoventral axis. Application of the single-limb stance-type loading pattern mimicked the experimental setup; a displacement driven load (0.1 mm per increment) was applied via a cup (\varnothing 30 mm) on the head of the femur (Figure 1B). Post yield material behaviour was not implemented in the surface elements underneath this cup in order to prevent distortion artefacts as a result of the load application. FE simulations were performed using MSC software (MSC.MARC2007r1, MSC Software Corporation, Santa Ana, CA, USA). The total reaction force in the loading direction was calculated; the maximum value of this force defined failure of the FE model. Displacements were calculated in a reference node on the femoral head, underneath the centre of the loading cup. The fracture location and fracture surface in the FE models were determined by elements that had undergone plasticity; i.e. elements that had passed the softening phase in the post yield material behaviour.

Sensitivity analysis on the parameters defining the Drucker-Prager yield criterion

In previous FE studies that were related to the prediction of the femoral bone strength, the VMYC was applied (Keyak, 2001; Keyak et al., 2005b; Tanck et al., 2009), assuming equal bone strength under tension and compression (Figure 2, left section). In this study, we first implemented the post yield material behaviour using the VMYC and used these predictions as a reference. Secondly, we adopted asymmetric yield behaviour using the DPYC (Figure 2, right sections) and performed a sensitivity analysis on the parameters defining the DPYC. In Figure 2, middle section) a 2-dimensional graphical representation of the DP yield envelope is presented. The horizontal axis represents the hydrostatic pressure axis, for which it holds:

$$p = \frac{1}{3}(\sigma_1 + \sigma_2 + \sigma_3) \quad (1)$$

with p = pressure, and $\sigma_1, \sigma_2, \sigma_3$ as the stresses in principal direction. Under uniaxial stress in the σ_1 direction at yielding, this formula reduces to:

$$p = \frac{1}{3}\sigma_{yield} \quad (2)$$

The vertical axis represents the shear stress axis, for which the following applies:

$$\tau_{max} = \frac{1}{2}\sigma_{yield} \quad (3)$$

with τ_{max} = maximum shear stress. Combining the relationships defined in (2) and (3), we can derive the following relationship between p and τ :

$$p = \frac{2}{3}\tau \quad (4)$$

This relationship is depicted by the dashed line in Figure 2 (middle panel). The two points of intersection of the DP yield surface with the dashed line correspond to the yield points in compressive and tensile direction in the one-dimensional stress-strain curve (Figure 2, right panel), when the specimen is loaded in one of the principal directions. Thus, the shape of the DP yield surface directly relates to the degree of asymmetry and is defined by the friction angle φ and the cohesion factor c (Figure 2, middle section):

$$\sin(\varphi) = \frac{3\alpha}{\sqrt{(1 - 3\alpha^2)}} \quad (5)$$

$$c = \frac{\sigma}{\sqrt{3(1 - 12\alpha^2)}} \quad (6)$$

with σ as the tensile yield stress and α representing the degree of asymmetry in tensile and compressive yield strength:

$$\alpha = (\sigma_{y,c} - \sigma_{y,t}) / [(\sigma_{y,c} + \sigma_{y,t}) * \sqrt{3}] \quad (7)$$

with $\sigma_{y,c}$ as the compressive yield stress and $\sigma_{y,t}$ as the tensile yield stress. From these equations and Figure 2 it should be clear that the position of the cone along the hydrostatic pressure axis depends on both α and the yield stress (σ), whereas the width of the cone is only determined by α . A larger difference in tensile and compressive bone strength results in a larger value of α , which in turn leads to an increase in c and φ , and thus in a wider yield envelope.

In this study, the sensitivity analysis on α was based on results from experiments and experimentally calibrated FE modelling as reported in literature (Table 1). The specimens used in these studies were rather diverse in terms of the species and the anatomic site they originated from. In order to diminish an eventual effect of these inconsistencies, we used data from experiments with human trabecular bone only. From these data a minimum, an average and a

Table 1. Literature overview of yield asymmetries.

	Bayraktar 2004	Keaveny 1994	Kopperdahl 1998	Morgan 2001	Kaneko 2003
Type of bone	trabecular	trabecular	trabecular	trabecular	cortical
Origin of specimens	human	bovine	human	human	human
Anatomic site	femur	tibia	vertebrae	femur	femur
Tensile yield stress (MPa)	82.80	15.60	1.75	10.93	83.90
Compressive yield stress (MPa)	133.60	21.30	1.92	17.45	153.00
Degree of asymmetry (α)	0.135	0.089	0.027	0.133	0.168

maximum value of α were calculated, i.e. $\alpha = 0.027, 0.082$ and 0.135 . The stress- strain curves for the three different values of α are given in Figure 3 (bottom section). Note that for these cases the choice was made to keep the compressive yield stress equal in all three graphs.

Previously, the VMYC was used to describe the post yield material behaviour of bone (Keyak et al., 2005b). On the basis of compressive yield stress found in experiments, the VM yield stress (VM σ_y) was calculated per element using:

$$\sigma_y = 102 * \rho_{ash}^{1.8} \quad (8)$$

We based the sensitivity analysis on yield stress on these fitted VM results. For the implementation of this post yield material behaviour with the DPYC we first let the MARC-FE package calculate the yield stresses in tension and compression with its default settings, resulting in a more negative compressive yield stress (DP $\sigma_{y,c}$) and a less positive tensile yield stress (DP $\sigma_{y,t}$) as compared to the VM simulations and experimental results. This case was defined as DEFAULT (Figure 3, upper section). Next, the DP $\sigma_{y,c}$ was equated to the VM σ_y , resulting in a less positive DP $\sigma_{y,t}$ as compared to the VM σ_y . This case was defined as the compression-equated case (COMP_EQ) (Figure 3). Although the VM σ_y was validated against compressive experiments, the calculated yield stress was applied in both tension and compression, since the VMYC assumes symmetric yielding. Hence, in the second variation, DP $\sigma_{y,t}$ was fitted to VM σ_y , resulting in a more negative DP $\sigma_{y,c}$ as compared to the VM simulations. We defined this condition as the tension-equated case (TENS_EQ) (Figure 3).

Data analyses

The effects of implementing variable yield asymmetries on bone failure were evaluated in terms of fracture location and failure forces. The fracture locations predicted by the FE model at the moment of failure were qualitatively compared to the fracture locations in the experiments.

The accuracy of the FE strength predictions was evaluated by determining the correlation and the linear regression equations between the actual experimental bone strength and the bone strength predicted by the FE model. More specifically, using SPSS (SPSS 16.02, SPSS Inc., Chicago, IL, USA), the coefficient of determination (R^2), the regression coefficient and intercept were calculated. In addition, we compared the mean, minimum and maximum relative differences between the experimental failure force and the failure forces predicted by the FE models for every parameter setting. The FE model adopting the VMYC served as a reference. The results of the sensitivity analysis of the two DP parameters were compared to this VM simulation in a descriptive manner.

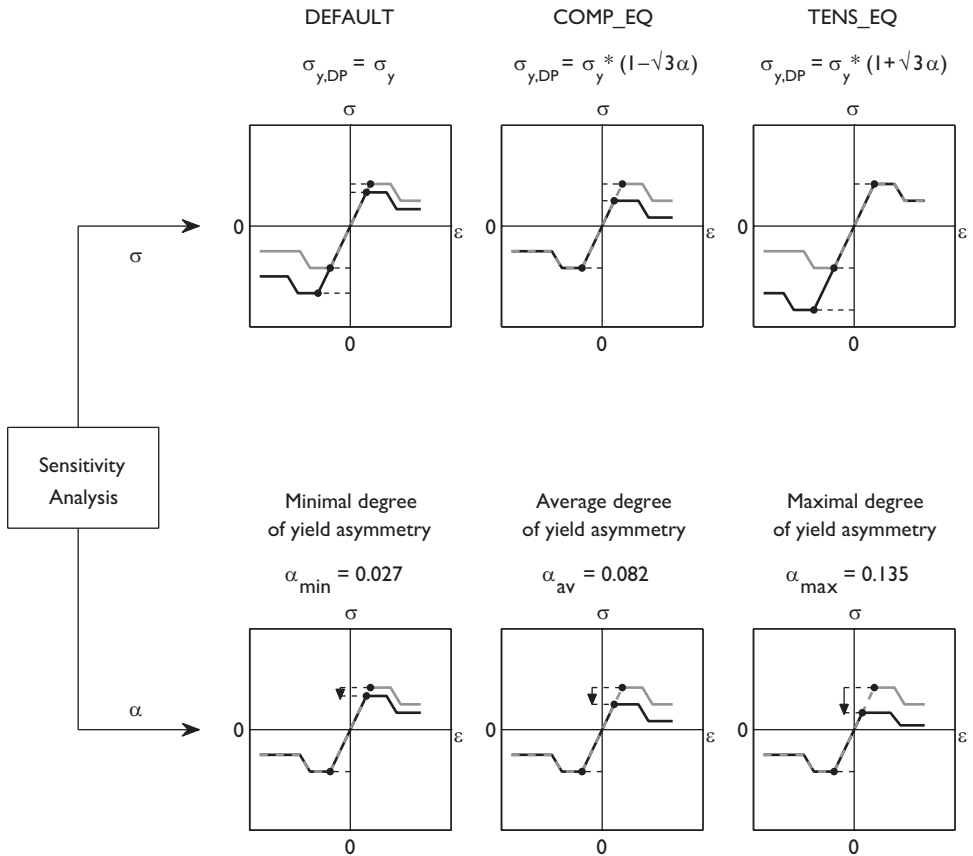


Figure 3. Overview of the different parameter settings in the sensitivity analysis on post-yield material behaviour, implemented using the DPYC. For the variations in fitting the yield stress (upper panels), the DP yield stress was not equated to the Von Mises yield stress (DEFAULT), equated to the Von Mises yield stress in compression (COMP_EQ), or in tension (TENS_EQ). For the variations in the degree of yield asymmetry (lower panels), the minimal and maximal values of α were based on yield asymmetry data reported in literature (Kopperdahl et al., 1998; Bayraktar et al., 2004b), and the average value was calculated as the mean of these two values.

Results

Fracture location

In the four bones without artificial metastases, the prediction of the fracture location improved by the implementation of the DPYC. For example, in Figure 4, the fracture location in one of the experiments, the VM simulation and the DP simulation (with a maximal α and the yield stress equated in compression, COMP_EQ) are shown. For two of the intact bones, a considerable improvement in the prediction of the fracture line was seen, whereas in the remaining two bones a more subtle effect of the use of yield asymmetry was found. In the experiments, intertrochanteric and transcortical fractures were seen. This pattern was reasonably reproduced when the DPYC was used but was not reproduced in the VM simulations. More specifically, the VM simulations mainly predicted subcapital fractures, whereas the implementation of the DPYC resulted in a fracture that was located more towards the greater and lesser trochanter. It was found that a larger degree of yield asymmetry, i.e. higher values of α , better predicted the fracture line. Variations in the yield stress did not have an effect on the location of the fracture line.

In the bones with artificial metastases, the VM simulations correctly predicted the fracture locations through the lesions. The same fracture location was found when using the DP yield criterion.

Failure force

The implementation of the DPYC improved the prediction of the ultimate bone strength. Due to the small number of specimens in this study, no significant differences were found between the different parameter settings in this study. However, we found a number of inte-

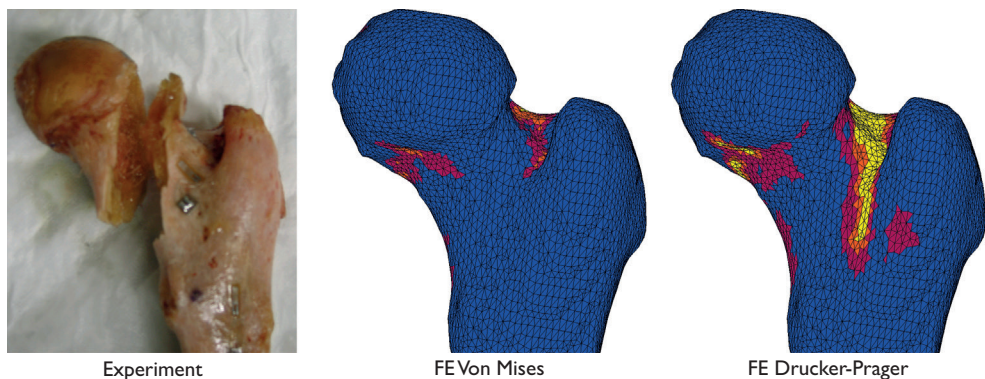


Figure 4. Location of fracture in the experiment, FE simulation using the VMYC and FE simulation using the DPYC. The fracture location was better predicted in the DP simulation than in the VM simulation.

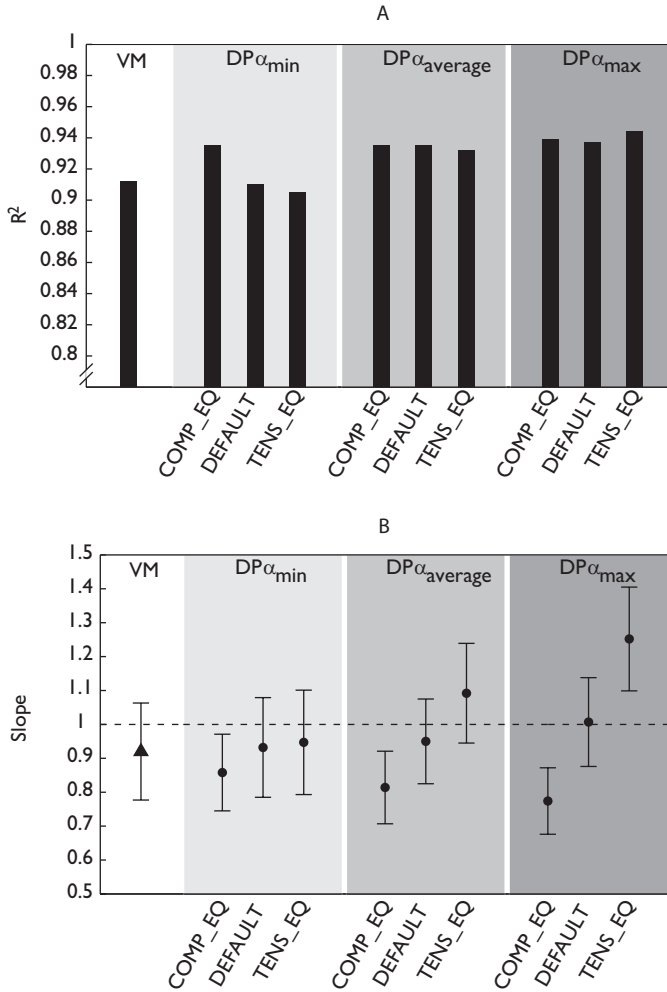


Figure 5. The accuracy of the FE strength predictions. We compared the bone strength predicted by the FE model to the actual experimental bone strength in terms of the correlation (A), and the slopes (with 95% confidence intervals) of the linear regression equations (B).

resting trends in this study. The predictions by the FE models using the VMYC were already fairly good ($R^2 = 0.91$, slope = 0.92, intercept = -629), but the correlations between the actual and predicted failure forces in the DPYC simulations were higher (R^2 values ranged from 0.91 to 0.94) (Figure 5A). The variations in the yield stress had a large effect on the predicted failure force. The DEFAULT simulations best approached the actual failure forces with high correlations ($0.91 < R^2 < 0.94$) and slopes that were close to 1 ($0.93 < \text{slope} < 1.01$) (Figure 5). Equating the DP compressive yield stress to the VM yield stress (COMP_EQ) resulted in

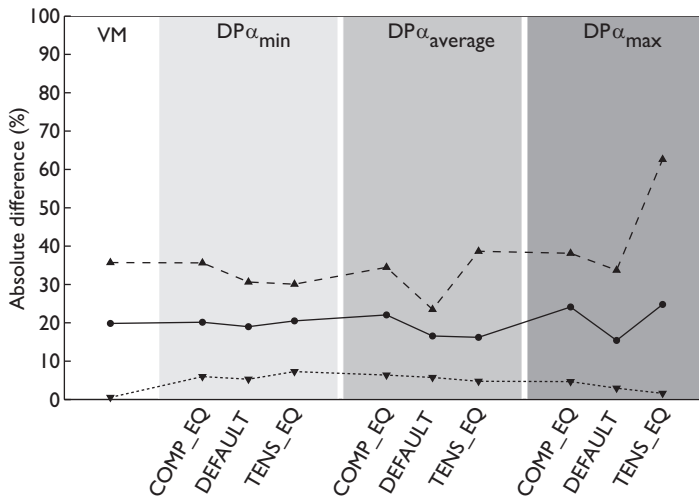


Figure 6. The mean (black circles), minimum (triangles, dotted) and maximum (triangles, dashed) absolute differences (in %) between the experimental failure force and the failure forces predicted by the FE models for every parameter setting.

high correlations as well ($R^2 = 0.94$ in all three settings of α) and slopes ranging between 0.77 and 0.86 (Figure 5). In the same vein, fitting the DP tensile yield stress to the VM yield stress (TENS_EQ) showed R^2 in between 0.91 and 0.94, whereas the slopes ranged between 0.95 and 1.25 (Figure 5). The intercepts of the regression equations ranged from -459 to -116, but were never significantly different from 0.

The mean, minimum and maximum absolute differences (in %) between the predicted and experimental failure forces are depicted in Figure 6. The simulations with a DEFAULT yield stress condition showed the lowest absolute differences compared to the experiments. From these results, and the finding that a larger degree of yield asymmetry improves the prediction of fracture locations, the best settings to implement asymmetric yielding in the FE prediction of the femoral bone strength were defined as a maximal degree of asymmetry and a default yield stress (i.e. no fit to the VM yield stresses under either compression or tension).

Furthermore, the combined variations in both α and yield stress had a synergetic effect on the failure forces. For example, the effect of variations in the yield stresses was larger when implemented with a larger degree of asymmetry (Figure 7).

In addition, we found that the effect of the sensitivity analysis was dependent on the ultimate strength of the bone (Figure 8). In the weakest bone, the range of predicted failure forces was 1000 N, whereas in the strongest bone this range increased to almost 5000 N, which in both cases approximated 50% of the failure force.

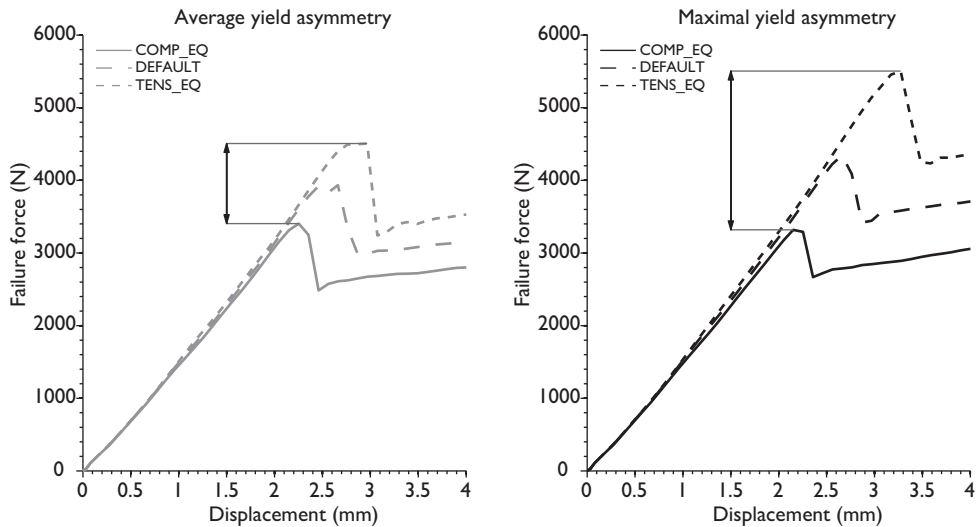


Figure 7. Force-displacement curves for combinations of variations in the yield asymmetry and the yield stress, which had a synergetic effect on the predicted failure forces.

Discussion

The aim of this study was to verify that asymmetric yielding in bone can be captured by the DPYC and can provide better results than the commonly used VMYC. In addition, we performed a sensitivity analysis on the parameters defining asymmetric yielding. We studied the subsequent effect on bone failure, in terms of failure force and failure location, and defined the best possible settings for using the DPYC in the prediction of the femoral bone strength by case-specific non-linear finite element models.

Although the highest correlations between predicted and actual failure forces were found when using the DPYC, all FE models in this study were able to adequately predict the femoral bone strength. FE predictions of the failure force related to the experimental failure force with coefficients of determination ranging between 0.91 and 0.94. These results are in line with previously reported work (R^2 values ranging between 0.83 (Keyak et al., 2005b) and 0.96 (Bessho et al., 2009)).

The variation in the degree of yield asymmetry mainly affected the fracture location, whereas variations in yield stress had a marked effect on the failure force. In the femora without metastatic lesions, fracture locations were better predicted by models using a large yield asymmetry. These results may be explained as follows. In studies based on experiments with human bone, it was shown that compressive bone strength is higher than the tensile strength (Keaveny et al., 1994; Kopperdahl et al., 1998; Morgan et al., 2001; Kaneko et al., 2003; Bayraktar et al., 2004b), thus the use of a symmetric yield criterion such as the VMYC would

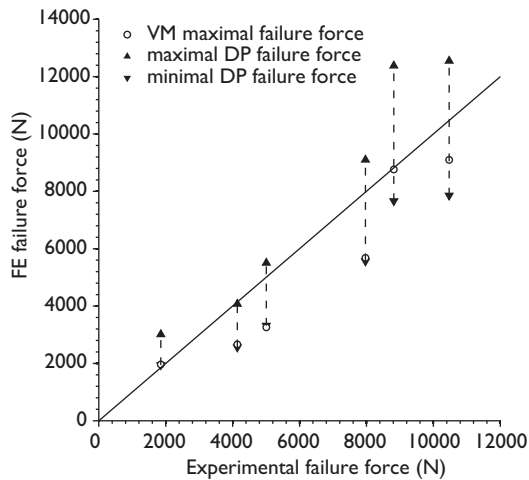


Figure 8. The sensitivity to the various parameter settings of the asymmetric yield criterion is dependent on the global bone strength. For every femur, the largest and smallest failure forces predicted by models using the DPYC are depicted, as well as the predictions by the models using the VMYC. In the weakest bone, the range of predicted failure forces was 1000 N, whereas in the strongest bone this range increased to almost 5000 N, which in both cases approximated 50% of the failure force.

consequently either overestimate the tensile bone strength or underestimate the compressive bone strength. In either case, the failure prediction by an FE model using the VMYC will be biased towards failure under compression. Under single-limb stance-type loading, as utilised in this study, the proximal-lateral femoral neck is assumed to be mainly loaded in tension, whereas the distal-medial part is mainly loaded in compression. Using a symmetric yield criterion would therefore lead to fractures that initiate in the distal-medial parts of the femoral neck, as predicted in the VM simulations. The use of an asymmetric yield criterion can account for this bias towards failure under compression. Indeed, when using the DPYC, the FE model predicted more failure in elements that were loaded under tension, and the resulting fracture locations were more in line with the experimental fracture locations. In the femora with artificial lesions, we found virtually no differences in fracture location predicted in VM simulations and DP simulations. The artificial lesions were located in the medial and anterior femoral shaft. Under single-limb stance-type loading, these areas are loaded primarily under compression, so that the effect of implementing yield asymmetry is reduced. In addition, by drilling holes that mimicked artificial metastases, the femoral cortex was interrupted. As a result, the large forces directed along the shaft of the femur had to be redirected through much weaker, trabecular bone. Consequently, extensive failure in the elements surrounding the artificial lesion was found. This effect might have overruled the more subtle effect of the implemented yield asymmetry. In order to verify this hypothesis, more femora with artificial

lesions in other locations (e.g. the lateral shaft or the femoral neck) should be tested.

The variations in the yield stress had a large effect on the failure forces predicted by the FE models. On the basis of the current set of specimens the best possible failure force prediction was obtained when using a yield stress not fitted to the VM yield stresses in tension nor compression (DEFAULT), in combination with the largest degree of yield asymmetry.

The combined variations in the degree of yield asymmetry and yield stress had a synergetic effect on the failure force. On the element level, the variations in yield stress gradually lead to an increase in the cohesion factor, in which $COMP_EQ < DEFAULT < TENS_EQ$. Furthermore, a larger degree of yield asymmetry (a larger value of α) increases both the friction angle (φ) and the cohesion factor (c) on the element level. A larger friction angle and cohesion factor result in a wider yield envelope and thus in a larger effect of the hydrostatic pressure on the yield stress. Thus, the increase in predicted bone strength as a result of variations in the degree of asymmetry and yield stress is depending on the 3D stress distribution, which implies that the effect on the global bone strength is sometimes difficult to comprehend.

In addition, on the global level, the effect of variable DP parameters was dependent on the ultimate bone strength. Variations in α and yield stress affect the ratio between the tensile and compressive yield strength. Therefore, absolute difference between tensile and compressive yield strength is larger in FE models with stronger elements. Again, this effect on the bone strength is dependent on the 3D stress distribution, such that the effect on the global strength is not so straightforward.

The results in this study are in line with previous studies investigating the implementation of asymmetric yielding on the micro level. Mullins et al. (2009) showed that micro level FE models implementing the DPYC better predicted bone failure parameters retrieved by nanoindentation than FE models using the VMYC. Furthermore, Keaveny and co-workers developed validated micromechanical FE models using an asymmetric yield criterion (Niebur et al., 2000; Bayraktar et al., 2004b) or a multiaxial yield surface (Bayraktar et al., 2004a), with which they were better able to capture experimentally measured yield behaviour of both human and bovine bone. In contrast, Keyak et al. (2000) performed a sensitivity analysis on global femoral FE models using various yield criteria. Their results showed that the implementation of complex yield behaviour (e.g. asymmetric yielding) worsened the prediction as compared to the use of symmetric, more simple yield criteria. However, they did not consider the implementation of the Drucker-Prager yield criterion which, as this study shows, has the capacity to improve the predictions relative to experimental measurements.

A few limitations of this study should be considered. First, it should be noted that we only used 4 intact femora and 2 femora with metastatic lesions, which is from a statistical point of

view a small population. With this number of specimens there is a lack of statistical power to qualify the one parameter setting above and beyond another one, i.e. no statistically significant differences were found between the various parameter settings. However, as a result of the three variations in α , three variations in the yield stress and one VM simulation, we ran 60 non-linear simulations in total. In order to confine calculation time, we used a limited number of specimens. In future work the best possible parameters found in this study will be applied to, and validated in, a larger population. Furthermore, we congregated the failure data of intact and metastatic femora. Since the failure process of those two groups is fairly different, this might affect the homogeneity of the sample and therefore the interpretation of the results. However, in a previous study of our group (Tanck et al., 2009) we found that the accuracy of the predictions by the FE model further increased when separately considering the results in the two groups. Obviously, analyses on large numbers of intact and metastatic femora are needed to confirm these results.

Second, in the intact femora, the predicted fracture locations did not perfectly overlay on the fracture locations as found in the experiments. The FE models predicted the fracture locations more towards the subcapital region, whereas the experimental fractures were located more in between the greater and lesser trochanter. This may be due to the fact that mechanical anisotropy was not implemented in this model. It has been shown that a significant part of the variation in bone strength is explained by the variable trabecular orientation of the bone (Lenaerts et al., 2009). According to Wolff's law, trabeculae in the femoral head and neck orient towards the physiological loading direction. More specifically, two different trabecular patterns can be distinguished, (i.e. a compressive band and a tensile band), which traverse in the centre of the femoral head (Kyle et al., 1995). The trabeculae in these bands are stronger when loaded in the preferential direction. Thus, by implementing anisotropy, elements in the subcapital region become more resistant to single-limb stance-type loading, being a daily physiological loading condition. Consequently, elements located more towards the greater trochanter might fail earlier, and the fracture location might be further improved. However, it is very difficult to retrieve local anisotropy parameters *in vivo* (Lenaerts et al., 2009), but taking into account these trabecular bands maybe a first step towards implementation of anisotropy in the FE models. Finally, we used a single-limb stance-type loading pattern, allowing us to exactly mimic the experiments. However, with this loading type, we could not cover complex loading conditions in daily activities. Although FE models incorporating this simple loading configuration have shown to be successful, more sophisticated loading patterns might further improve the accuracy of the FE predictions. Therefore, future work will focus on the application of muscle forces and hip joint contact forces determined by musculoskeletal models in order to apply

such complex loading configurations to the FE model.

In conclusion, in this study we further developed our subject specific non-linear finite element model. By implementing a large degree of yield asymmetry using the DPYC, we showed an improvement in the prediction of bone strength as well as in the prediction of the fracture location.

Acknowledgments

This project has been funded by the Dutch Science Foundation NWO-STW (NPG.06778), the Furlong Research Charitable Foundation and Stichting Anna Fonds.

References

- Bayraktar HH, Gupta A, Kwon RY, Papadopoulos P, Keaveny TM. 2004a. The modified super-ellipsoid yield criterion for human trabecular bone. *J Biomech Eng* 126(6): 677-684.
- Bayraktar HH, Morgan EF, Niebur GL, Morris GE, Wong EK, Keaveny TM. 2004b. Comparison of the elastic and yield properties of human femoral trabecular and cortical bone tissue. *J Biomech* 37(1): 27-35.
- Bessho M, Ohnishi I, Matsumoto T, Ohashi S, Matsuyama J, Tobita K, Kaneko M, Nakamura K. 2009. Prediction of proximal femur strength using a CT-based nonlinear finite element method: Differences in predicted fracture load and site with changing load and boundary conditions. *Bone* 45(2): 226-231.
- Bessho M, Ohnishi I, Matsuyama J, Matsumoto T, Imai K, Nakamura K. 2007. Prediction of strength and strain of the proximal femur by a CT-based finite element method. *J Biomech* 40(8): 1745-1753.
- Body JJ. 2003. Rationale for the use of bisphosphonates in osteoblastic and osteolytic bone lesions. *Breast* 12: S37-S44.
- Harvey HA. 1997. Issues concerning the role of chemotherapy and hormonal therapy of bone metastases from breast carcinoma. *Cancer* 80(8 Suppl): 1646-1651.
- Hipp JA, Springfield DS, Hayes WC. 1995. Predicting pathologic fracture risk in the management of metastatic bone defects. *Clin Orthop Relat Res* 312: 120-135.
- Hoskin PJ. 2003. Bisphosphonates and radiation therapy for palliation of metastatic bone disease. *Cancer Treat Rev* 29(4): 321-327.
- Kaneko TS, Pejčić MR, Tehranzadeh J, Keyak JH. 2003. Relationships between material properties and CT scan data of cortical bone with and without metastatic lesions. *Med Eng Phys* 25(6): 445-454.
- Keaveny TM, Wachtel EF, Ford CM, Hayes WC. 1994. Differences between the Tensile and Compressive Strengths of Bovine Tibial Trabecular Bone Depend on Modulus. *J Biomech* 27(9): 1137-1146.
- Keyak JH. 2001. Improved prediction of proximal femoral fracture load using nonlinear finite element models. *Med Eng Phys* 23(3): 165-173.
- Keyak JH, Kaneko TS, Rossi SA, Pejčić MR, Tehranzadeh J, Skinner HB. 2005a. Predicting the strength of femoral shafts with and without metastatic lesions. *Clin Orthop Relat Res* 439: 161-170.
- Keyak JH, Kaneko TS, Skinner HB, Hoang BH. 2007. The effect of simulated metastatic lytic lesions on proximal femoral strength. *Clin Orthop Relat Res* 459: 139-145.
- Keyak JH, Kaneko TS, Tehranzadeh J, Skinner HB. 2005b. Predicting proximal femoral strength using structural engineering models. *Clin Orthop Relat Res* 437: 219-228.
- Keyak JH, Rossi SA. 2000. Prediction of femoral fracture load using finite element models: an examination of stress- and strain-based failure theories. *J Biomech* 33(2): 209-214.
- Kopperdahl DL, Keaveny TM. 1998. Yield strain behavior of trabecular bone. *J Biomech* 31(7): 601-608.
- Kyle RF, Cabanela ME, Russell TA, Swiontkowski MF, Winquist RA, Zuckerman JD, Schmidt AH, Koval KJ. 1995.

Fractures of the proximal part of the femur. Instr Course Lect 44: 227-253.

- Lenaerts L, van Lenthe GH. 2009. Multi-level patient-specific modelling of the proximal femur. A promising tool to quantify the effect of osteoporosis treatment. *Philos Trans A Math Phys Eng Sci* 367(1895): 2079-2093.
- Mirels H. 1989. Metastatic disease in long bones. A proposed scoring system for diagnosing impending pathologic fractures. *Clin Orthop Relat Res* 249: 256-264.
- Morgan EF, Keaveny TM. 2001. Dependence of yield strain of human trabecular bone on anatomic site. *J Biomech* 34(5): 569-577.
- Mullins LP, Bruzzi MS, McHugh PE. 2009. Calibration of a constitutive model for the post-yield behaviour of cortical bone. *J Mech Behav Biomed Mater* 2(5): 460-470.
- Niebur GL, Feldstein MJ, Yuen JC, Chen TJ, Keaveny TM. 2000. High-resolution finite element models with tissue strength asymmetry accurately predict failure of trabecular bone. *J Biomech* 33(12): 1575-1583.
- Orwoll ES, Marshall LM, Nielson CM, Cummings SR, Lapidus J, Cauley JA, Ensrud K, Lane N, Hoffmann PR, Koppe-dahl DL, Keaveny TM, Osteoporotic Fractures in Men Study G. 2009. Finite element analysis of the proximal femur and hip fracture risk in older men. *J Bone Miner Res* 24(3): 475-483.
- Tanck E, van Aken JB, van der Linden YM, Schreuder HWB, Binkowski M, Huizenga H, Verdonschot N. 2009. Pathological fracture prediction in patients with metastatic lesions can be improved with quantitative computed tomography based computer models. *Bone* 45(4): 777-783.
- van der Linden YM, Dijkstra PD, Kroon HM, Lok JJ, Noordijk EM, Leer JW, Marijnen CA. 2004. Comparative analysis of risk factors for pathological fracture with femoral metastases. *J Bone Joint Surg Br* 86(4): 566-573.
- van der Linden YM, Kroon HM, Dijkstra SP, Lok JJ, Noordijk EM, Leer JW, Marijnen CA, Dutch Bone Metastasis Study G. 2003. Simple radiographic parameter predicts fracturing in metastatic femoral bone lesions: results from a randomised trial. *Radiother Oncol* 69(1): 21-31.

4

Finite element analysis and CT-based structural rigidity analysis to assess failure load in bones with simulated lytic defects

*Lorenzo Anez-Bustillos, Loes C. Derikx, Nico Verdonschot, Nathan Calderon,
David Zurakowski, Brian D. Snyder, Ara Nazarian, Esther Tanck.
Bone 2014; 58, 160-167.*



Introduction

After lungs and liver, bone tissue constitutes the third most common site for the development of metastases in cancer (Schulman et al., 2007). Carcinomas of the breast, prostate, lungs, and thyroid are the most prone to metastasizing to the skeleton, accounting for approximately 80% of all bone metastases (Hage et al., 2000; Coleman, 2006; Clezardin et al., 2007). Although prognosis after development of metastatic bone disease is better than that seen after visceral invasion, the morbidity associated with these lesions considerably affects patients' quality of life. Main clinical features include intractable pain, metabolic alterations such as hypercalcaemia, neurological deficit in cases of spinal involvement, and spontaneous pathological fracture (Coleman, 2006; Toma et al., 2007). The latter is considered the most important and troublesome complication for both the patient and the physician. Management of these types of fractures accounts for the majority of the calculated national cost burden of patients with metastatic bone disease, estimated to be \$12.6 billion in the United States (Schulman et al., 2007). As survival rates from patients with primary cancer continue to improve, so will the incidence of these major complications (Papagelopoulos et al., 2006).

Primary cancer site, presence of pain, and risk of fracture represent main factors to consider while choosing the most appropriate treatment following the diagnosis of a suspiciously malignant bone lesion (Johnson et al., 2008). Given the detrimental effects of bone fractures, the main challenge for the treating physician is to effectively determine the extent of the lesion, and decide whether it has weakened the bone enough to cause a pathological fracture. Patients with a low risk of pathological fracture are effectively treated for pain using nonsurgical approaches such as radiation therapy, immunotherapy, endocrine or cytotoxic chemotherapy, and bisphosphonates (Houston et al., 1995; Bickels et al., 2009). On the other hand, operative treatment is indicated for cases of impending and pathological fractures in long bone and pelvic girdle metastases. As for patients with spinal lesions, surgical intervention is recommended when evidence of spinal cord compression and/or spinal instability ensues (Bickels et al., 2009).

Although evolving, fracture risk assessment is still based on inaccurate predictors estimated from previous retrospective studies. In 1989, Mirels proposed a weighted scoring system combining clinical and radiographic criteria to quantify the risk of sustaining a pathologic fracture through a metastatic long bone lesion (Mirels, 1989). Although Mirels' score is often used for screening of metastatic appendicular skeletal lesions, it is associated with a variety of limitations. It is based on a 2D radiographic representation of a 3D lesion which is rather imprecise in evaluating the size and nature of the lesions compared to current imaging modalities such as computed tomography and magnetic resonance imaging. Despite the low

false-positive rate for lesions with scores of 9 and above, the low specificity of less than 35% (Damron et al., 2003) means that strict application of these criteria will result in unnecessary surgery in approximately two thirds of cases. A comparative analysis of risk factors conducted by Van der Linden et al. (2004) provided proof of the overestimation of fracture risk when making decisions based on conventional risk factors. As an alternative to existing methods, Van der Linden et al. proposed an approach based on axial cortical involvement, the accuracy of which was further demonstrated in a randomised trial (van der Linden et al., 2003). There are also conflicting data on reproducibility and reliability of the results obtained from different specialties (El-Husseiny et al., 2010) and anatomical sites (Evans et al., 2008), further emphasizing the need for a more accurate clinical tool to assess fracture risk in the presence of metastatic lesions.

We have previously demonstrated the effective use of non-invasive imaging techniques using quantitative computed tomography (QCT) for the assessment of structural rigidity and prediction of failure loads in *ex vivo* and *in vivo* models (Whealan et al., 2000; Hong et al., 2004; Snyder et al., 2006; Nazarian et al., 2010; Entezari et al., 2011). Additionally, using the same principle, we and others have shown that case-specific finite element (FE) models are capable of effectively simulating the mechanical behaviour of bones under axial loading with a relatively high level of precision (Cody et al., 1999; Keyak et al., 2003; Taddei et al., 2006; Bessho et al., 2007; Schileo et al., 2008; Tanck et al., 2009; Derikx et al., 2012b). However, the prediction accuracies of computed tomography rigidity analysis (CTRA) and FE analysis have never been directly compared. In the current study we aim to establish and assess statistical comparisons between QCT structural rigidity analyses and FE analyses, in their accuracy for the estimation of femoral failure load. For that purpose, we use an experimental dataset and the corresponding FE simulations as described previously (Tanck et al., 2009; Derikx et al., 2012a). Based on these experiments, we performed a QCT structural rigidity analysis and compared these results to the results from the FE analyses.

Materials and Methods

Quantitative Computed Tomography and Mechanical Experiments

For the validation of CTRA and FEA we relied on the exact results of mechanical experiments as performed previously (Tanck et al., 2009; Derikx et al., 2012a). For an elaborate description of the setup of these experiments, the reader is referred to this previous work. In short, ten paired femurs from fresh-frozen human cadavers (mean age 81.7 ± 10.65 years) were obtained from the Department of Anatomy, Radboud university medical center, with institutional approval. One of the femurs in each pair was left intact and assigned to the control group.



Figure 1. Anterior view of the FE-model, generated from a QCT scan. Displacement was applied to the model via the cup on the head of the femur, while the bottom of the model was fixated by means of high stiffness springs.

The contralateral femur was assigned to the metastatic group, while one or more defects were created. Size and location of these lesions resembled clinical appearance of lytic metastatic lesions, as discussed with orthopaedic oncologists (Table 3). Hence, they were not related to the femoral size or geometry. QCT images were acquired with the following settings: 120 kVp, 220 mA, slice thickness 3 mm, pitch 1.5, spiral and standard reconstruction, in-plane resolution 0.9375 mm (ACQSim/Brilliance Big Bore, Philips, Eindhoven, The Netherlands). The femurs were scanned in a water basin, on top of a solid calibration phantom (Image Analysis, Columbia, KY, USA). Following imaging, the specimens underwent mechanical testing in a hydraulic mechanical testing system (MTS) machine. An axial load was applied on the head of the femur, with 10 N/s from 0 N until failure, while force and displacement of the plunger were recorded. The failure location of each femur was photographically documented.

Finite Element Analysis

The mesh generation for the FE models was accomplished by segmenting the QCT images and converting them to a solid mesh (Patran 2005 r2, MSC Software Corporation, Santa Ana, CA, USA) (Derikx et al., 2012a). Calibration of the QCT scans and material property assignment was performed using the DICOM Toolkit software package, developed at the Orthopaedic Research Lab in Nijmegen (Derikx et al., 2012a). The experimental boundary conditions were reproduced in the FE simulations (Figure 1). The FE simulations, adopting non-linear isotropic material behaviour (Keyak et al., 2005), were performed using MSC Marc (MSC.

MARC2007r1, MSC Software Corporation, Santa Ana, CA, USA). The global failure load (F_{FE}) was defined as the maximum total reaction force, i.e., the sum of the contact normal forces in the model. The elements that plastically deformed at the moment of maximal total reaction force defined the failure location (Derikx et al., 2012a).

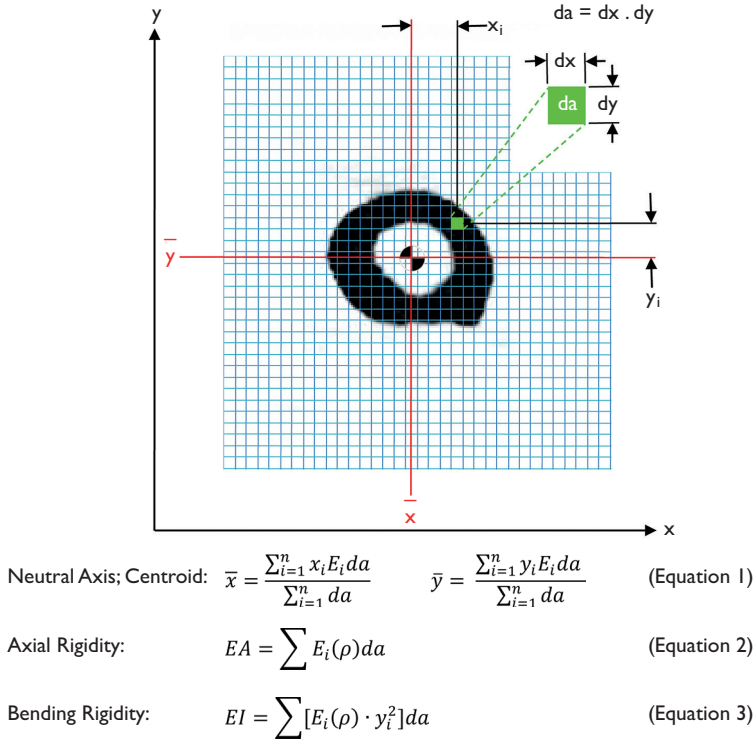


Figure 2. Schematic diagram illustrating the pixel-based CTRA analysis algorithm to calculate axial (EA) and bending (EI) rigidities. Each grid element is intended to represent one pixel (the exaggeration of the grid element size is done solely for illustration purposes). The different equations are presented, where ρ represents bone density, x_i and y_i represent the distance of each pixel from the x and y axes respectively, da represents the area of each pixel, E_i represents Young's modulus of elasticity (defined as the ratio of tensile strength to strain in the linear region), and G_i represents the shear modulus (defined as the ratio of shear stress to shear strain in the linear region).

The modulus neutral axis and centroid (Equation 1) are determined based on the coordinates of the i^{th} pixel, its modulus (E_i), area (da), and total number of pixels in the bone cross-section (n). Axial rigidity, which provides a measure of the bone's resistance to deformation when subjected to uniaxial tensile or compressive loads (Equation 2), is estimated by summing the products of each pixel's elastic modulus (E_i) and pixel area (da). Bending rigidity provides a measure of the bone's resistance to flexure deformation when subjected to bending moments. Its rigidity about the y-axis (Equation 3) is the sum of the products of the elastic modulus (E_i), square of the i^{th} pixel distance to the neutral axis (\bar{y}), and the pixel area (da).

CT-based Structural Rigidity Analysis

For CTRA, the grey values in the CT scan were converted to equivalent mineral density by using the linear relationship between Hounsfield units (HU) and equivalent mineral density as established by the hydroxyapatite phantom scanned with each bone. Then, the mineral density of each pixel was converted to modulus of elasticity (E) for axial (EA) and bending (EI) rigidity measurements, using empirically derived constitutive relationships for cancellous (Rice et al., 1988) and cortical (Snyder et al., 1991) bone (Figure 2). The modulus neutral axis and centroid were calculated based on the coordinates of the i^{th} pixel and its corresponding area (da), modulus (E_i), and total number of pixels in the cross section (n), as depicted in Equation 1.

$$\bar{x} = \frac{\sum_{i=1}^n x_i E_i da}{\sum_{i=1}^n da} \quad \bar{y} = \frac{\sum_{i=1}^n y_i E_i da}{\sum_{i=1}^n da} \quad (1)$$

where x_i and y_i represent the distance of each pixel from the x and y axes, respectively. The Young's modulus of elasticity (E_i) is defined as the ratio of tensile strength to strain in the linear region.

Axial rigidity provides a measure of the bone's resistance to uniaxial (tensile or compressive) loads, whereas bending rigidity provides a measure of the bone's resistance to bending moments. For each trans-axial image, EA and EI were calculated by summing the modulus-weighted area of each pixel within the bone contour by the position of the pixel relative to the centroid of the bone cross-section as described in Equations 2 and 3:

$$EA = \sum E_i(\rho) da \quad (2)$$

$$EI = \sum [E_i(\rho) \cdot y_i^2] da \quad (3)$$

The cross-section through the affected bone that has the lowest rigidity value is the weakest and assumed to govern failure of the entire bone. Therefore, the cross section with the lowest rigidity in the tested area is considered the failure region.

Data Analysis

CTRA-based axial (EA) and bending (EI) rigidities and FE-based failure load results were correlated with the experimental failure load from mechanical testing. Paired t -tests were used to assess the mean difference in failure load (N) determined by mechanical testing (F_{mech})

and CTRA-based EA and FE-based failure load (F_{FE}).

The Bland-Altman technique was applied to assess agreement in CTRA-based axial rigidity and FE-based failure load compared to the gold standard mechanical testing with limits of agreement determined as mean difference ± 1.96 standard deviations (i.e. 95% confidence interval of the difference) (Bland et al., 1986). The Bland-Altman technique is based on plotting the difference between two sets of measurements and plots the difference on the y-axis and the average of the two measurements on the x-axis (this is done for each pair of observations; hence the paired comparison between the two methods). By convention, a line is drawn to represent the mean difference and this is called the “bias”. In addition, two lines are drawn to represent the precision of agreement, called the “limits of agreement” and are calculated as $1.96 \times$ standard deviations of the mean difference (i.e., these are analogous to the 95% confidence interval) and by definition will encompass 95% of the data points.

The correlation between the difference in CTRA-based EA and FE-based failure load with the gold standard failure load was calculated to assess whether the bias was constant across the range of possible loads to failure. Although CTRA does not provide a direct failure load prediction, the output parameters in FE (failure load in N) and CTRA-based EA (axial rigidity in N) are the same and therefore comparable using the Bland-Altman method. In contrast, the output parameters in CTRA-based EI (in Nm^2) are not the same unit-wise and therefore not directly comparable using this particular analysis.

To test the robustness of the two methods in predicting failure load, the size and location of the artificial lesions were varied as much as possible. Obviously, this makes it impossible to study lesion-specific prediction accuracy between the two methods as a large variation in lesion characteristics comes with a small number of specimens per variation. Therefore we studied differences in prediction accuracy between subgroups, i.e. for the intact specimens and the specimens with a defect, in addition to the analyses on total group of specimens.

In addition, the output parameters were used to rank the femurs from weak to strong; this was done for both the outcome parameters of FE and CTRA. These rankings were subsequently compared with the experimental ranking and with each other using the Kendall rank correlation coefficient (τ), which allowed for studying prediction accuracy among the different methods.

The fracture locations in the experiments were qualitatively compared to the fracture lines predicted by the FE model and to the cross-section that was assumed to govern failure of the femur in the CTRA analysis.

Power analysis indicated that 10 femur pairs ($n = 20$) were required (Moore et al., 2003). Statistical analyses were performed using MedCalc version 12.2.1 (MedCalc Software, Mariaker-

ke, Belgium) and STATA (Statistics/Data Analysis 11.2, College Station, TX, USA) software packages. Two-tailed $p < 0.05$ was considered statistically significant.

Results

As reported previously (Derikx et al., 2012a), mechanical testing procedures were successfully completed on every specimen. Overall, the axial and bending rigidities obtained through CTRA correlated well with the load capacity obtained from mechanical testing (Figures 3A and 3B). The coefficients of determination for the femurs were 0.82 for EA and 0.86 for EI ($p < 0.001$ for all cases). As shown in previous work, the simulated FE models accurately predicted the failure load of the intact as well as the metastatic femurs as measured in the experiments ($R^2 = 0.89$ and $p < 0.001$) (Figure 3C).

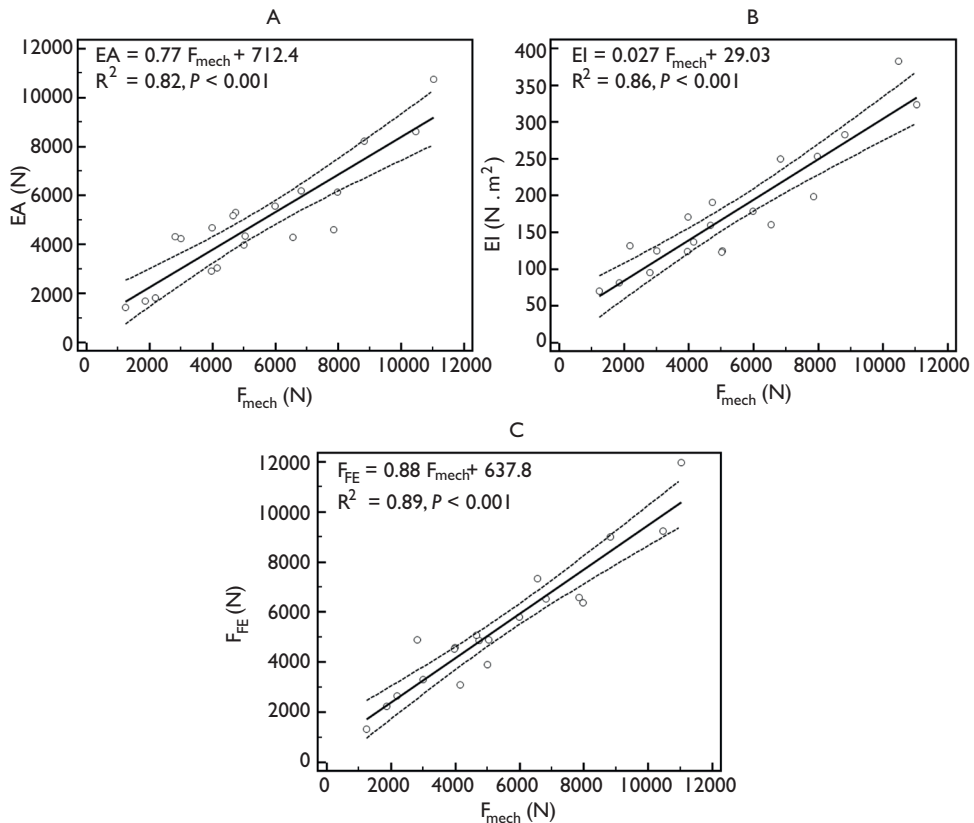


Figure 3. Linear regression between failure load from mechanical testing versus A) axial rigidity and B) bending rigidity and C) failure load predicted by the FE models.

When considering all specimens, paired t-tests did not indicate differences between CTRA-based EA index and mechanical testing with an average underestimation of 534 N for failure load (Table 1, $p = 0.06$). FE demonstrated a mean difference of -9 N compared to mechanical testing, which was not significant ($p = 0.96$). Bland-Altman analysis revealed that the limits of agreement defined as 95% confidence intervals were moderate for CTRA-based EA (Figure 4A). For example, the mean difference of 534 N for EA is associated with a precision between -1779 to 2847 N, implying that 95% of the time, EA will provide an estimate of failure in this range compared to the gold standard. For EA, the bias was constant across the magnitude of failure load as judged by non-significant correlation between the average versus the difference

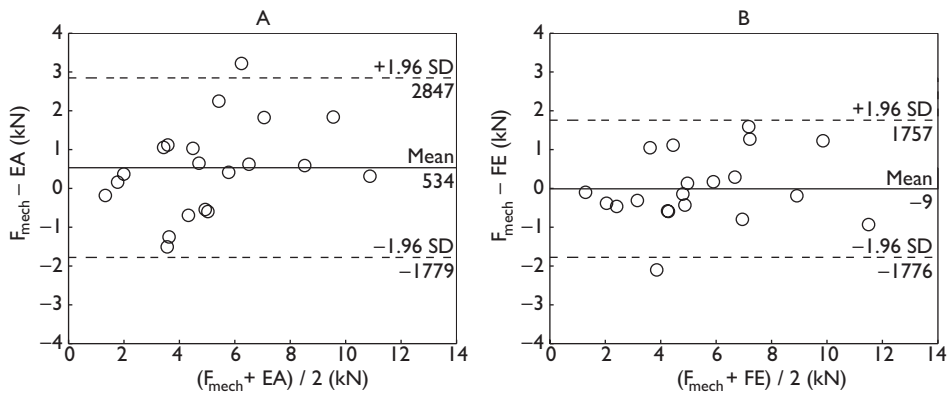


Figure 4. Bland-Altman plots for CTRA based axial rigidity (A) and FE based failure load (B). In Figure 4A, the Bland-Altman plot compares the force (N) between mechanical testing and EA for 20 human femurs and shows that the mean difference is 534 N, indicating that on average, force as measured by mechanical testing was 534 N greater than force determined by EA (solid line). The dashed lines represent the 95% limits of agreement and indicate that the difference between the two methods, while averaging 534 N, may range between 1779 N lower to 2847 N higher for mechanical testing compared to EA. There was no significant correlation between the difference on the y-axis and the mean on the x-axis of the two methods, suggesting that the bias is approximately constant throughout the range of values for the 20 human specimens. Regarding Figure 4B, the Bland-Altman plot shows the mean difference in force between mechanical testing and finite element (FE) analysis to be only -9 N, meaning that on average the difference or bias between the two sets of measurements is very close to 0, (i.e., about 9 N greater with FE than with mechanical testing). In addition, the limits of agreement as denoted by the dashed lines ($\pm 1.96 \times \text{SD}$ of the mean difference) reveals that 95% of the time the force using mechanical testing can be somewhere 1776 N lower than FE to 1757 N higher than FE. Again, the bias appears to be constant throughout the range of values, meaning that the variability of the paired measurements between mechanical and FE vary almost equally above and below the mean (solid) line. The Bland-Altman plots in essence provide an excellent graphical representation for assessing agreement between two different methods of measurement and the limits of agreement demarcate the width of the difference that can be expected 95% of the time. The Bland-Altman technique does not require having a “gold standard,” but typically the “new method of interest” (e.g., EA or FE) is subtracted from the conventional method (in this case, mechanical testing) on the y-axis.

Table 1. Comparison of CTRA based EA and FE based failure load for estimation of experimental failure load

	TOTAL			INTACT			DEFECT		
	EXP	EA	FE	EXP	EA	FE	EXP	EA	FE
Failure load (N)	5404 ± 2764	4870 ± 2347	5413 ± 2583	6771 ± 2498	5823 ± 2297	6255 ± 2634	4037 ± 2394	3916 ± 2081	4572 ± 2362
P-value (paired t-test)		0.06*	0.96*		0.03**	0.09**		0.74**	0.02**
Mean ± SD of difference vs. Mechanical Testing		534 ± 1180	-9 ± 901		948 ± 1153	517 ± 850		120 ± 1108	-535 ± 615
Bland-Altman Method [#] , 95% CI		-1779 to 2847	-1776 to 1757		-1311 to 3208	-1149 to 2183		-2052 to 2292	-1740 to 670

* Plus-minus values are mean ± SD and data are based on 10 paired femurs.

** Plus-minus values are mean ± SD and data are based on 10 single femurs.

Bland-Altman method evaluating limits of agreement between each method (QCT and FEA) versus mechanical testing based on mean difference (bias) and 95% confidence interval of difference (± 1.96 SDs).

Table 2. Correlations between rankings of the femurs in the experiments and the predictions by FE and CTRA using Kendall Tau ranking coefficients

		Intact femurs	Defect femurs
Experiments vs.	FE	0.73 *	0.87 *
	EA	0.64 *	0.73 *
	EI	0.64 *	0.73 *

* indicates significant correlations at the p -level of 0.05.

($r = 0.36$, $p = 0.12$). FE showed more accurate estimates of failure load than each of the two CT-based rigidity parameters (all $p < 0.001$, paired t -tests on the deltas versus mechanical testing). The limits of agreement in the Bland-Altman plot indicate that the FE estimated failure load on average is nearly the same as mechanical testing (mean difference of -9 N) and provides estimates that are within the range of -1776 to 1757 N (Figure 4B, Table 1). Moreover, the bias throughout the magnitude of possible failure loads is constant as indicated by a non-significant correlation between the average versus the difference ($r = 0.20$, $p = 0.39$).

To further study differences in prediction accuracy between the two methods, the paired t -tests and Bland-Altman analysis were repeated for the intact and defect specimens separately (Table 1). Paired t -tests then showed a significant difference between mechanical testing and EA for the intact femurs and between mechanical testing and FE for the metastatic femurs. In addition, for EA the bias varied over the different analyses (total group and both subgroups), but the limits of agreement were constant. For FE there were differences in both the bias and the limits of agreement over the analyses. The more narrow limits of agreement in the subgroup analysis of the defect specimens suggested a higher accuracy at the cost of a larger systemic error (as the bias was larger than in the overall analysis). For the defect femurs, which are of main interest here, CTRA showed the smallest bias (120 N vs. -535 N for FE), whereas FE showed a higher agreement among predictions (SD 615 N vs. 1108 N for CTRA). High Kendall rank correlations between the experiments and the predictions by either FE or CTRA (all significant at the $p = 0.05$ level) were found (Table 2). Furthermore, Kendall rank correlations between the FE rankings and the CTRA rankings showed moderate to good correlations (Figure 5). No significant differences in prediction accuracy were found between the two methods.

The fracture locations in the experiments were qualitatively compared to the fracture lines predicted by the FE model and to the minimum rigidity cross-section from CTRA analysis. (Figure 6 provides a graphic presentation of a representative specimen). The results indicated that the fracture locations were always directed through the lesion in the defect specimens, if

applicable. Overall, the fracture locations were reasonably well predicted by both FE (Derikx et al., 2012a) and CTRA methods as highlighted in Table 3.

Discussion

In recent years, different diagnostic tools have been developed to address the common quandary encountered by physicians when assessing fracture risk prediction in patients found to have a metastatic bone lesion. The choice for the most appropriate therapeutic approach should be objectively determined by methods that consider bone as a structure, whose mechanical behaviour depends on both material and geometric properties. This study compa-

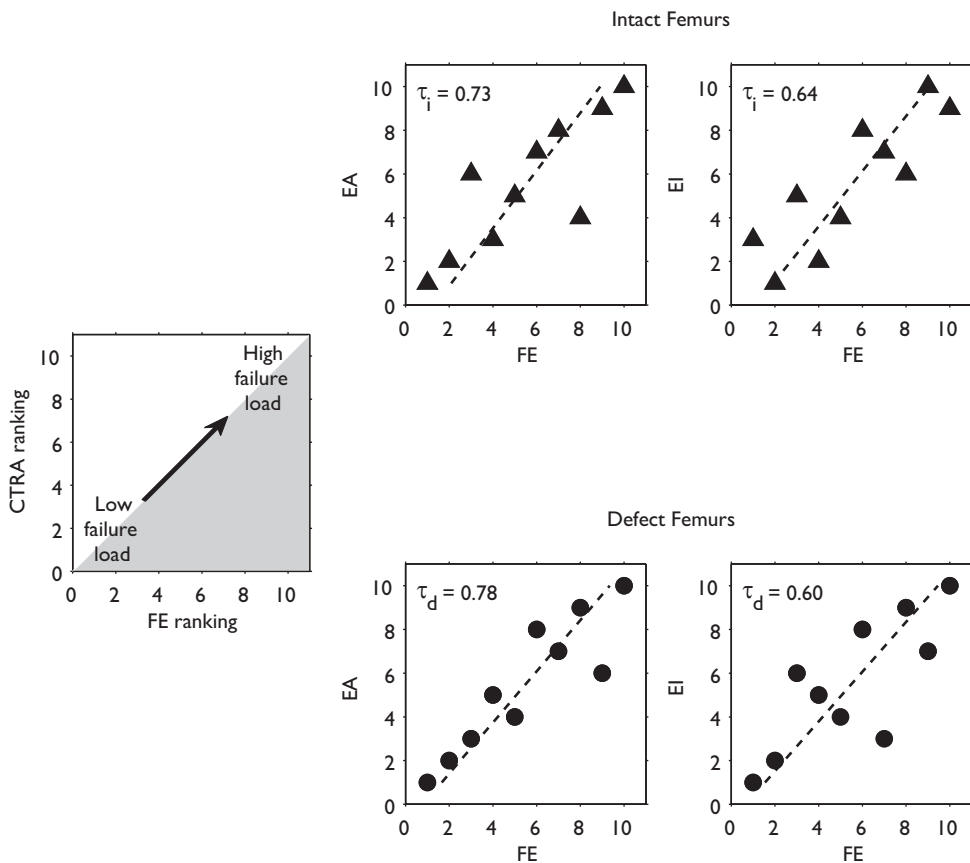


Figure 5. The output parameters (failure load for FE and EA and EI for CTRA) were used to rank the femurs from weak to strong. These rankings were subsequently compared by calculating the Kendall rank correlation coefficient (τ). This figure shows Kendall rank correlation coefficients between failure load predicted by the FE models and axial (left panel) and bending (right panel) rigidities calculated by CTRA, both for intact (τ_i , triangles) and metastatic femurs (τ_d , circles).

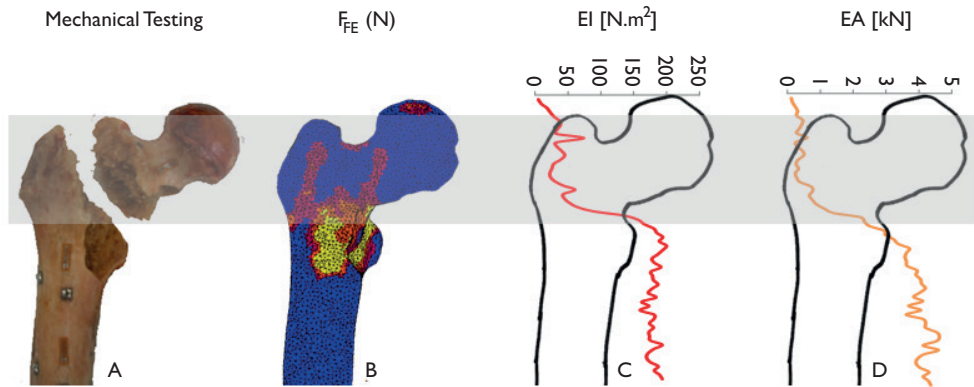


Figure 6. Fracture location as demonstrated by mechanical testing (A), FE (B) and CTRA analysis (C and D) on a representative specimen. The grey band highlights the failed area as outlined from mechanical testing (panel A). The FE results indicate the elements that underwent plastic deformation in this region (red to yellow sections in panel B), and the bending and axial rigidities (panel C and D) show the lowest EI and EA values for the CT slices residing in the grey fracture zone. The horizontal bar at the top provides the EA and EI axes, and the vertical axis (not shown in axis, which is collinear with the long axis of the bone) is the slice number of the CT data stack.

red the prediction accuracy of CTRA to the prediction accuracy of FEA, determined on the basis of actual mechanical experiments using paired femurs with and without simulated lytic lesions. We were able to demonstrate that structural rigidity retrieved from CTRA, as well as failure loads predicted by FE correlated well with the actual failure loads obtained from mechanical testing. There were no significant differences in prediction accuracy between the two modelling techniques.

As reported previously (Derikx et al., 2012a), the correlation coefficients between the FE predicted and the actual measured failure forces ($R^2 = 0.89$) were similar to those obtained in other FE studies (Bessho et al., 2004; Keyak et al., 2005; Tanck et al., 2009; Dragomir-Daescu et al., 2011). Similarly, relatively high correlation coefficients between CTRA and mechanical testing data were evidenced ($R^2 = 0.82$ and 0.86 , EA and EI respectively). These results are comparable to those obtained by Hong et al. (2004), who showed high coefficients of determination when comparing reductions in failure loads versus reductions in axial, bending and torsional rigidity ($R^2 = 0.84$, 0.80 and 0.71 , respectively) in samples from whale trabecular bone. Similarly, Whealan et al. (2000) demonstrated the effectiveness of QCT derived measurements of rigidity for the prospective prediction of yield loads of vertebrae with simulated lytic lesions ($r_c = 0.74$). Finally, by assessing fracture prediction through benign skeletal lesions in children and young adults, Snyder et al. (2006) indicated that bending and torsional rigidities were each highly significant predictors of fracture occurrence and combined, these

measures could predict femoral fractures with 97% accuracy.

Studying the intact and defect specimens separately allowed for further evaluating potential differences in prediction accuracy between the two methods. Especially in the specimens with an artificial defect, contrasting results were seen. CTRA seemed to have a higher accuracy (as the bias was lowest), whereas FE showed a higher precision (due to smaller limits of agreement). This could indicate that FE calculations need a correction for the systemic bias but could more closely approach the failure load in defect femurs on a subject-specific level. In contrast, CTRA will provide more accurate estimates of axial rigidity (as a surrogate for failure load) on the group level. However, further studies using larger numbers of specimens should confirm our findings.

Unlike previously proposed radiographic guidelines, both methods are able to deliver objective predictions while considering important biomechanical aspects of the bone, being a three-dimensional structure governed by its material and geometric properties; even if these are affected by the presence of a lytic lesion. Both techniques are based on QCT imaging, but computational times differ considerably between the two methods. Generating and running the FE simulations in this study takes about 8 hours per sample, and the sophisticated

Table 3. Fracture locations for all specimens as predicted by FEA and CTRA methods

Specimen	Lesion Characteristics			CTRA		
	Size (mm)	Location	Mech. Testing	FEA	EA	EI
1	-	-	Neck	Neck	Neck	Neck
1	40	Med, prox	Intertroch.	Intertroch.	Intertroch.	Intertroch.
2	-	-	Neck	Neck	Neck	Neck
2	40	Med, shaft	Midshaft	Midshaft	Midshaft	Midshaft
3	-	-	Intertroch.	Neck	Intertroch.	Intertroch.
3	22	Med, prox	Intertroch.	Intertroch.	Intertroch.	Intertroch.
4	-	-	Neck	Neck	Neck	Neck
4	40	Post, prox	Intertroch.	Neck/Intertroch.	Intertroch.	Intertroch.
5	-	-	Neck	Neck	Neck	Neck
5	45	Med, prox	Subtroch.	Subtroch.	Subtroch.	Subtroch.
6	-	-	Neck	Neck	Neck	Neck
6	40	Lat, prox	Subtroch.	Neck	Subtroch.	Subtroch.
7	-	-	Neck	Neck	Neck	Neck
7	2x22	Med, prox&shaft	Neck	Neck	Neck	Neck/Intertroch
8	-	-	Neck	Neck	Neck	Neck
8	40	Ant, prox	Intertroch.	Neck/Intertroch.	Intertroch.	Intertroch.
9	-	-	Neck	Neck	Neck	Neck
9	22	Ant, prox	Neck	Neck	Neck	Neck
10	-	-	Neck	Neck	Neck	Neck
10	2x30	Ant, prox&shaft	Proximal Shaft	Neck	Proximal Shaft	Proximal Shaft

and relatively complex FE software required asks for a certain level of expertise as well as background in biomechanics. CTRA takes only approximately 30 minutes, as this software is intentionally designed to be simple and be readily usable on a regular computer with an operator without expertise in structural mechanics. For those reasons, one would choose CTRA analysis. In contrast, FE simulations would be more suitable for the implementation of complex loading conditions. It is likely that the decrease in bone strength resulting from metastatic lesions is very focal and can differ a lot between patients. As a result, small muscle forces that insert on the femur close to the lesion site can be more dangerous than larger forces such as for example the hip contact force. The comprehension of such potentially important anatomical characteristics might be more straightforward using FEA.

Furthermore, prospective patient studies should resolve whether the two modelling techniques have equal prediction accuracy in clinical practice. That is, clinical experts have difficulties relating predicted biomechanical parameters, such as global strength or rigidity, to the clinical fracture risk for a certain patient.

Limitations of our study are shared with many previous works done in the field using *ex vivo* models for the assessment of failure load prediction using non-invasive imaging methods. On a group level, both methods accurately predict the femoral load capacity, but on the individual level there can be rather large over- and under-estimations of the femoral strength. These subject-specific over- and under-estimations should be improved before either of the methods can be implemented in clinical practice.

Moreover, isotropic material behaviour was implemented in the FE models. We found that fracture locations in intact femora were often predicted in the subcapital region, whereas the experimental fractures were located more in between the greater and lesser trochanter. The implementation of isotropic material behaviour rather than anisotropic behaviour is a plausible cause for this. However, it is not yet possible to practically implement realistic anisotropic material behaviour in FE models based on clinical CT images. Trabecular architecture is only visible on the micro-level, and as such anisotropic measures can only be determined from micro-CT scans or high-resolution CT-scans. In contrast, CTRA is an axial analysis by default, where it uses compressive and tensile constitutive properties in their axial direction to convert pixel density to modulus of elasticity. Therefore, it does not take into consideration mechanical properties of the bone in the transverse direction.

Furthermore, it is a universal rule that *ex vivo* experimental results introduce a certain amount of limitation when extrapolating to *in vivo* conditions. Evident differences exist between the metastatic lytic lesions that were artificially simulated in this study and those seen in patients in the clinical practice. In our case, regularly shaped defects were limited to cortical lesions,

while metastatic bone lesions generally show an irregular pattern and additionally involve trabecular tissue. However, QCT would be readily able to detect these irregularities and incorporate them into both algorithmic analytical processes, although accurately modelling the material properties of blastic metastatic tissue might be challenging. Moreover, we are currently working on the evaluation of the FE simulations for the prediction of femoral failure load using *in vivo* patient data, and the preliminary results are promising (Derikx et al., 2012b). In summary, the results of our study showed that non-invasive subject-specific fracture risk assessment techniques correlate evenly well with actual failure loads measured in mechanical experiments. This suggests that both methods could be further developed into a tool that can be used in clinical practice. When analyzing the defect femurs only, the results suggested that predictions by FEA are slightly more accurate on a subject-specific level, yet CTRA analysis can be conducted expediently by non-expert operators. However, validation in prospective patient studies should confirm these preliminary findings. Such future clinical studies should additionally resolve how these methods can be implemented in clinical settings in order to improve the prediction of the fracture risk in metastatic bone disease.

Acknowledgements

This work has been funded by the Dutch Science Foundation NWO-STW (NPG.06778), Stichting Anna Fonds, the Furlong Research Charitable Foundation and Fonds NutsOhra. This work has also been funded by the National Institute of Health Loan Repayment Program (AN) and internal funds from the Department of Orthopaedic Surgery at Boston Children's Hospital (BDS).

References

- Bessho M, Ohnishi I, Matsuyama J, Matsumoto T, Imai K, Nakamura K. 2007. Prediction of strength and strain of the proximal femur by a CT-based finite element method. *J Biomech* 40(8): 1745-1753.
- Bessho M, Ohnishi I, Okazaki H, Sato W, Kominami H, Matsunaga S, Nakamura K. 2004. Prediction of the strength and fracture location of the femoral neck by CT-based finite-element method: a preliminary study on patients with hip fracture. *J Orthop Sci* 9(6): 545-550.
- Bickels J, Dadia S, Lidar Z. 2009. Surgical management of metastatic bone disease. *J Bone Joint Surg Am* 91(6): 1503-1516.
- Bland JM, Altman DG. 1986. Statistical Methods for Assessing Agreement between Two Methods of Clinical Measurement. *Lancet* 1(8476): 307-310.
- Clezardin P, Teti A. 2007. Bone metastasis: pathogenesis and therapeutic implications. *Clin Exp Metastasis* 24(8): 599-608.
- Cody DD, Gross GJ, Hou FJ, Spencer HJ, Goldstein SA, Fyhrie DP. 1999. Femoral strength is better predicted by finite element models than QCT and DXA. *J Biomech* 32(10): 1013-1020.
- Coleman RE. 2006. Clinical features of metastatic bone disease and risk of skeletal morbidity. *Clin Cancer Res* 12(20

Pt 2): 6243s-6249s.

- Damron TA, Morgan H, Prakash D, Grant W, Aronowitz J, Heiner J. 2003. Critical evaluation of Mirels' rating system for impending pathologic fractures. *Clin Orthop Relat Res* 415 Suppl: S201-207.
- Derikx LC, van Aken JB, Janssen D, Snyers A, van der Linden YM, Verdonshot N, Tanck E. 2012a. The assessment of the risk of fracture in femora with metastatic lesions: comparing case-specific finite element analyses with predictions by clinical experts. *J Bone Joint Surg Br* 94(8): 1135-1142.
- Derikx LC, van der Linden YM, Snyers A, Verdonshot N, Tanck E. 2012b. Patient-specific finite element models differentiate between patients with and without a pathological fracture in metastatic bone disease. *Proceedings of ESB 2012, 18th Congress of the European Society of Biomechanics*. Lisbon.
- Dragomir-Daescu D, Op Den Buijs J, McEligot S, Dai Y, Entwistle RC, Salas C, Melton LJ, 3rd, Bennet KE, Khosla S, Amin S. 2011. Robust QCT/FEA models of proximal femur stiffness and fracture load during a sideways fall on the hip. *Ann Biomed Eng* 39(2): 742-755.
- El-Husseiny M, Coleman N. 2010. Inter- and intra-observer variation in classification systems for impending fractures of bone metastases. *Skeletal Radiol* 39(2): 155-160.
- Entezari V, Basto PA, Vartanians V, Zurakowski D, Snyder BD, Nazarian A. 2011. Non-invasive assessment of failure torque in rat bones with simulated lytic lesions using computed tomography based structural rigidity analysis. *J Biomech* 44(3): 552-556.
- Evans AR, Bottros J, Grant W, Chen BY, Damron TA. 2008. Mirels' rating for humerus lesions is both reproducible and valid. *Clin Orthop Relat Res* 466(6): 1279-1284.
- Hage WD, Aboulafia AJ, Aboulafia DM. 2000. Incidence, location, and diagnostic evaluation of metastatic bone disease. *Orthop Clin North Am* 31(4): 515-528, vii.
- Hong J, Cabe GD, Tedrow JR, Hipp JA, Snyder BD. 2004. Failure of trabecular bone with simulated lytic defects can be predicted non-invasively by structural analysis. *J Orthop Res* 22(3): 479-486.
- Houston SJ, Rubens RD. 1995. The systemic treatment of bone metastases. *Clin Orthop Relat Res* 312: 95-104.
- Johnson SK, Knobf MT. 2008. Surgical interventions for cancer patients with impending or actual pathologic fractures. *Orthop Nurs* 27(3): 160-171; quiz 172-173.
- Keyak JH, Falkinstein Y. 2003. Comparison of in situ and in vitro CT scan-based finite element model predictions of proximal femoral fracture load. *Med Eng Phys* 25(9): 781-787.
- Keyak JH, Kaneko TS, Tehranzadeh J, Skinner HB. 2005. Predicting proximal femoral strength using structural engineering models. *Clin Orthop Relat Res* 437: 219-228.
- Mirels H. 1989. Metastatic disease in long bones. A proposed scoring system for diagnosing impending pathologic fractures. *Clin Orthop Relat Res* 249: 256-264.
- Moore D, McCabe G. 2003. *Introduction to the Practice of Statistics*. 4 ed. W.H. Freeman and Company, New York.
- Nazarian A, Pezzella L, Tseng A, Baldassarri S, Zurakowski D, Evans CH, Snyder BD. 2010. Application of structural rigidity analysis to assess fidelity of healed fractures in rat femurs with critical defects. *Calcif Tissue Int* 86(5): 397-403.
- Papagelopoulos PJ, Savvidou OD, Galanis EC, Mavrogenis AF, Jacofsky DJ, Frassica FJ, Sim FH. 2006. Advances and challenges in diagnosis and management of skeletal metastases. *Orthopedics* 29(7): 609-620; quiz 621-602.
- Rice JC, Cowin SC, Bowman JA. 1988. On the dependence of the elasticity and strength of cancellous bone on apparent density. *J Biomech* 21(2): 155-168.
- Schileo E, Taddei F, Cristofolini L, Viceconti M. 2008. Subject-specific finite element models implementing a maximum principal strain criterion are able to estimate failure risk and fracture location on human femurs tested in vitro. *J Biomech* 41(2): 356-367.
- Schulman KL, Kohles J. 2007. Economic burden of metastatic bone disease in the U.S. *Cancer* 109(11): 2334-2342.
- Snyder BD, Hauser-Kara DA, Hipp JA, Zurakowski D, Hecht AC, Gebhardt MC. 2006. Predicting fracture through benign skeletal lesions with quantitative computed tomography. *Journal of Bone and Joint Surgery Am* 88A(1): 55-70.
- Snyder SM, Schneider E. 1991. Estimation of mechanical properties of cortical bone by computed tomography. *J Orthop Res* 9(3): 422-431.

- Taddei F, Cristofolini L, Martelli S, Gill HS, Viceconti M. 2006. Subject-specific finite element models of long bones: An in vitro evaluation of the overall accuracy. *J Biomech* 39(13): 2457-2467.
- Tanck E, van Aken JB, van der Linden YM, Schreuder HWB, Binkowski M, Huizenga H, Verdonschot N. 2009. Pathological fracture prediction in patients with metastatic lesions can be improved with quantitative computed tomography based computer models. *Bone* 45(4): 777-783.
- Toma CD, Dominkus M, Nedelcu T, Abdolvahab F, Assadian O, Krepler P, Kotz R. 2007. Metastatic bone disease: a 36-year single centre trend-analysis of patients admitted to a tertiary orthopaedic surgical department. *J Surg Oncol* 96(5): 404-410.
- van der Linden YM, Dijkstra PD, Kroon HM, Lok JJ, Noordijk EM, Leer JW, Marijnen CA. 2004. Comparative analysis of risk factors for pathological fracture with femoral metastases. *J Bone Joint Surg Br* 86(4): 566-573.
- van der Linden YM, Kroon HM, Dijkstra SP, Lok JJ, Noordijk EM, Leer JW, Marijnen CA, Dutch Bone Metastasis Study G. 2003. Simple radiographic parameter predicts fracturing in metastatic femoral bone lesions: results from a randomised trial. *Radiother Oncol* 69(1): 21-31.
- Whealan KM, Kwak SD, Tedrow JR, Inoue K, Snyder BD. 2000. Noninvasive imaging predicts failure load of the spine with simulated osteolytic defects. *J Bone Joint Surg Am* 82(9): 1240-1251.

5

Can patient-specific finite element models better predict fractures in metastatic bone disease than experienced clinicians? Towards introducing computational modelling into daily clinical practice

*Loes C. Derikx, Yvette M. van der Linden, Florieke Eggermont, H.W. Bart Schreuder,
An Snyers, Tom Rozema, Nico Verdonschot, Esther Tanck.*



Introduction

Specific cancer types, e.g. breast, prostate, lung, kidney and thyroid cancer, have a preference to metastasise to bone (Coleman, 1997; Johnson et al., 2008; Gralow et al., 2009). This may cause the patient pain and, when left untreated, these metastases carry a risk of developing serious complications such as hypercalcaemia, pathological fractures or, in case of vertebral metastases, spinal cord compression (Coleman, 1997; Coleman, 2006; Gralow et al., 2009). Pathological fractures in extremities have a negative influence on the quality of life. Especially when these fractures occur in weight bearing long bones, such as the femur, they instantly hamper the patient's mobility and self-care.

Femoral metastases with a low risk of fracture are conservatively treated for pain, e.g. with local radiotherapy. Metastases with a high risk of fracture require prophylactic surgery to retain mechanical strength and stability of the bone (van der Linden et al., 2004). This is an invasive procedure requiring anaesthesia, which is generally complex in cancer patients with limited life expectancy and a deteriorating condition. Thus, the decision for either a non-invasive treatment with e.g. radiotherapy or a prophylactic surgical treatment should be carefully made.

However, current clinical practice lacks an accurate tool to guide clinicians to the correct treatment decision. Numerous studies have evaluated lesion or patient factors, however, none has shown sufficient predictive power (van der Linden et al., 2004). A potential tool to improve clinical fracture risk assessments is finite element (FE) modelling, which predicts human femoral bone strength fairly accurately (Keyak et al., 2005b; Bessho et al., 2007; Lenaerts et al., 2009; Schileo et al., 2014). Our group showed, for example, that the FE model accurately calculates failure load and fairly predicts fracture locations in cadaver femurs with and without artificial lesions compared to mechanical experiments (Tanck et al., 2009; Derikx et al., 2011; Derikx et al., 2012). Moreover, we demonstrated that the ranking on FE failure load better resembled the experimentally measured failure loads than rankings by experienced clinicians (Derikx et al., 2012).

In this prospective cohort study, we investigated whether patient-specific FE models are able to identify patients at risk of pathological femoral fracturing resulting from metastatic bone disease. For this purpose, we included patients referred for radiotherapy to treat painful femoral metastases. Against expectations, some of these patients sustained pathological fractures in the femur during follow-up. We calculated the femoral failure loads and compared those between patients who did or did not sustain a fracture. In addition, we compared the FE predictions to assessments by experienced clinicians. We hypothesised that the FE models more accurately identify patients with a high fracture risk than experienced clinicians.

Methods and Materials

Study design

Between August 2006 and September 2009, all patients referred for palliative radiotherapy of the femur to three participating radiotherapy institutes in the Netherlands (Radiotherapeutic Institution Friesland, Leiden University Medical Center and Radboud university medical center) were asked to participate in this prospective cohort study (ethical approval was obtained from all participating centres). These patients received palliative radiotherapy following Dutch clinical guidelines: lesions with an axial cortical involvement < 30 mm have an expected low risk of fracture ($< 5\%$) and were treated with a single dose of 8 Gy (van der Linden et al., 2003). If the axial cortical involvement was >30 mm the risk of fracture was substantial (23%) (van der Linden et al., 2004). In such case, patients with an acceptable condition were referred for prophylactic stabilizing surgery and excluded from this study (van der Linden et al., 2003). If the patient's condition was hampered and surgery undesirable or impossible, the patient was referred for multiple fraction radiotherapy (e.g. 6 x 4 Gy) to induce remineralisation of the bone (Koswig et al., 1999). These patients were included in this study. Further inclusion criteria are depicted in Table 1. Power analysis revealed that 52 patients are needed to detect improvement of the specificity from 58% (van der Linden et al., 2004) to 79% with 90% power; the total number of patients was increased to 60 patients because of the limited life expectancy of these patients. During the study period, 66 patients gave their informed consent and were included in the study.

The time schedule of this study is depicted in Table 2. Baseline characteristics of the patients were recorded prior to and 28 and 70 days after radiotherapy. Furthermore, quantitative computed tomography (QCT) scans of the femoral region were retrieved. Patients filled out questionnaires on pain (BPI (Fairbank et al., 1980)), the level of activity and quality of life (i.e. parts of LAPAQ (Stel et al., 2004), SF-36 (Ware et al., 1992) and WOMAC (Bellamy et

Table 1. Inclusion criteria for this study

Inclusion criteria
• Proven malignancy
• Karnofsky score ≥ 60
• No clinical or radiological evidence of pathological fracturing of the femur
• No prior palliative surgery for the current treatment site of the femur
• No planned surgical intervention of the femoral bone
• No systemic radiotherapy 30 days prior to entry into the study
• No previous radiotherapy to the current treatment site of the femur
• Patient is able and willing to fill out baseline and follow-up forms on pain and quality of life
• Patient is willing to undergo additional CT scans for the femoral region

al., 1988)), but these were not included in the current study. Patients referred for multiple fraction radiotherapy underwent an additional QCT scan on the final day of their radiation schedule, to capture a potential short term effect of multiple fraction radiotherapy. Through their hospital records, the patients were followed for six months after inclusion or until a fracture occurred, or until death, as competing risk, whichever occurred first. Based on having sustained a fracture yes or no, the patients were divided into either the fracture group (F) or the non-fracture group (NF).

Table 2. Follow-up protocol for the two treatment schedules. Patients with multiple fraction radiotherapy underwent an additional QCT scan on the final day of their radiation schedule, which aimed to capture any potential short term effect of multiple fraction radiotherapy.

	Baseline (t=0)	Day 8 (t=1)	Day 28 (t=2)	Day 70 (t=3)
Single Fraction	QCT-1	-	QCT-3	QCT-4
Multiple Fraction	QCT-1	QCT-2	QCT-3	QCT-4

Subselection of patients for current study

Recent work by Carpenter et al. (2014), has shown that the use of different CT scanners can have a significant effect on bone mineral density measurements and subsequent failure loads, and is difficult to correct for. In the current study, two different scanners from one manufacturer were used in the three institutes. Although QCT scan settings were protocolled as far as possible, such inter-scanner effect may have been present in the input to our FE models, which could potentially lead to incorrect or at least incomparable FE failure loads. Therefore, in this study, we only analysed the data of 23 patients who were accrued at the Radboud university medical center. It should be noted that our previous *in vitro* validation study was also conducted in this institute using the same scanning equipment.

FE modelling

Patient-specific femoral FE models were generated, for the greater part using the workflow reported previously (Derikx et al., 2012). Summarizing, QCT images were generated using a standard protocol (as far as allowed by clinical practice), with the following settings: 120 kVp, 220 mA, slice thickness 3 mm, pitch 1.5, spiral and standard reconstruction, in-plane resolution 0.9375 mm. The patient-specific femoral geometry was segmented from the most recent CT images available and converted to a 3D surface mesh (Mimics 11.0 and 14.0, Materialise, Leuven, Belgium) and a solid mesh (Patran 2005 r2, MSC Software Corporation, Santa Ana, CA, USA), subsequently. A solid calibration phantom containing known calcium equivalent densities (Image Analysis, Columbia, KY, USA) was scanned along with the pa-



Figure 1. Boundary conditions for the FE model. The model was distally fixed by springs with a very high stiffness and the load was applied by means of a cup on the head of the femur, which incrementally displaced in distal direction.

tient at the level of the proximal femur. Using this phantom, we performed a mean diaphysial slice calibration to convert the grey values to calcium equivalent densities, ash densities and non-linear isotropic material behaviour (Keyak et al., 2005b), respectively. The FE simulations of the proximal femur were performed using MSC Marc (MSC.MARC2007r1, MSC Software Corporation, Santa Ana, CA, USA).

The FE models were loaded in axial direction, while distally fixed by two bundles of high-stiffness springs (Figure 1), which roughly resembles the single legged stance. The maximum total reaction force determined the failure load of the femur, which was normalised for body weight. The failure location was defined by elements that had plastically deformed at the moment of structural failure, and was compared to the post-fracture radiograph.

Clinical assessment

To compare the FE predictions to clinical fracture risk assessments, we generated digitally reconstructed radiographs (DRRs) from the CT scans in this study (Jacobs et al., 1998). We asked two radiation oncologists and two orthopaedic surgeons to individually assess the DRRs of the cases in this study, without providing any further information. First, they indica-

ted whether or not they thought the patient to carry a high risk of fracture requiring elective stabilizing surgery. Subsequently, we asked them to judge whether the cortical disruption caused by the metastasis was larger than 3 cm (van der Linden et al., 2003). To compare these clinical assessments to the predictions by the FE model, a critical FE failure load was defined, classifying a patient with a high or a low fracture risk. More specifically, sensitivity and specificity were calculated for different thresholds using increments of 0.5 x BW. Assuming equal weights for unexpected fractures and unnecessary surgeries, the threshold with the highest combined specificity and sensitivity was chosen as a threshold for comparison with clinical assessments.

Table 3. Characteristics of the three patients who sustained fractures during follow-up.

	Patient 1		Patient 2		Patient 3
Gender	M		F		M
Age at inclusion	70		53		64
	Right femur (F1)	Left femur (F2)	Right femur (F3)	Left femur (F4)	Left femur (F5)
Treatment (dose/no of fractions)	24 Gy/6	24 Gy/6	8 Gy/1	-	24 Gy/6
Time to fracture (days)	123	123	92	92	7
Type of fracture	Collum fracture	Collum fracture	Pertrochanteric fracture	Collum fracture	Subtrochanteric fracture
Activity while fracture occurred	Walking	Walking	Spontaneously	Spontaneously	Spontaneously

Statistical Analyses

We compared the failure load corrected for body weight (BW) between the fractured and the non-fractured femurs using Mann-Whitney U tests. Baseline data were compared between groups on the femur level using Chi-square (primary tumour), Fisher's Exact tests (gender, radiation schedule) or Mann-Whitney U tests (age, bodyweight, KPS). Interobserver agreement among clinicians was calculated using the Gwet's AC1. Like Cohen's kappa, this coefficient calculates the chance-corrected agreement between different observers but has shown to be less sensitive to the prevalence of observations (Wongpakaran et al., 2013). For all tests, the level of significance was defined at $p < 0.05$.

Results

Patients

Twenty-three patients with painful bone metastases were included in this study. Three pa-

tients sustained five fractures (F group) during follow-up (average time to fracture 87.4 days, range 7 - 123 days). One of these fractures occurred in a contralateral femur that was not irradiated (Table 3, Figure 4). Fractures F1 and F2 occurred during walking, the other three femurs (F3 - F5) fractured spontaneously. Two other patients sustained a fracture well after follow-up, i.e. 441 and 500 days after inclusion, and were therefore included as patients with non-fractured femurs. One patient without a fracture was excluded from the study, as a hip prosthesis in the contralateral femur severely distorted the CT images. Thus, in the NF group

Table 4. Baseline characteristics on the group level.

	Fracture group (F) 5 femurs ^a	Non-fracture group (NF) 24 femurs ^a	p-value
Gender			
Male	3 (60%)	13 (54%)	1.00
Female	2 (40%)	11 (46%)	
Age in years			
Median (IQR)	64.0 (17.0)	62.0 (19.8)	1.00
Body weight in kg			
Median (IQR)	73.0 (8.5)	65.5 (25.3)	0.08
Radiation schedule ^b			
SF	1 (25%)	14 (58%)	0.31
MF	3 (75%)	10 (42%)	
KPS			
Median (IQR)	80.0 (10.0)	70.0 (10)	0.72
Time since primary tumour in years			
Median (IQR)	3.6 (1.7)	4.3 (5.2)	0.45
Time since first metastasis in years			
Median (IQR)	3.2 (1.6)	2.5 (2.8)	0.32
Primary cancer site			
Breast	2 (40%)	7 (29%)	0.41 ^e
Prostate	1 (20%)	8 (33%)	
Kidney	0 (0%)	3 (13%)	
Rectum	0 (0%)	2 (8%)	
M. Kahler	2 (40%)	1 (4%)	
Urethra	0 (0%)	1 (4%)	
Cervix	0 (0%)	1 (4%)	
aCUP ^c	0 (0%)	1 (4%)	
Time to death since inclusion in months			
Median (IQR)	11.0 (9)	8.0 (17) ^d	0.91
Time to most recent CT in days			
Median (IQR)	28.0 (15)	31.5 (71.8)	0.30

IQR: interquartile range. ^a Fracture group: 5 femurs in 3 patients. Non-fracture group: 24 femurs in 19 patients. ^b One femur in the fracture group was not treated with radiotherapy. ^c Cancer of Unknown Primary origin. ^d Date of death missing for one non-fracture patient. ^e P-value for Pearson Chi-Square; since Fisher's Exact tests can only be performed in 2x2 contingency tables.

19 patients with 24 treated non-fractured femurs were included. Baseline characteristics are shown in Table 4; there were no significant differences between groups.

FE models

Figure 2A shows the BW-corrected failure loads for all femurs in this study. It should be mentioned that the body weight of three patients (four femurs) in the non-fracture group was not filed in their medical record. Hence, those femurs had to be excluded from the FE analyses. The median failure load of fractured femurs was 4.89 x BW (IQR = 2.13) and 10.02 x BW

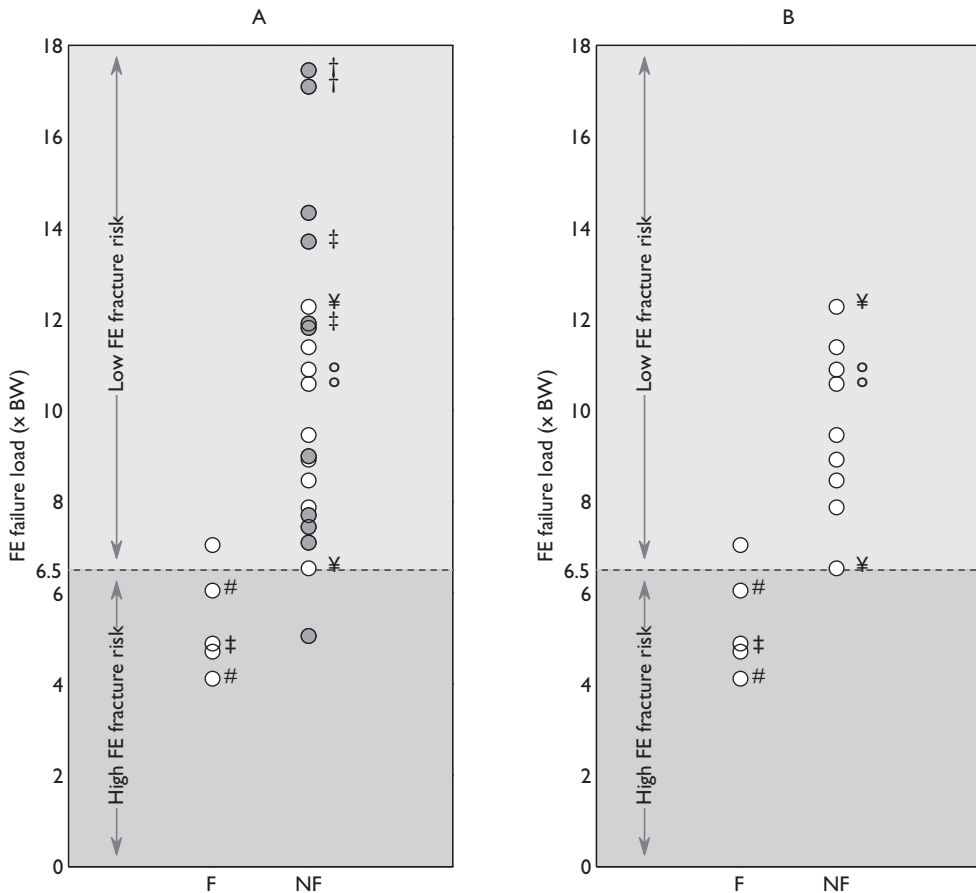


Figure 2. Femoral failure load for patients who did (F) or did not (NF) sustain a femoral fracture during follow-up, corrected for bodyweight for all femurs (A) and after exclusion of blastic lesions (B). Femurs with blastic lesions are indicated in grey, femurs with lytic or mixed type lesions are indicated with open circles. The threshold at 6.5 x BW is used to compare the predictive power of the FE model vs. experienced clinicians. Symbols indicate paired femurs.

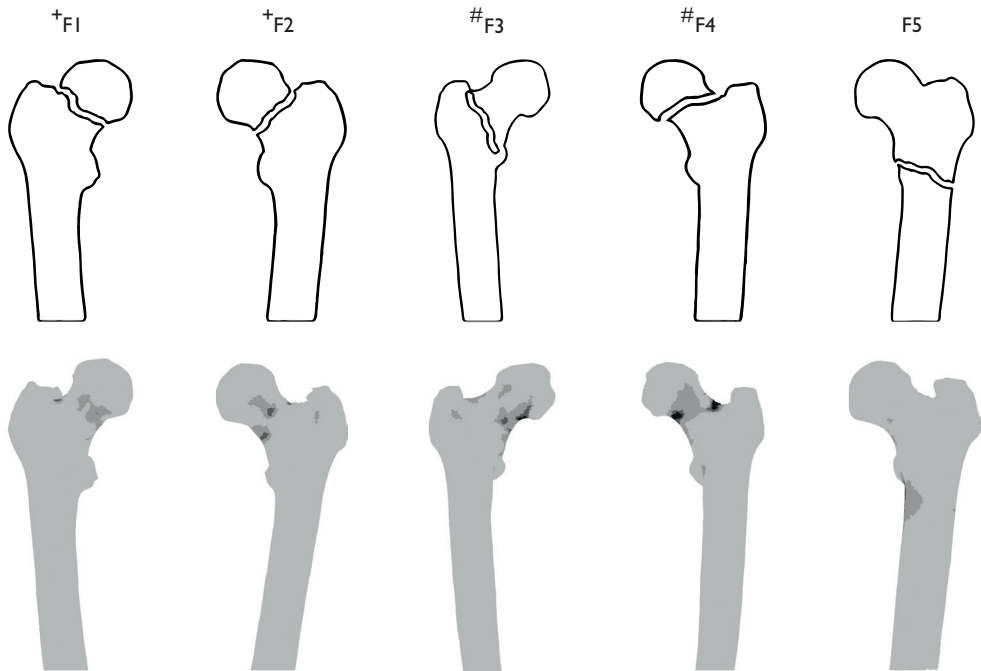


Figure 3. Schematic overview of clinical fracture locations (upper panel), indicated by an experienced clinician who was blinded to the predicted fracture locations, and the fracture locations at failure (mid-coronal plane) predicted by the FE models (lower panel). Femurs indicated with + and # are paired femurs.

(IQR = 4.43) for the non-fractured femurs. A Mann-Whitney U test showed that this difference was significant ($p < 0.001$). Some of the non-fractured femurs' failure loads were extremely high. Clinical re-assessment of the CT images by a radiation oncologist (blinded to the failure loads) revealed that these patients suffered from blastic lesions, which, as generally thought, decrease the structural strength of the bone despite their high degree of mineralisation.

We excluded these femurs and re-ran the statistical analysis (Figure 2B). The difference between groups remained significant after exclusion of femurs with pure blastic lesions (4.89 x BW (IQR = 2.13) vs. 9.46 x BW (IQR = 2.97); $p = 0.002$). Furthermore, four out of five FE fracture locations well resembled the actual fractures as gleaned from postfracture radiographs (Figure 3). In the remaining case, the FE model predicted a femoral neck fracture whereas this patient clinically presented with a peritrochanteric fracture.

Clinical assessment

A critical failure load of 6.5 x BW was used for comparing the predictions of the FE models

to clinical assessments. More patients were correctly identified with a high fracture risk by the FE model than by clinicians who relied on their clinical experience (Figure 4). For the non-fractured femurs, the performance of the model and the experienced clinicians was comparable, particularly when omitting femurs for which the body weight was not reported. Both the clinicians and the FE model more often correctly identified non-fracture patients than fracture patients, as the specificity (SP) was higher than the sensitivity (SE) (Table 5). The FE model identified 20 femurs with a low fracture risk. However, one femur did fracture during follow-up, and as such was wrongly assessed (negative predictive value (NPV) = 0.95). NPV values for clinicians ranged between 0.81 and 0.90.

Table 5. Summary statistics for the prediction accuracy of the FE model and the experienced clinicians when relying on their experience. 95% Confidence intervals are given between brackets.

		F	NF	SE	SP	PPV	NPV
FE ^a	F predicted	4	1	0.80 (0.29-0.97)	0.95 (0.75-0.99)	0.80 (0.29-0.97)	0.95 (0.75-0.99)
	NF predicted	1	19				
RO1	F predicted	1	7	0.20 (0.03-0.71)	0.71 (0.49-0.87)	0.13 (0.02-0.53)	0.81 (0.58-0.94)
	NF predicted	4	17				
RO2	F predicted	1	7	0.20 (0.03-0.71)	0.71 (0.49-0.87)	0.13 (0.02-0.53)	0.81 (0.58-0.94)
	NF predicted	4	17				
OS1	F predicted	3	5	0.60 (0.15-0.94)	0.79 (0.58-0.93)	0.38 (0.09-0.75)	0.90 (0.70-0.99)
	NF predicted	2	19				
OS2	F predicted	3	5	0.60 (0.15-0.94)	0.79 (0.58-0.93)	0.38 (0.09-0.75)	0.90 (0.70-0.99)
	NF predicted	2	19				

^a The bodyweight of three patients (four femurs) in the non-fracture group were not available, and could therefore not be included in the scoring by the FE model and in the subsequent calculation of these statistics. SE: Sensitivity, SP: specificity, PPV: positive predictive value, NPV: negative predictive value.

Furthermore, the FE model identified five femurs with a high fracture risk, four of which actually fractured during follow-up (positive predictive value (PPV) = 0.80). The PPV values for clinicians were lower and ranged between 0.13 and 0.38, however, 95% confidence intervals overlapped. The highest interobserver agreement was found between the two orthopaedic surgeons and between one of the radiation oncologists and one of the orthopaedic surgeons, while agreement between radiation oncologists was lower (Table 6). However, 95% confidence intervals were again large and overlapping (Table 6). When the experienced clinicians were asked to base their decision on a 30 mm cortical disruption (Figure 5), mainly the radiation oncologists identified fewer non-fractured femurs with a high fracture risk, at the cost of a slight increase in the number of fractured femurs that were incorrectly identified with a low fracture risk.

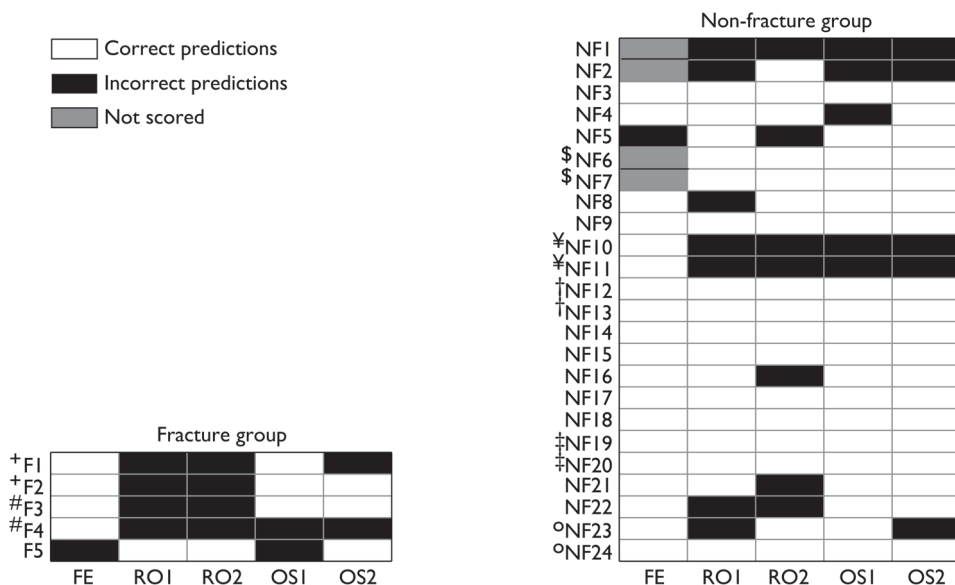


Figure 4. Correct and incorrect fracture predictions by the FE model and the experienced clinicians (ROI, RO2, OS1, OS2). Clinicians judged the reconstructed radiographs of the patients based on their experience, without any further guidelines prescribed. For the FE predictions a threshold of 6.5 x BW was used to indicate fracture or non-fracture. Results are shown per group (F and NF). The body weight of three patients (four femurs) were not available, and could therefore not be included in the scoring by the FE model ('not scored').

Discussion

Previously, we showed that FE-models calculated femoral failure loads that were comparable to those measured in mechanical experiments (Derikx et al., 2012). In the current study, we applied these FE-models *in vivo* by comparing the model predictions with clinical follow-up data. We verified whether the model could have predicted the pathological fractures that patients with painful bone metastases sustained during follow-up in a prospective study.

We showed a difference in median failure load between patients who sustained a pathological fracture and those who did not. This shows that finite element models are able to comprehend many factors that contribute to the *in vivo* load capacity of metastatic femurs, such as the

Table 6. Interobserver agreement between experienced radiation oncologists (ROI, RO2) and orthopaedic surgeons (OS1, OS2), expressed in Gwet's AC1 Coefficient. 95% Confidence intervals are given between brackets.

	ROI	RO2	OS1
RO2	0.66 (0.37 – 0.94)	-	-
OS1	0.54 (0.21 – 0.87)	0.43 (0.06 – 0.79)	-
OS2	0.77 (0.53 – 1.00)	0.54 (0.21 – 0.87)	0.77 (0.53 – 1.00)

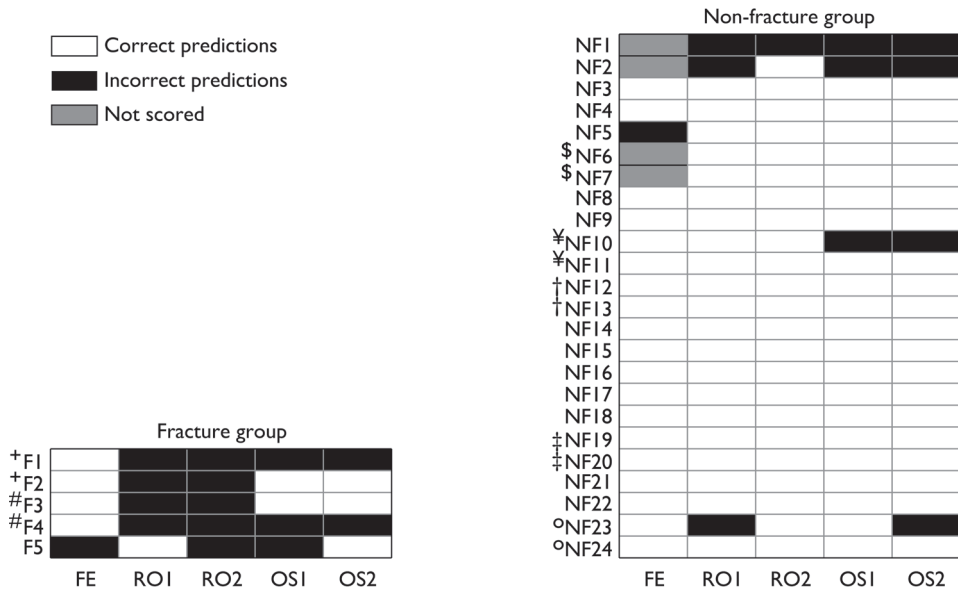


Figure 5. Correct and incorrect fracture predictions by the FE model and the experienced clinicians (ROI, RO2, OS1, OS2). Based on reconstructed radiographs of the patients, clinicians indicated whether the cortical disruption in the lesion was larger than 3 cm. If so, a fracture was predicted. For the FE predictions a threshold of $6.5 \times BW$ was used to indicate fracture or non-fracture. Results are shown per group (F and NF). The body weight of three patients (four femurs) were not available, and could therefore not be included in the scoring by the FE model ('not scored').

bone quality and the bone geometry, or compromise it, such as the location and the size of the lesion. Such findings have been shown in other *in vivo* studies as well, for example in the field of osteoporosis (e.g. (Keyak et al., 2013; Kopperdahl et al., 2014)). These studies showed that FE strength was highly correlated with fracture (Keyak et al., 2013) and that FE bone strength remained predictive for fracture after correction for total hip areal bone mineral density in men and women (Kopperdahl et al., 2014).

Furthermore, although confidence intervals were large, the FE predictions in the present study demonstrated higher sensitivity and PPV values compared to clinical assessments, suggesting a better identification of patients who will sustain a fracture by the FE model. The specificity and NPVs were comparable, which indicates that both the model and the experienced clinicians were equally able to identify patients who are not at risk of fracture. These results support the hypothesis that FE models can serve as a useful clinical tool, since current clinical guidelines have shown high negative predictive power but low positive predictive power (van der Linden et al., 2004).

In four out of five cases, the predicted fracture locations resembled the actual clinical fracture

locations. However, it should be noted that compressive fractures were predicted, whereas tensile fractures would be expected under axial loading conditions. The implementation of more realistic material behaviour can improve the prediction of the fracture location (Derikx et al., 2011), but an extensive sensitivity analysis should first reveal the appropriate parameters to do so. In case F3, the FE fracture location did not resemble the clinical fracture line. Since the patient did not notice during which activity the bilateral fractures occurred, the axial load applied in this study might be inappropriate to simulate the correct fracture line. Hence, modelling more and realistic loading conditions may therefore further improve the predicted fracture location and could additionally help the attending physician to instruct the patient which activities could be performed safely in daily life.

Although the results in this study are promising, some limitations should be mentioned here. First of all, we realise that the sample size in this study is limited, and the statistics, especially in the fracture group, should therefore be replicated in the full dataset including patients from all three participating radiotherapy institutions ($n = 66$) after we have quantified and corrected for the inter-scanner effects.

A second limitation in this study relates to the modelling of metastatic tissue. The FE model predicted very high failure loads in the femurs of one patient in the non-fracture group. In this patient blastic femoral lesions were confirmed, which generally show very high CT intensities. In the current FE model, these CT intensities were converted to material behaviour using relationships that are defined based on experiments with human tissue affected by metastases as well as healthy bone (Keyak et al., 2005b). Although not all femurs with extensive blastic lesions showed such aberrant failure loads (Figure 2), these empirical relationships may need to be adapted for blastic metastatic tissue. So far, differences in microarchitecture have been described for metastases (e.g. (Sone et al., 2004)), but the mechanical behaviour has yet not been established unequivocally (Kaneko et al., 2003; Kaneko et al., 2004). Moreover, adapted material models did not yet improve the predictive power of FE models with metastatic lesions (Keyak et al., 2005a). Hence, further research is required to determine the mechanical behaviour of different types of metastatic tissue.

Thirdly, we used the most recent CT scan available to capture the mechanical status of the femur closest to the moment of fracture. However, it has been demonstrated that the bone mineral content may decrease after radiotherapy and can be (over-)compensated in a subsequent recalcification process (Koswig et al., 1999). Thus, the mechanical status of the femur over time may be confounded by the effect of radiotherapy treatment, as well as by progression of the metastatic disease. Future work is to quantify this effect using the temporal CT data in this study. Nevertheless, the assessments by the experienced clinicians were based

on DRRs generated from the same QCT scans, so the better performance of the FE model over the experienced clinicians remains. Additionally, it should be mentioned that the clinicians pointed out that the quality of the DRRs was suboptimal compared to conventional radiographs they normally use, which obviously may have affected their assessments.

Finally, it should be noted that the failure loads of four femurs from three patients in the non-fracture group could not be normalised as their body weight and length were not filed. Since the failure loads of two of these femurs (NF1 and NF2) were rather low, and estimated body masses were relatively high, we should note that the FE model would probably have incorrectly predicted a high fracture risk for these non-fractured femurs, similar to the clinicians.

In conclusion, we showed that FE models are potential tools to improve clinical fracture risk predictions in metastatic bone disease in patients with disseminated cancer. The FE models provided an accurate identification of patients with high fracture risk. Future work in a larger patient population should confirm the higher predictive power of the FE models over current clinical guidelines.

Acknowledgements

The authors would like to thank Wouter Gevers for his help in generating the DRRs, and Femke Peters, MD, PhD (LUMC) and Ingrid van der Geest, MD, PhD (Radboud university medical center) for their input to this study. This work was funded by the Dutch Cancer Society and Fonds NutsOhra.

References

- Bellamy N, Buchanan WW, Goldsmith CH, Campbell J, Stitt LW. 1988. Validation study of WOMAC: a health status instrument for measuring clinically important patient relevant outcomes to antirheumatic drug therapy in patients with osteoarthritis of the hip or knee. *J Rheumatol* 15(12): 1833-1840.
- Bessho M, Ohnishi I, Matsuyama J, Matsumoto T, Imai K, Nakamura K. 2007. Prediction of strength and strain of the proximal femur by a CT-based finite element method. *J Biomech* 40(8): 1745-1753.
- Carpenter RD, Saeed I, Bonaretti S, Schreck C, Keyak JH, Streeper T, Harris TB, Lang TF. 2014. Inter-scanner differences in in vivo QCT measurements of the density and strength of the proximal femur remain after correction with anthropomorphic standardization phantoms. *Med Eng Phys* 36(10): 1225-1232.
- Coleman RE. 1997. Skeletal complications of malignancy. *Cancer* 80(8 Suppl): 1588-1594.
- Coleman RE. 2006. Clinical features of metastatic bone disease and risk of skeletal morbidity. *Clin Cancer Res* 12(20 Pt 2): 6243s-6249s.
- Derikx LC, van Aken JB, Janssen D, Snyers A, van der Linden YM, Verdonshot N, Tanck E. 2012. The assessment of the risk of fracture in femora with metastatic lesions: comparing case-specific finite element analyses with predictions by clinical experts. *J Bone Joint Surg Br* 94(8): 1135-1142.
- Derikx LC, Vis R, Meinders T, Verdonshot N, Tanck E. 2011. Implementation of asymmetric yielding in case-specific finite element models improves the prediction of femoral fractures. *Comput Methods Biomech Biomed Engin*

- 14(2): 183-193.
- Fairbank JC, Couper J, Davies JB, O'Brien JP. 1980. The Oswestry low back pain disability questionnaire. *Physiotherapy* 66(8): 271-273.
- Gralow JR, Biermann JS, Farooki A, Fournier MN, Gagel RF, Kumar RN, Shapiro CL, Shields A, Smith MR, Srinivas S, Van Poznak CH. 2009. NCCN Task Force Report: Bone Health in Cancer Care. *J Natl Compr Canc Netw* 7 Suppl 3: S1-S2; quiz S33-35.
- Jacobs F, Sundermann E, De Sutter B, Christiaens M, Lemahieu I. 1998. A fast algorithm to calculate the exact radiological path through a pixel or voxel space. *J. Comput. Inf. Technol* 6(1): 89-94.
- Johnson SK, Knobf MT. 2008. Surgical interventions for cancer patients with impending or actual pathologic fractures. *Orthop Nurs* 27(3): 160-171; quiz 172-173.
- Kaneko TS, Bell JS, Pejcić MR, Tehranzadeh J, Keyak JH. 2004. Mechanical properties, density and quantitative CT scan data of trabecular bone with and without metastases. *J Biomech* 37(4): 523-530.
- Kaneko TS, Pejcić MR, Tehranzadeh J, Keyak JH. 2003. Relationships between material properties and CT scan data of cortical bone with and without metastatic lesions. *Med Eng Phys* 25(6): 445-454.
- Keyak JH, Kaneko TS, Rossi SA, Pejcić MR, Tehranzadeh J, Skinner HB. 2005a. Predicting the strength of femoral shafts with and without metastatic lesions. *Clin Orthop Relat Res* 439: 161-170.
- Keyak JH, Kaneko TS, Tehranzadeh J, Skinner HB. 2005b. Predicting proximal femoral strength using structural engineering models. *Clin Orthop Relat Res* 437: 219-228.
- Keyak JH, Sigurdsson S, Karlsdóttir GS, Oskarsdóttir D, Sigmarsdóttir A, Kornak J, Harris TB, Sigurdsson G, Jonsson BY, Siggeirsdóttir K, Eiríksdóttir G, Gudnason V, Lang TF. 2013. Effect of finite element model loading condition on fracture risk assessment in men and women: the AGES-Reykjavik study. *Bone* 57(1): 18-29.
- Kopperdahl DL, Aspelund T, Hoffmann PF, Sigurdsson S, Siggeirsdóttir K, Harris TB, Gudnason V, Keaveny TM. 2014. Assessment of incident spine and hip fractures in women and men using finite element analysis of CT scans. *J Bone Miner Res* 29(3): 570-580.
- Koswig S, Budach V. 1999. [Remineralization and pain relief in bone metastases after after different radiotherapy fractions (10 times 3 Gy vs. 1 time 8 Gy). A prospective study]. *Strahlenther Onkol* 175(10): 500-508.
- Lenaerts L, van Lenthe GH. 2009. Multi-level patient-specific modelling of the proximal femur. A promising tool to quantify the effect of osteoporosis treatment. *Philos Trans A Math Phys Eng Sci* 367(1895): 2079-2093.
- Schileo E, Balistreri L, Grassi L, Cristofolini L, Taddei F. 2014. To what extent can linear finite element models of human femora predict failure under stance and fall loading configurations? *J Biomech* 47(14): 3531-3538.
- Sone T, Tamada T, Jo Y, Miyoshi H, Fukunaga M. 2004. Analysis of three-dimensional microarchitecture and degree of mineralization in bone metastases from prostate cancer using synchrotron microcomputed tomography. *Bone* 35(2): 432-438.
- Stel VS, Smit JH, Pluijm SM, Visser M, Deeg DJ, Lips P. 2004. Comparison of the LASA Physical Activity Questionnaire with a 7-day diary and pedometer. *J Clin Epidemiol* 57(3): 252-258.
- Tanck E, van Aken JB, van der Linden YM, Schreuder HWB, Binkowski M, Huizenga H, Verdoncote N. 2009. Pathological fracture prediction in patients with metastatic lesions can be improved with quantitative computed tomography based computer models. *Bone* 45(4): 777-783.
- van der Linden YM, Dijkstra PD, Kroon HM, Lok JJ, Noordijk EM, Leer JW, Marijnen CA. 2004. Comparative analysis of risk factors for pathological fracture with femoral metastases. *J Bone Joint Surg Br* 86(4): 566-573.
- van der Linden YM, Kroon HM, Dijkstra SP, Lok JJ, Noordijk EM, Leer JW, Marijnen CA, Dutch Bone Metastasis Study G. 2003. Simple radiographic parameter predicts fracturing in metastatic femoral bone lesions: results from a randomised trial. *Radiother Oncol* 69(1): 21-31.
- Ware JE, Jr., Sherbourne CD. 1992. The MOS 36-item short-form health survey (SF-36). I. Conceptual framework and item selection. *Med Care* 30(6): 473-483.
- Wongpakaran N, Wongpakaran T, Wedding D, Gwet KL. 2013. A comparison of Cohen's Kappa and Gwet's AC1 when calculating inter-rater reliability coefficients: a study conducted with personality disorder samples. *Bmc Medical Research Methodology* 13: 61.

6

Muscle optimisation techniques impact the magnitude of calculated hip joint contact forces

Mariska Wesseling, Loes C. Derikx*, Friedl de Groot, Ward Bartels,
Christophe Meyer, Nico Verdonschot, Ilse Jonkers. * joint first authorship
J Orthop Res 2015; 33(3), 430-438.*



Introduction

The hip contact force (HCF) is a relevant measure of joint loading. Changes in HCF have been related to osteoarthritis (OA) of the hip and knee (Felson, 2004; Lenaerts et al., 2009). However, experimental measurement of HCFs is not trivial and relies on the use of instrumented prostheses in hip arthroplasty patients (Bergmann et al., 1993; Bergmann et al., 2001). Therefore, data collection is limited to a selected group of patients who underwent total hip surgery, resulting in a relatively small and specific dataset. Alternatively, musculoskeletal models in combination with dynamic simulations of motion have been used to calculate muscle forces and joint contact forces, so that larger populations comprising both healthy and diseased subjects can be studied.

The calculation of joint contact forces relies on the use of musculoskeletal models in combination with an optimisation procedure to determine the muscle force distribution (Heller et al., 2001; Stansfield et al., 2003; Lenaerts et al., 2008; Modenese et al., 2012). The resulting calculated joint forces have previously been validated using instrumented prostheses (Bergmann et al., 2001; Heller et al., 2001; Stansfield et al., 2003; Modenese et al., 2012). Most analyses use a static optimisation (SO) technique to calculate muscle forces. SO uses an inverse dynamics approach: joint moments are used as a constraint to calculate individual muscle forces that satisfy the moment equilibrium at each time frame by minimising muscle activation or muscle stress. As such, this method is a simplification of muscle physiology and does not account for muscle dynamics. Therefore, alternative methods were developed. Computed muscle control (CMC) (Thelen et al., 2003) combines a forward integration of the dynamic equations with a static optimisation to compute muscle excitations and muscle forces respectively, and therefore complies with time dependency of force production. Alternatively, the physiological inverse approach (PIA) includes muscle activation and contraction dynamics to calculate muscle forces and optimises performance globally over time (De Groote et al., 2009). Several authors have compared the effect of different optimisation techniques on calculated muscle activations (Anderson et al., 2001; De Groote et al., 2009; De Groote et al., 2012) and compared them to experimentally measured electromyography (EMG) signals. Some have shown there is not much difference between static and dynamic simulations (Anderson et al., 2001). Others show that PIA produces excitations and activations in closer agreement with the EMG signals (De Groote et al., 2009; De Groote et al., 2012).

However, the effect of specific muscle optimisation techniques on calculated HCFs is not documented, while the optimisation method and related boundary conditions used to calculate muscle forces can be assumed to strongly influence the calculated joint contact forces (Correa et al., 2010). This effect of specific muscle optimisation techniques on calculated HCFs is

important to acknowledge when utilizing these forces as loading conditions in orthopaedic research applications, to study for example implant loading and bone adaptation (Speirs et al., 2007; van der Ploeg et al., 2012; Pankaj, 2013). Hence, the effect of the optimisation technique on the output parameters is analysed, as this may influence such research applications. Therefore, the goal of this study was to quantify differences in 1) muscle forces and 2) the magnitude and orientation of the resultant HCFs when using four optimisation techniques. Calculated HCFs were additionally compared against contact forces measured using instrumented prostheses (the HIP98 dataset (Bergmann et al., 2001)).

Methods

Movement analysis

Five healthy subjects (age 56 ± 3 yrs., range 52-61 yrs.; BMI 22.3 ± 1.59 , range 20.6-24.0), 2 male and 3 female, were included in the study and signed informed consent. All subjects performed gait at self-selected speed (walking speed 1.28 ± 0.13 m/s, range 1.1 - 1.4 m/s) as well as a sit to stand movement (sit to stand time 0.60 ± 0.09 s, range 0.51 - 0.69 s) from an adjusted stool position imposing a 90° knee flexion angle. The sit to stand movement was defined from the moment of lift-off from the stool until the moment of minimal vertical ground reaction force after lift-off, i.e. just before standing upright (McGibbon et al., 2004). A Plug-in-Gait marker set containing lower limb and trunk was used (Davis et al., 1991) including a three-marker cluster on both upper and lower legs and one additional marker on both medial knees and ankles during the static trials. Thus, a total of 40 markers were included. 3D marker trajectories were captured using Vicon (100 Hz, VICON, Oxford Metrics, Oxford, UK) and force data was measured using two AMTI force platforms (1500 Hz, Advanced Mechanical Technology Inc., Watertown, MA).

Musculoskeletal Modelling

The Gait2392 musculoskeletal model installed with OpenSim (Delp et al., 2007) was used, which consists of 12 segments, 19 degrees of freedom and 92 musculotendon actuators. Simulations and analyses were performed in OpenSim 2.4.0 (Delp et al., 2007). To calculate HCFs, the model was first scaled based on the marker locations in a static pose. The scaled model was then used for an inverse kinematics procedure based on measured 3D marker trajectories to determine the kinematics of the movement. Subsequently, a residual reduction algorithm (RRA) (Thelen et al., 2006) was applied, which minimises the dynamic inconsistency between ground reaction forces and whole body kinematics introduced by errors in modelling and marker kinematics. This inconsistency is compensated by changing the kinematics

and by adjusting the mass of the segments and the centre of mass of the torso. Since RRA is only applicable if ground reaction forces, exerted on both feet, are available, the gait cycle was restricted from toe off of the left leg until heel strike of the right leg.

To calculate muscle forces, four different methods were used. First, we used the static optimisation procedure as provided in OpenSim (SO1) (Anderson et al., 2001). Muscle forces at each time instance of the movement are calculated while minimising the instantaneous total squared muscle activation. A quadratic optimisation criterion was adopted, since this has shown to produce the best agreement between EMG and muscle forces and reliably predict measured hip contact forces (Modenese et al., 2011). This method further includes muscle force-length-velocity relationships and reserve actuators that are activated whenever the total muscle moment is insufficient to balance the net joint moment. A second static optimisation procedure (SO2) was developed in-house, based on Lenaerts et al. (2008). This optimisation uses a cost function similar to SO1, but adds constraints to the cost function to impose a physiological increase and decrease of muscle activation in time. In addition to the work of Lenaerts et al. (2008), passive muscle forces were accounted for following the work of Rodrigo et al. (2008). Thirdly, we used CMC (Thelen et al., 2003) which combines a static optimisation with feedforward and feedback controls to calculate muscle excitations, and subsequent muscle forces. As this method is based on a forward simulation, the time dependency of the activation and contraction dynamics is explicitly accounted for. Fourthly, we applied the PIA (De Groote et al., 2009), which globally optimises squared muscle activations over the complete movement cycle while imposing muscle activation and contraction dynamics. The objective functions for all methods are provided in appendix A. The muscle forces were normalised to body weight and compared between the four methods. At the first and second peak, the magnitudes of the muscle forces were summed to indicate the total muscle load calculated by the optimisation techniques.

Finally, for the four methods, HCFs of the right leg were calculated using the JointReaction analysis in OpenSim (Steele et al., 2012). The time history of model-based HCFs as well as muscle activations and forces are provided in the supplementary material.

Validation of the muscle activations

During all trials, the EMG activity of the mm. tensor fasciae latae, rectus femoris, biceps femoris, medial hamstrings, gluteus maximus and the posterior, medial and anterior bundles of the m. gluteus medius were recorded using a wireless EMG system (Zero-wire EMG, Aurio, Milan, Italy). After appropriate skin cleaning, disposable surface electrodes (Pre-gelled Nutrode mini P10M0, 30 mm diameter, GE Medical Accessories Europe) were placed

following the SENIAM guidelines (Hermens et al., 2000) and based on manual palpation. EMG signals were band pass filtered (4th order, zero-lag Butterworth filter, cut-off-frequency between 20 and 400 Hz), rectified and then low pass filtered (4th order, zero-lag Butterworth filter, cut-off frequency of 10 Hz) (Steele et al., 2012). All signals were normalised to their maximum in the gait cycle or sit to stand movement. The muscle activations were calculated using the four optimisation methods and compared to the measured EMG signals.

Validation of the hip joint contact forces

The calculated HCFs were evaluated against contact forces measured in four subjects (age 62 ± 11 yrs., range 51 - 78 yrs.; BMI 29.0 ± 2.65 , range 26.2 - 32.6) with instrumented hip implants (HIP98) (Bergmann et al., 2001) during walking (walking speed 1.18 ± 0.12 m/s, range 1.08 - 1.35 m/s) and rising from a chair (sit to stand time 0.81 ± 0.03 s, range 0.76 - 0.82s).

Data Analysis

For each of the four optimisation methods the magnitude of the resultant HCFs were calculated per subject, both for gait and sit to stand. HCFs were normalised to body weight (BW) for comparison between optimisation techniques. For comparing with HIP98, HCFs were normalised to the peak in ground reaction force (pGRF) (Martelli et al., 2011) to better accommodate for differences in gait dynamics between subjects. The contact forces were subsequently averaged over the subjects by calculating 'typical signals' (Bender et al., 2012). This was done for the minimum, maximum, 25th and 75th percentile, median and average of the normalised resultant forces of the five subjects, respectively. Similarly, typical signals were calculated for the HCFs measured in the four HIP98 subjects.

During normal gait, the HCF measured in instrumented prostheses shows two peaks, i.e. at 15 - 20% of gait cycle (first peak) and at 45 - 55% of gait cycle (second peak). Muscle forces were compared between optimisation techniques at these two peaks in gait and at the peak in sit to stand. Subsequently, the difference between HIP98 and the calculated HCFs at these peaks was determined. Furthermore, the 3D orientation of the HCF was averaged over subjects and compared with the orientation of the typical signal in the HIP98 dataset.

Results

Hip contact forces

For gait trials, the CMC contact forces were highest throughout the entire gait cycle (Figure 1A). The other optimisation techniques resulted in rather similar HCF patterns, especially during stance phase. During swing phase, a more distinct difference was seen with the lowest

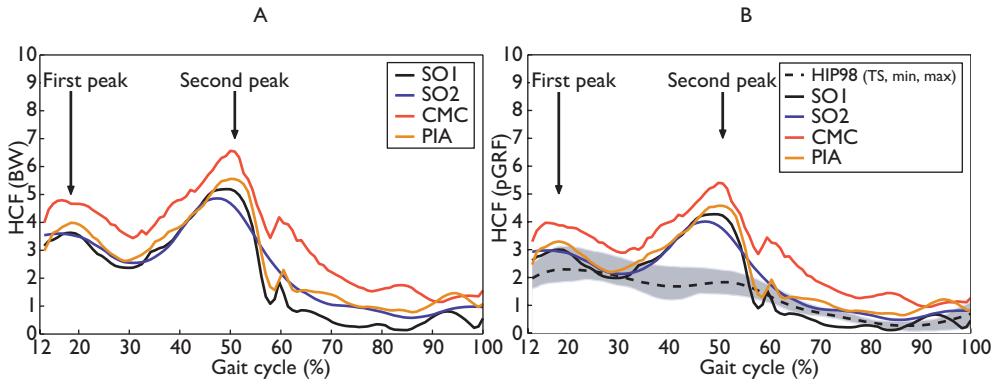


Figure 1. A) Average hip contact forces (normalised to body weight (BW)) over the five subjects for gait calculated using different optimisation techniques, shown from toe off of the left leg until heel strike of the right leg. Two peaks were defined, i.e. the first (at 15-20% of gait cycle) and second peak (at 45-55% of gait cycle). B) Calculated hip contact forces compared with experimental hip contact forces from HIP98. HCFs were normalised to the peak in ground reaction force (pGRF) to account for the differences in gait dynamics between subjects.

average HCF for SO1 (Figure 1A). At the first peak, the contact forces calculated using CMC was highest (median of 3.9 pGRF), while both static optimisations were closest to HIP98 forces (median of 3.0 and 3.1 pGRF for SO1 and SO2, respectively; Figure 2A). The PIA calculated contact forces close to SO1 and SO2 (median of 3.2 pGRF). At the second peak (Figure 2B), again HCFs were highest when using CMC (median of 5.6 pGRF). All optimisation techniques tended to overestimate the HCF compared to the measured forces (Figure 1B, Table 1). The 3D orientation angles of the calculated HCFs were very similar, but they differed from the HCF described in HIP98. At both peaks in the gait cycle, calculated HCFs generally resulted in a more anterior and medial loading compared to the HIP98 data (Figure 3 A and B). For sit to stand trials, the use of CMC induced the largest HCF (Figure 4A, Table 1). When using both SO techniques, peak contact forces, just after lift-off, were closest to the measured HIP98 data (median of 4.7 and 5.3 pGRF for SO1 and SO2, respectively; Figure 5). HCFs resulting from PIA were only slightly lower than for CMC at the peak (median of 5.6 and 5.9

Table 1. The range of differences between calculated HCF and HIP98 [%] among subjects at the first and second peak in gait and at the peak during sit to stand. HCFs were calculated using different optimisation techniques and normalised to the peak in ground reaction force (pGRF) to account for the differences in gait dynamics between subjects.

		SO1	SO2	CMC	PIA
Gait	Difference with HIP98 at the first peak [%]	4.5-56	3.6-47	46-88	12-69
	Difference with HIP98 at the second peak [%]	56-162	62-139	120-238	72-187
Sit to stand	Difference with HIP98 at the peak [%]	20-67	32-76	34-127	38-118

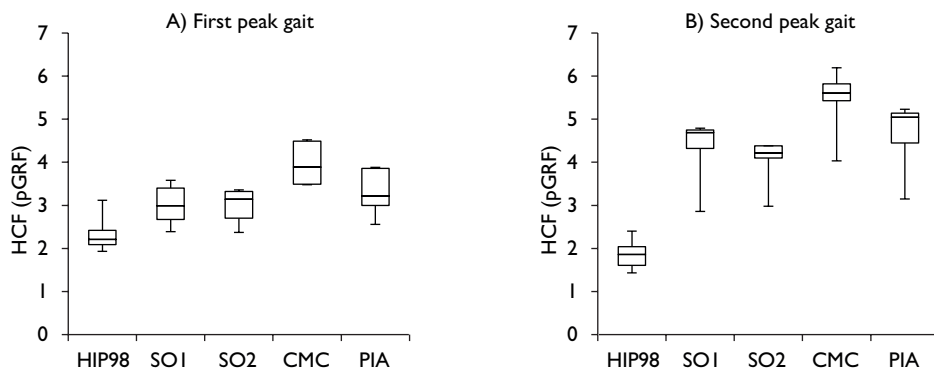


Figure 2. Distribution of hip contact force (normalised to the peak in ground reaction force (pGRF)) among subjects at the first (A) and second peak (B) during a gait cycle using different optimisation techniques. The minimum, 25th percentile, median, 75th percentile and maximum values are shown.

pGRF respectively), but were closer to measured data in the second part of the movement (Figure 4B). The calculated orientation angles showed that HCFs presented a more anterior and lateral loading than in HIP98 (Figure 3C). The use of PIA resulted in an orientation angle that was most comparable to HIP98.

Muscle forces

The sum of the magnitudes of the muscle forces calculated by CMC was higher than for other optimisation techniques at both HCF peaks during walking and at the HCF peak during sit to stand (Figure 6). Muscle forces calculated by PIA are slightly lower during gait and more comparable to SO1 and SO2 in sit to stand. At the second peak in gait the total muscle force found for CMC was up to 22% larger compared to SO2. Specifically, the force calculated for the bundles of the gluteus maximus (first peak) and medius (second peak) were higher for CMC. Appendix B shows the results of a qualitative comparison between the average normalised EMG activation patterns and the average muscle activation patterns calculated using the different optimisation techniques.

Discussion

This study compared muscle forces and the subsequent HCFs calculated using four different optimisation techniques. CMC calculated the largest sum of muscle forces for both gait and sit to stand while particularly SO2 calculated lower forces (Figure 6). The same trend was seen in the calculation of the HCFs; both static optimisation techniques showed the lowest HCFs. The additional constraints to include a physiological increase and decrease of muscle activation in time and the inclusion of passive muscle forces (SO2) did not majorly affect the

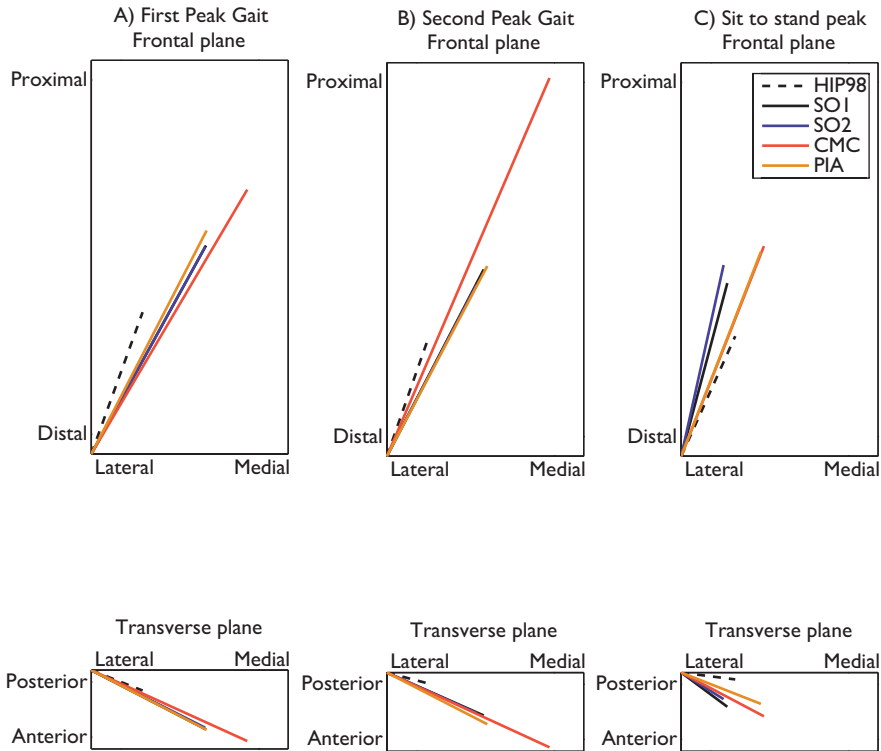


Figure 3. Direction of hip contact force (HCF) in the frontal and transverse planes calculated using different optimisation techniques and measured in vivo (HIP98), at the first (A) and second peak (B) during gait and at the peak HCF during sit to stand (C). The force vectors of the different optimisation techniques have a similar direction and are therefore difficult to distinguish.

HCFs compared to a standard SO formulation (SO1, Figure 1A). In contrast, HCFs increased drastically when using CMC (Figure 1A). The agreement in HCF between SO techniques and PIA shows that the activation and contraction dynamics can be integrated without inducing an excessive overestimation of the HCFs as observed by CMC.

There may be two causes for the increased muscle force production found for CMC relative to other optimisation techniques. First, the higher muscle forces may reflect co-contraction of agonists and antagonists to satisfy the 3D joint moments around the hip, which may explain the increased HCFs found for this method. More specifically, a post hoc analysis of the muscle moments of the primary muscles acting around the hip joint confirmed these co-contractions, particularly at the second peak in gait (Figure 7B). At this time instant, an internal hip abduction and flexion moment is present. The recruitment of the bundles of the gluteus medius muscle induces this hip abduction moment, but also produces a hip extension

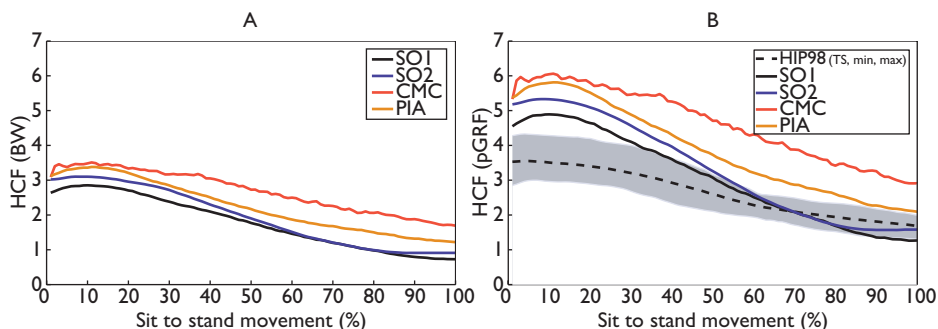


Figure 4. A) Average hip contact forces (normalised to body weight (BW)) over the five subjects for sit to stand calculated using different optimisation techniques. B) Calculated hip contact forces compared with experimental hip contact forces from HIP98. HCFs were normalised to the peak in ground reaction force (pGRF) to account for the differences in motion dynamics between subjects.

moment. Therefore additional contraction of the mm. iliacus and psoas is induced to deliver the required hip flexion moment. Although this co-contraction is seen in all optimisation techniques, for both peaks in gait (Figure 7A and B) and sit to stand (Figure 7C), the effect is largest for CMC. This may be explained by the fact that passive muscle forces and muscle dynamics are accounted for. More specifically, muscle forces cannot change instantaneously due to activation and contraction dynamics and hence force build-up in the agonists will coincide with force build-off in the antagonists.

The second possible cause for the increased muscle and contact force found by CMC could be the fact that this implementation allows for calculating a muscle generated moment that deviates slightly more from the moment necessary to counteract the net joint moments. This results in a larger difference between the muscle generated moments and net joint moments,

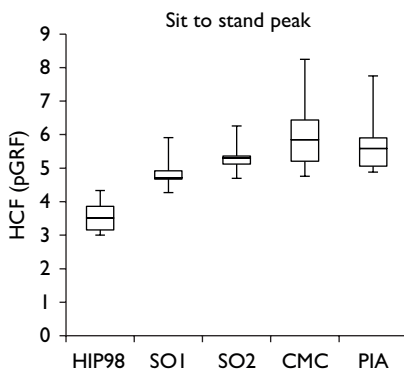


Figure 5. Distribution of hip contact force (normalised to the peak in ground reaction force (pGRF)) among subjects at the peak in sit to stand using different optimisation techniques. The minimum, 25th percentile, median, 75th percentile and maximum values are shown.

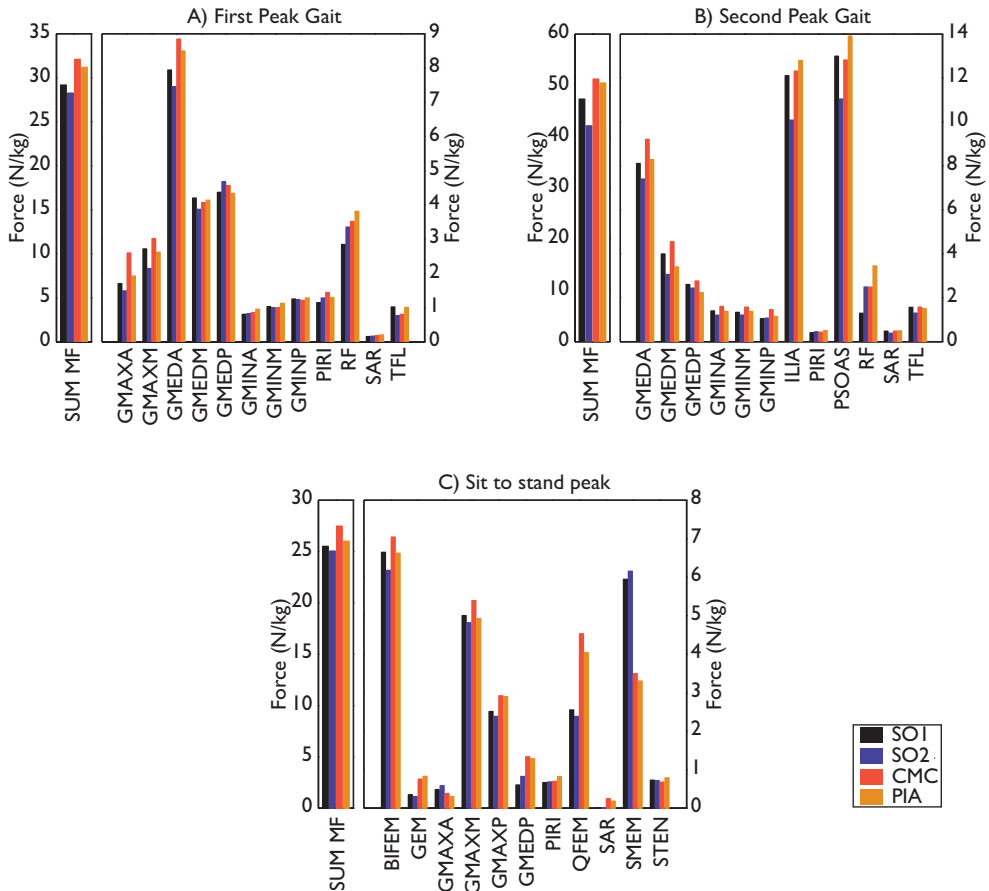


Figure 6. Calculated muscle forces and sum of the muscle forces (SUM MF) for the different optimisation techniques for the first and second peak in gait (A and B respectively) and peak in sit to stand (C). The most active muscles spanning the hip joint are shown. The force delivered by other muscles is generally lower than 1 N.

mainly in the frontal and sagittal planes (Figure 8). Although defined in different manners, all optimisation techniques allow for a deviation from the net joint moment. Largest deviations were found for CMC, mainly for abduction. This might be explained by the feedforward and feedback controls imposed by CMC for tracking the kinematics combined with the physiological constraints on muscle force rise and decay which cause increased muscle generated moments around the hip.

HCFs calculated using CMC deviated most from other optimisation techniques, especially during gait trials (Figure 1B). Since the input (musculoskeletal model, kinematics and ground reaction forces) was identical for all of the optimisation procedures, the differences in the resulting HCFs must be attributed to the different optimisation techniques. However, all techni-

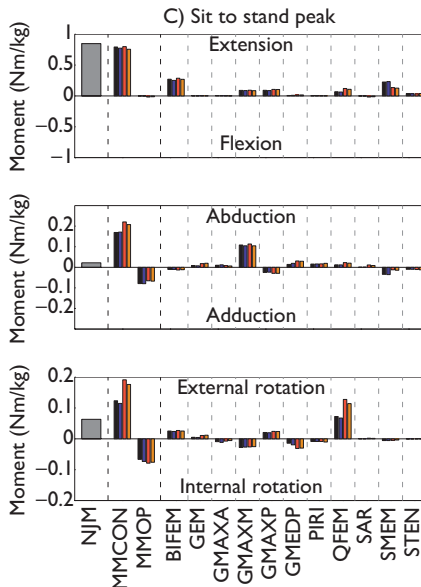
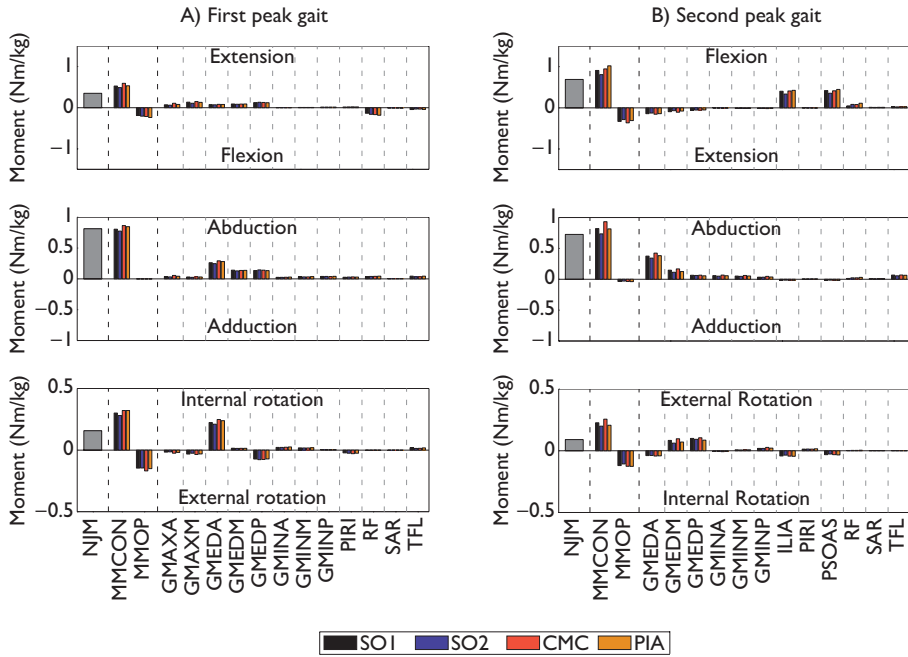


Figure 7. Contribution of muscles to the hip moments at the first (A) and second (B) peak during gait and the peak in sit to stand (C). NJM is the net the joint moment calculated using an inverse dynamics procedure, MMCON and MMOP are respectively the sum of muscle moments contributing to and opposing the net joint moment. Note the different scales on the vertical axes.

ques systematically overestimated the magnitude of the HCFs as compared to those measured using instrumented prostheses (Bergmann et al., 2001). In addition to overestimated magnitudes, the calculated contact forces showed a more out of plane loading of the hip joint in the frontal plane, i.e. a more anterior loading (Figure 3). These differences with the HIP98 data may have arisen from modelling choices that were made before the optimisation step, since there are many parameters in musculoskeletal models, e.g. attachment points, number of muscles in the model and muscle parameters that affect the estimated muscle forces and the consequential effect on the HCF. Hence, further research is warranted to unravel the complexity of these issues to obtain more robust and reliable musculoskeletal predictions. Additional contraction was seen in all optimisation techniques, for both peaks in gait and sit to stand, which may partly explain the overestimation on HIP98. The optimisation procedures solve the redundancy problem by minimising the total of the squared muscle activations after the joint moment equilibrium at the hip and other joints of the lower limb have been satisfied. The resulting co-activations will contribute to the overestimation of the contact forces (Pedersen et al., 1987). Specifically at the second peak in gait, large opposing moments are found in the sagittal and transversal planes (Figure 7B). At the first peak in gait, only mm.

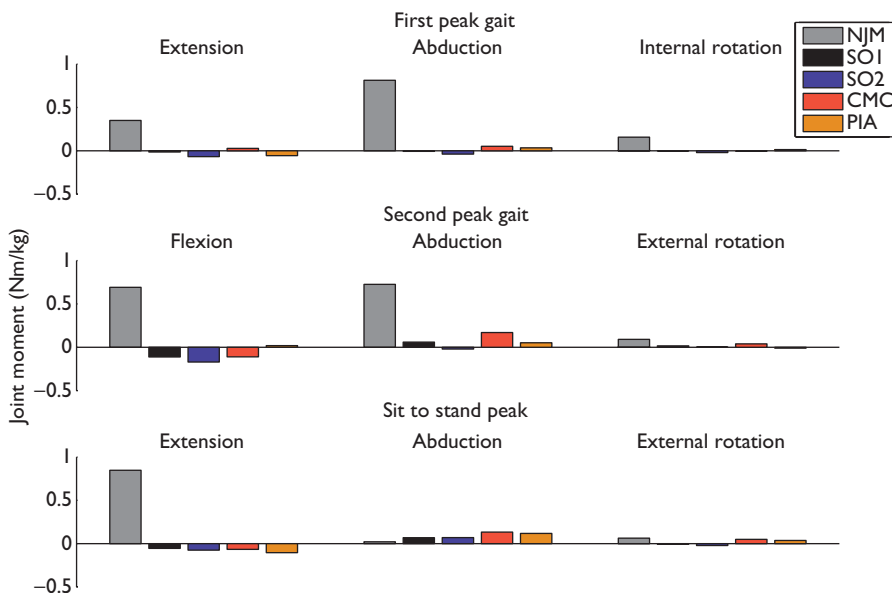


Figure 8. Net joint moment (NJM) and the difference between absolute muscle generated moment and net joint moment for the different optimisation techniques, e.g. the deviation from the net joint moment. When the net joint moment is satisfied by the optimisation, the muscle moment and joint moment will be equal, i.e. the difference between muscle moment and net joint moment is zero.

rectus femoris and tensor fasciae latae opposed the required extension moment (Figure 7A) which may explain why HCF overestimations were lower at this time instance. Also for sit to stand overestimations of HCFs were lower compared to the first peak in gait, as none of the recruited muscles opposed the external flexion moment (Figure 7C).

The overestimation of joint contact forces has been described before. Klein Horsman (2007) compared one young and healthy subject with the HIP98 data, using inverse forward dynamic optimisation (van der Kooij et al., 2003) and an energy related criterion (Praagman et al., 2006) and found that the second peak was 200% larger than the measured HCF. Although a different muscle optimisation technique was used, the magnitude of the second peak was also much larger than the first peak, and comparable to the present study. Moreover, Mellon et al. (2013) found contact forces up to 229% larger than those found by Bergmann et al. (2001), although this difference was not statistically significant. For sit to stand more comparable results were found.

In contrast, several other studies showed HCFs that are closer to HIP98 data than those reported in the current study (Heller et al., 2001; Stansfield et al., 2003; Martelli et al., 2011; Modenese et al., 2012), which may be attributed to different modelling choices. First of all, these simulations were based on the subjects from the HIP98 dataset (Heller et al., 2001; Stansfield et al., 2003; Modenese et al., 2012) and therefore differences between healthy subjects and the HIP98 patients were not applicable. Furthermore, Stansfield et al. (2003) used a static optimisation which included a minimization of the contact forces. This additional criterion redistributes muscle forces to synergists without increasing the HCF. Heller et al. (2001) used a linear optimisation that minimised the sum of muscle forces and limited the maximal muscle force. Furthermore, others showed that the number of muscles and lines of action in the musculoskeletal model affect the HCF (Modenese et al., 2012). Besides that, several studies included subject-specific information in their models. Martelli et al. (2011) included a subject that was body-matched to the cadaver from which a subject-specific model was created. Alternatively, CT images have been used to further personalise the model (Stansfield et al., 2003; Mellon et al., 2013). Comparing these studies to the results in the current work show that musculoskeletal modelling involves many steps starting from kinematic and kinetic measurements, the choice of a musculoskeletal model, adapting that model to the subject-specific anatomy and the choice of an optimisation criterion. All these steps have a major effect on the end results, however, in this study we only focussed on the potential effects of the choice of optimisation technique.

When interpreting the results of this study, a number of limitations should be taken into account. The calculated muscle activations compared only moderately to experimental EMG

for both gait and sit to stand (appendix B), which has been reported in previous research as well (Anderson et al., 2001; De Groote et al., 2009; De Groote et al., 2012). However, since only very few muscles around the hip can be appropriately measured using surface EMG, the comparison of activation to EMG signals can only partially reflect the effect of the optimisation techniques.

As a second limitation, we used experimental data from healthy subjects to calculate HCFs and compared these to an average HCF measured in four patients with instrumented prostheses. Consequently, observed differences between measured and calculated HCFs may partially result from subject characteristics. First, gait speeds in our population of control subjects were higher than in the normal walking trials in HIP98 (1.28 m/s vs. 1.18 m/s), which can lead to increased contact forces (Bergmann et al., 2001). Second, hip moments were generally lower in the HIP98 patients than in our healthy control subjects, mainly around 50% of the gait cycle (in hip flexion 3.5 vs. 6.7 % BW*m and in hip adduction 6.5 vs. 7.2 % BW*m). These higher external moments determine the muscle forces that need to be produced to satisfy the moment equilibrium and therefore influence the HCF. A fairer comparison would have been to calculate the HCFs using the experimental data made available via Orthoload (Bergmann, 2008) and compare them with their measured HCFs. However, the restricted number of experimental markers made the calculation of the joint angles highly sensitive to the marker definition in the model, which could only be partially reproduced based on the available documentation.

In conclusion, this study showed that the calculation of hip contact forces was sensitive to the optimisation method used to calculate muscle forces. Both SO techniques produced results closest to measured HCFs, while CMC calculated the highest HCFs. PIA showed that activation and contraction dynamics can be included in the optimisation without excessively increasing contact forces. However, other modelling choices had a distinct effect on the calculated loads as well, although identification of these factors was not within the scope of this study. Further research is therefore required to assess the effects of other modelling steps to come to a valid and robust prediction of muscle and joint contact forces in the lower limb.

Acknowledgments

This work was funded by the Agency for Innovation by Science and Technology (IWT-TBM no. 100786), Fonds NutsOhra and the Dutch Cancer Society.

Appendix A. Objective functions

Four different optimisation techniques were used to calculate muscle forces. To solve the redundancy problem, each method minimises an objective function.

SO1 (Anderson et al., 2001)

This static optimisation uses an inverse dynamics approach. It uses the joint moments to calculate individual muscle forces that satisfy the moment equilibrium at each time frame by minimising the total squared muscle activation. It minimises the objective function:

$$J = \sum_{m=1}^n (A_m(t_i))^2,$$

where n is the number of muscles and $A_m(t_i)$ is the activation level of muscle m (limited between 1 and 0) at time instant t_i . The force generated by the muscle to satisfy the moment equilibrium is constrained by the force-length-velocity relationship:

$$\sum_{m=1}^n [A_m(t_i)F_{max,m}(t_i)]r_{m,k}(t_i) = M_{joint,k}(t_i),$$

where $F_{max,m}(t_i)$ is the maximal force-generating capacity of muscle m , taking into account the force-length-velocity relationship of the muscle; $r_{m,k}$ is its moment arm about the k^{th} joint axis and $M_{joint,k}(t_i)$ represents the joint moment. Reserve actuators are included which are activated whenever the total muscular moment is insufficient to balance the net joint moment.

SO2 (Lenaerts et al., 2008)

The second static optimisation also calculates muscle forces that satisfy the moment equilibrium at each time frame by minimising the total squared muscle activation. However, additional constraints are imposed on the muscle activation values to impose a physiological increase and decrease in muscle activation. Furthermore, in this optimisation the joint moments are included with a weight factor W (in squared muscle activation per Newton-meter) in the cost function. In contrast to SO1, the joint moment term also includes passive muscle forces (Rodrigo et al., 2008). The cost function that is minimised is:

$$J = \sum_{m=1}^n [A_m(t_i)]^2 + W \sum_{k=1}^K w_k \left[M_{joint,k}(t_i) - \sum_{m=1}^n r_{m,k}(t_i) \left(F_{min,m}(t_i) + A_m(t_i) \left(F_{max,m}(t_i) - F_{min,m}(t_i) \right) \right) \right]^2,$$

where K are the degrees of freedom, W and w_k are weight factors; and $F_{min,m}(t_i)$ and $F_{max,m}(t_i)$ are the minimal and maximal force-generating capacity of muscle respectively, taking into

account the force-length relationship of the muscle. The minimal muscle force $F_{min,m}(t)$ is the passive force generated by a muscle that is not activated. The optimisation is constrained by:

$$A_m(t_i) \leq 1 - (1 - A_m(t_{i-1})) \exp\left(\frac{-\Delta t}{\tau_a}\right)$$

$$A_m(t_i) \geq A_m(t_{i-1}) \exp\left(\frac{-\Delta t}{\tau_d}\right)$$

where Δt is the time between two time instants (1/sample frequency); and τ_a (11 ms) and τ_d (68 ms) are the activation and deactivation time constants respectively (Raasch et al., 1997). This way a physiological increase and decrease in muscle activation is imposed.

CMC (Thelen et al., 2006)

Computed muscle control combines a forward integration of the dynamic equations with a static optimisation to compute muscle excitations, and muscle forces respectively. The time dependency of the excitation and contraction dynamics is therefore explicitly accounted for. In a first step, a set of desired joint angular accelerations that will drive the model coordinates toward the experimental coordinates is computed:

$$\ddot{q}_k^{des}(t_{i+1}) = \ddot{q}_k^{exp}(t_{i+1}) + k_v[\dot{q}_k^{exp}(t) - \dot{q}_k(t)] + k_p[\bar{q}_k^{exp}(t) - \bar{q}_k(t)],$$

where \ddot{q}_k^{des} are the desired joint angular accelerations; \bar{q}_k^{exp} , \dot{q}_k^{exp} , \ddot{q}_k^{exp} are the generalised positions, velocities and accelerations respectively derived from gait analysis; \bar{q}_k , \dot{q}_k are the model joint position and velocity respectively; and k_v and k_p are feedback gains for the velocity and position errors respectively.

Next, a static optimisation is used to compute a set of desired muscle forces that produce the desired accelerations and minimise the cost function:

$$J = \sum_{m=1}^n A_m^2 + \sum_{k=1}^K w_k (\ddot{q}_k^{des} - \ddot{q}_k)^2,$$

where \ddot{q}_k is the model joint acceleration. Muscle excitations are then input into the forward dynamic simulation and held constant during integration of the entire set of system state equations from t_i till t_{i+1} .

PIA (De Groot et al., 2012)

The physiological inverse approach also includes activation and contraction dynamics, but optimises performance globally over time. The global performance criterion (f_{per}) sums the sum of squared activation across all muscles, over all time instants:

$$f_{per} = \sum_{i=1}^I \sum_{m=1}^n (A_m(t_i))^2,$$

Skeleton dynamics is imposed by appending the following penalty term to the performance criterion:

$$f_{pen} = W \sum_{k=1}^K \sum_{i=1}^I \left(w_i \cdot \left(M_{joint,k}(t_i) - \sum_{m=1}^n r_{i,m,k} F_{i,m} \right) \right)^2,$$

where I is the total number of frames, $F_{i,m}$ is the muscle force and w_i is a weight factor defined as:

$$w_i = \frac{1}{\max_i (M_{joint,k}(t_i))}.$$

The objective function then results in:

$$J = f_{per} + f_{pen}.$$

Appendix B. Validation of muscle activations

Average muscle activation patterns during gait are depicted in Figure S1, showing that the high activation levels of the glutei muscles were fairly well predicted in the first part of the gait cycle. However, calculated activations remained high for a longer time period and dropped more suddenly than experimentally measured EMG. The rectus femoris showed aberrant activations compared to EMG, which has been reported before (Lenaerts et al., 2009). Besides that, variation was large within the group of subjects, which may indicate some corrupted signals, possibly due to cross talk. In addition, gait speed can be of influence on the shape of the signals and therefore might also partially explain the variation between the different subjects (Barr et al., 2010). Comparing the different optimisation techniques, Figure S1 shows that SO1 and SO2 as well as PIA resulted in comparable activation patterns. In addition, CMC muscle activations for the m. biceps femoris were much higher than for the other optimisation techniques and compared poorly to EMG.

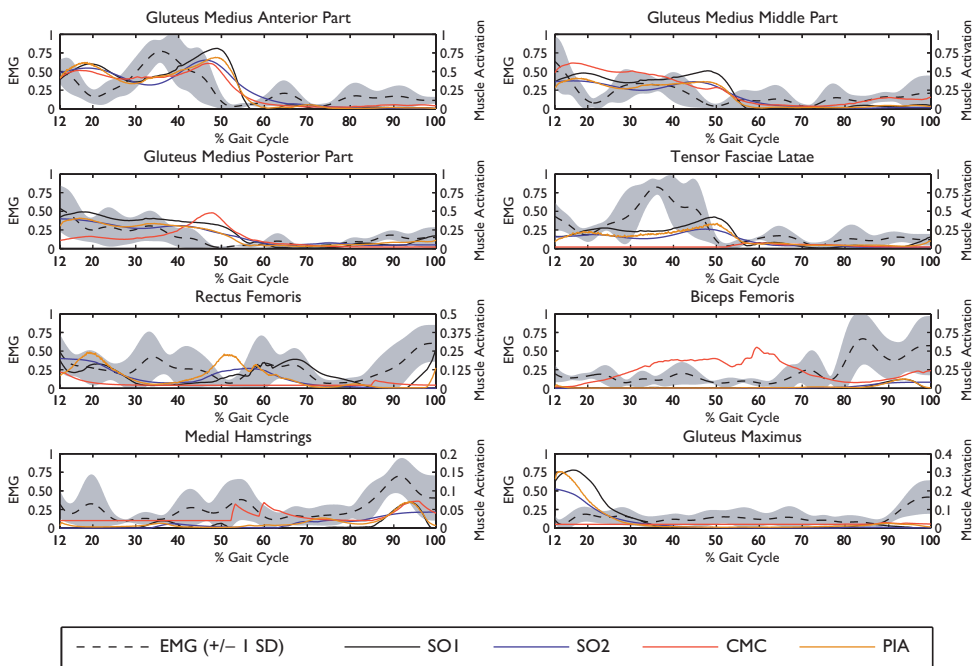


Figure S1. Muscle activations during gait, recorded using EMG and calculated using different optimisation techniques, shown from toe off of the left leg until heel strike of the right leg..

For sit to stand, activation of all parts of the m. gluteus medius and tensor fasciae latae was very low (Figure S2). Results therefore poorly compared to EMG signals, as for muscles that do not show a high activation, EMG will be normalised to a relatively low value. This results in apparently high activations, which will emphasise any irregularities in the signals. The decreasing activation for the mm. rectus femoris, and gluteus maximus after lift-off agreed between EMG signals and calculated activations. When comparing activations calculated using the different optimisation techniques, SO2 and CMC showed a much higher activation for the medial hamstrings, while SO1 and PIA showed a higher activation in the m. biceps femoris.

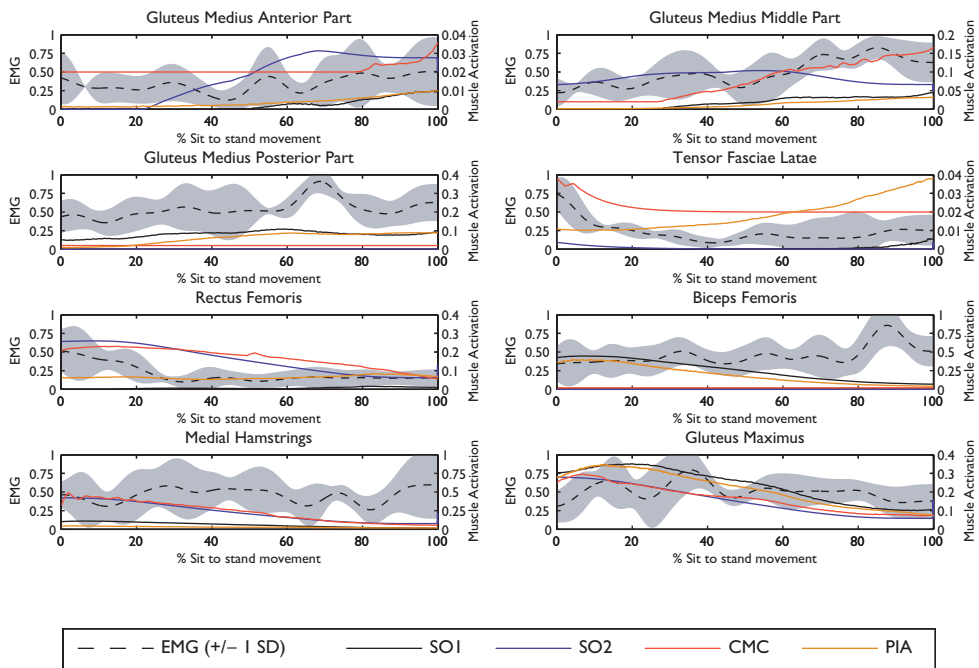


Figure S2. Muscle activations for sit to stand, recorded using EMG and calculated using different optimisation techniques.

References

- Anderson FC, Pandy MG. 2001. Static and dynamic optimization solutions for gait are practically equivalent. *J Biomech* 34(2): 153-161.
- Barr KM, Miller AL, Chapin KB. 2010. Surface electromyography does not accurately reflect rectus femoris activity during gait: impact of speed and crouch on vasti-to-rectus crosstalk. *Gait Posture* 32(3): 363-368.
- Bender A, Bergmann G. 2012. Determination of typical patterns from strongly varying signals. *Comput Methods Biomech Biomed Engin* 15(7): 761-769.
- Bergmann G (ed). 2008. Charité Universitaetsmedizin Berlin. Orthoload. Accessed 13 March 2012 from <http://www.OrthoLoad.com>.
- Bergmann G, Deuretzbacher G, Heller M, Graichen F, Rohlmann A, Strauss J, Duda GN. 2001. Hip contact forces and gait patterns from routine activities. *J Biomech* 34(7): 859-871.
- Bergmann G, Graichen F, Rohlmann A. 1993. Hip joint loading during walking and running, measured in two patients. *J Biomech* 26(8): 969-990.
- Correa TA, Crossley KM, Kim HJ, Pandy MG. 2010. Contributions of individual muscles to hip joint contact force in normal walking. *J Biomech* 43(8): 1618-1622.
- Davis RB, Ounpuu S, Tyburski D, Gage JR. 1991. A Gait Analysis Data-Collection and Reduction Technique. *Hum Mov Sci* 10(5): 575-587.
- De Groot F, Demeulenaere B, Swevers J, De Schutter J, Jonkers I. 2012. A physiology-based inverse dynamic analysis of human gait using sequential convex programming: a comparative study. *Comput Methods Biomech Biomed Engin* 15(10): 1093-1102.
- De Groot F, Pipeleers G, Jonkers I, Demeulenaere B, Patten C, Swevers J, De Schutter J. 2009. A physiology based inverse dynamic analysis of human gait: potential and perspectives. *Comput Methods Biomech Biomed Engin* 12(5): 563-574.
- Delp SL, Anderson FC, Arnold AS, Loan P, Habib A, John CT, Guendelman E, Thelen DG. 2007. OpenSim: open-source software to create and analyze dynamic simulations of movement. *IEEE Trans Biomed Eng* 54(11): 1940-1950.
- Felson DT. 2004. Obesity and vocational and avocational overload of the joint as risk factors for osteoarthritis. *J Rheumatol Suppl* 70: 2-5.
- Heller MO, Bergmann G, Deuretzbacher G, Durselen L, Pohl M, Claes L, Haas NP, Duda GN. 2001. Musculo-skeletal loading conditions at the hip during walking and stair climbing. *J Biomech* 34(7): 883-893.
- Hermens HJ, Freriks B, Disselhorst-Klug C, Rau G. 2000. Development of recommendations for SEMG sensors and sensor placement procedures. *J Electromyogr Kinesiol* 10(5): 361-374.
- Klein Horsman MD. 2007. The Twente lower extremity model: consistent dynamic simulation of the human locomotor apparatus. Thesis. University of Twente, Enschede, The Netherlands.
- Lenaerts G, De Groot F, Demeulenaere B, Mulier M, Van der Perre G, Spaepen A, Jonkers I. 2008. Subject-specific hip geometry affects predicted hip joint contact forces during gait. *J Biomech* 41(6): 1243-1252.
- Lenaerts G, Mulier M, Spaepen A, Van der Perre G, Jonkers I. 2009. Aberrant pelvis and hip kinematics impair hip loading before and after total hip replacement. *Gait Posture* 30(3): 296-302.
- Martelli S, Taddei F, Cappello A, van Sint Jan S, Leardini A, Viceconti M. 2011. Effect of sub-optimal neuromotor control on the hip joint load during level walking. *J Biomech* 44(9): 1716-1721.
- McGibbon CA, Goldvasser D, Krebs DE, Moxley Scarborough D. 2004. Instant of chair-rise lift-off can be predicted by foot-floor reaction forces. *Hum Mov Sci* 23(2): 121-132.
- Mellon SJ, Grammatopoulos G, Andersen MS, Pegg EC, Pandit HG, Murray DW, Gill HS. 2013. Individual motion patterns during gait and sit-to-stand contribute to edge-loading risk in metal-on-metal hip resurfacing. *Proc Inst Mech Eng H* 227(7): 799-810.
- Modenese L, Phillips AT, Bull AM. 2011. An open source lower limb model: Hip joint validation. *J Biomech* 44(12): 2185-2193.
- Modenese L, Phillips ATM. 2012. Prediction of hip contact forces and muscle activations during walking at different

- speeds. *Multibody System Dynamics* 28(1-2): 157-168.
- Pankaj P. 2013. Patient-specific modelling of bone and bone-implant systems: the challenges. *Int J Numer Method Biomed Eng* 29(2): 233-249.
- Pedersen DR, Brand RA, Cheng C, Arora JS. 1987. Direct comparison of muscle force predictions using linear and nonlinear programming. *J Biomech Eng* 109(3): 192-199.
- Praagman M, Chadwick EK, van der Helm FC, Veeger HE. 2006. The relationship between two different mechanical cost functions and muscle oxygen consumption. *J Biomech* 39(4): 758-765.
- Raasch CC, Zajac FE, Ma B, Levine WS. 1997. Muscle coordination of maximum-speed pedaling. *J Biomech* 30(6): 595-602.
- Rodrigo S, Ambrosio J, Tavares da Silva M, Penisi O. 2008. Analysis of Human Gait Based on Multibody Formulations and Optimization Tools. *Mechanics Based Design of Structures and Machines* 36(4): 446-477.
- Speirs AD, Heller MO, Duda GN, Taylor WR. 2007. Physiologically based boundary conditions in finite element modelling. *J Biomech* 40(10): 2318-2323.
- Stansfield BW, Nicol AC, Paul JP, Kelly IG, Graichen F, Bergmann G. 2003. Direct comparison of calculated hip joint contact forces with those measured using instrumented implants. An evaluation of a three-dimensional mathematical model of the lower limb. *J Biomech* 36(7): 929-936.
- Steele KM, Demers MS, Schwartz MH, Delp SL. 2012. Compressive tibiofemoral force during crouch gait. *Gait Posture* 35(4): 556-560.
- Thelen DG, Anderson FC. 2006. Using computed muscle control to generate forward dynamic simulations of human walking from experimental data. *J Biomech* 39(6): 1107-1115.
- Thelen DG, Anderson FC, Delp SL. 2003. Generating dynamic simulations of movement using computed muscle control. *J Biomech* 36(3): 321-328.
- van der Kooij H, van der Helm FC. 2003. Human gait analysis application of a new inverse/forward dynamic optimization (IFDO) method to solve the load sharing problem. *Proceedings of ISCSB, International symposium on computer simulation in biomechanics*. Sydney, Australia.
- van der Ploeg B, Tarala M, Homminga J, Janssen D, Buma P, Verdonchot N. 2012. Toward a more realistic prediction of peri-prosthetic micromotions. *J Orthop Res* 30(7): 1147-1154.

7

Physiological load cases combined with plasticity in patient-specific finite element models in metastatic bone disease: does it affect fracture predictions?

*Loes C. Derikx, Dennis Janssen, Yvette M. van der Linden, Mariska Wesseling,
Ilse Jonkers, Nico Verdonschot, Esther Tanck.*



Introduction

Assessing femoral fracture risks in patients with cancer and metastatic bone disease is troublesome. Despite previous efforts investigating potential determinants for such pathological fractures (e.g. Mirels (1989) and Van der Linden et al. (2003)), no predictors that identify impending fractures with sufficient sensitivity and specificity have been defined yet (van der Linden et al., 2004). These previous studies mainly included clinical features, such as the radiological appearance of the lesion or the lesion size, whereas biomechanical characteristics, such as the initial bone strength, were largely ignored. However, it is extremely difficult to capture and comprehend these biomechanical parameters in clinical fracture risk assessments. Finite element (FE) models show great promise to improve these clinical fracture risk predictions. Previous work, for the larger part *in vitro* studies, has shown that FE models predict femoral bone strength fairly accurately (Keyak et al., 2005; Bessho et al., 2007; Schileo et al., 2014). Yet, these studies used one or few simple load cases, resembling for example single legged stance (Derikx et al., 2012) or a fall (van der Zijden et al., 2015), mainly to simulate experimental loading conditions in order to validate the models. Such simplified load cases, however, do not resemble the loads imposed on the femur during daily life activities and may therefore be suboptimal for *in vivo* fracture risk predictions. Hence, the question is how to simulate femoral fracturing *in vivo*, in patients with cancer suffering from metastatic bone disease. This question comprises two different aspects.

The first aspect concerns the applied loading conditions which should obviously be as physiological as possible. Ideally, motion analysis on relevant daily activities should be performed for every individual patient. By using personalised musculoskeletal models, a tailored load case for each patient should be generated, so that hip joint forces and muscle forces at multiple instances of motion can be applied to the femur. However, metastatic bone disease severely affects the mobility of patients, due to pain and mechanical instability caused by the lesion(s) in the femoral bone. Hence, it is neither ethical nor feasible to perform gait analysis on these patients in order to develop a fully personalised FE load case. Alternatively, load cases based on the calculated hip contact forces (HCFs) and muscle forces of multiple healthy subjects could be used (rather than modelling a load case from one representative subject). In this way, some of the biomechanical variation that exists among humans could be covered.

Recent work has shown the importance of modelling multiple loading conditions. Falcinelli et al. (2014) defined a range of physiological hip contact forces, resembling different phases of gait or a fall on the greater trochanter to load the femoral FE models of osteoporotic/osteopenic patients. They showed an increased association between calculated FE bone strength and femoral fracture when modelling multiple loading conditions in these patients. Falcinelli

et al., however, only included variations in the hip contact forces. Adding muscle forces to the loading profile may constitute another step towards physiological loading conditions. This may especially hold for femurs with in metastatic lesions, in which case the bone tissue is most often very locally affected by metastases that may be located in the vicinity of muscle insertion sites.

The second important aspect is the selection of a material model that is sensitive to these variations in hip joint forces and muscle forces. In literature, FE predictions using both linear elastic material models (Schileo et al., 2014) and non-linear elastic-plastic models (Keyak et al., 2005; Tanck et al., 2009; Derikx et al., 2012) have shown to correlate well with fracture under simple loading conditions. However, it is unknown whether the modelling of multiple physiological load cases requires complex elastic-plastic material models, or whether a linear elastic simulation provides the same results in terms of fracture prediction. Namely, during cyclic loading, plastic deformation may accumulate over time, which is ignored by linear elastic calculations. More specifically, if elements in a model reach plasticity, this does not necessarily mean that the bone is failing at the structural level. However, the plasticity in a specific region will reduce the load bearing capacity of the bone. Inclusion of multiple load cases in combination with the accumulation of plasticity may therefore lead to failure loads that are lower than those calculated without considering plasticity, as is the case in linear elastic calculations. On the other hand, including plasticity increases the simulation complexity and therefore computational expenditure. If inclusion of plasticity does not alter the fracture predictions, then failure simulations can remain relatively simple by leaving out the actual simulation of plasticity.

Hence, in this study we investigated 1) whether modelling physiological load cases obtained from different healthy subjects and including hip contact as well as muscle forces majorly affect failure predictions and 2) whether non-linear elastic-plastic material properties need to be modelled to fully capture these variable effects on failure predictions. To this end, we applied the muscle forces and hip contact forces of five healthy subjects to the femurs of two patients with cancer and metastatic bone disease who sustained a pathological fracture. We compared the effects of these different load cases on the failure behaviour simulated using linear elastic as well as non-linear elastic-plastic material models, in terms of failure volume and fracture location.

Material and Methods

Patients

Two femurs of two patients diagnosed with cancer and metastatic bone disease were selected

for FE modelling. These patients were previously included in a large prospective study, of which full details are described elsewhere in this thesis (Chapter 5). In short, one patient (P1) suffered from lytic lesions in both femurs. The patient was treated for pain with multiple fraction radiotherapy and sustained bilateral femoral neck fractures during normal walking, 123 days after onset of therapy. Only the right femur of this patient was modelled in this study. The other patient (P2) suffered from both blastic and lytic lesions and sustained a spontaneous fracture through a lytic lesion under the lesser trochanter of the left femur, 7 days after treatment for pain with multiple fraction radiotherapy. Further patient characteristics are given in Table 1.

Table 1. Characteristics of the two patients included in this study.

	Patient 1 Right femur	Patient 2 Left femur
Gender	M	M
Age at inclusion	70	64
Body weight (kg)	73	90
Primary tumour	M. Kahler	Prostate
Type of fracture	Collum fracture	Subtrochanteric fracture
Activity while fracture occurred	Walking	Spontaneously

Obtaining loading conditions using musculoskeletal modelling

In a previous musculoskeletal modelling study published by our group (Wesseling et al., 2015b), five healthy subjects (HS1 to HS5, mean age 56 years, range 52-61) were included. Using different optimisation techniques, subject-specific muscle forces and HCFs were calculated during a normal gait cycle. The use of static optimisation (Anderson et al., 2001) implemented in OpenSim (Delp et al., 2007) resulted in calculated HCFs that best resembled HCFs measured *in vivo* (Bergmann et al., 2001). After additional model adaptations (Wesseling et al., 2015a) the analyses were rerun in OpenSim 3.2 (Delp et al., 2007) and used in the current study.

First, using a spline function, the data were resampled to 21 frames representing every 5% of the gait cycle. As the HCF peaks (at 15-20% and 45-55% of the gait cycle) not necessarily coincided with a resampled frame, these particular frames were specifically added to make sure the peak loads were included. In this way, the muscle forces and hip contact force during the full gait cycle were discretised to 23 frames. Subsequently, the subject-specific muscle and hip contact forces were normalised to the body weights of the two patients (P1 and P2), and transformed to the FE coordinate system, which was defined using anatomical landmarks. The hip joint centre (HJC) was determined using a sphere fit through the femoral head. Subsequent-

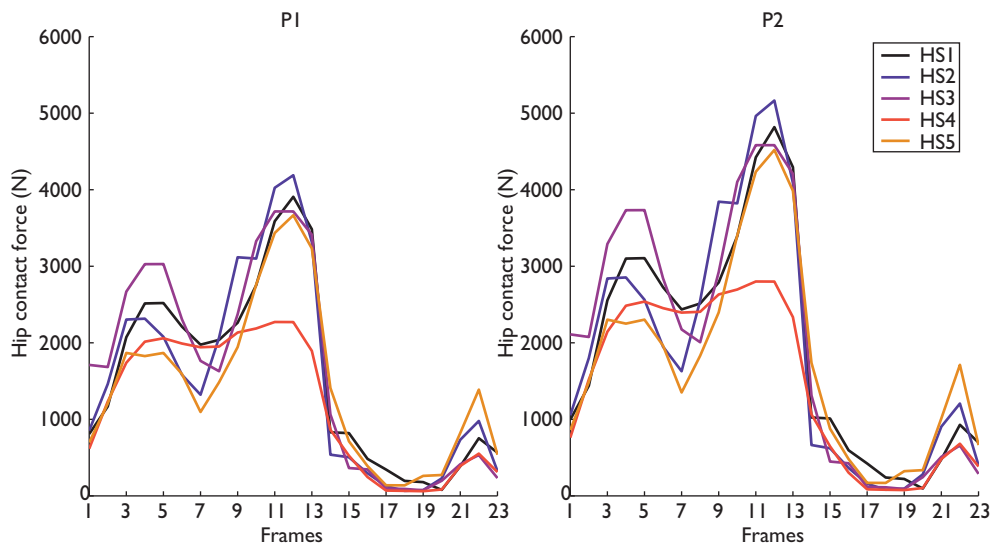


Figure 1. Magnitudes of HCF over a full gait cycle as applied to the FE models of P1 (left) and P2 (right) based on musculoskeletal modelling results of 5 healthy subjects (HS1 to HS5).

ly, the knee joint centre (KJC) was determined halfway a transcondylar axis connecting the centres of two circles fitted through the posterior condyles. The KJC defined the origin of the coordinate system. By orienting the HJC over the KJC, and using the plane defined by the transcondylar axis and the HJC, the coordinate system was defined. In this way, the femur was positioned in an orientation coming closest to the orientation in OpenSim.

Figure 1 depicts the magnitudes of the hip contact forces for each of the five healthy subjects, applied to the two patient femurs. In general, HCFs were relatively high, except for HS4. The HCFs at the second peak in the gait cycle ranged between 3.2 x BW (HS4) and 5.9 x BW (HS2). Over the full gait cycle, the applied HCF was smallest for HS4 and largest for HS3. HS1, HS2 and HS5 showed roughly the same pattern with a lower HCF at the first peak and a relatively high HCF at the second peak. The HCF at the first peak was more comparable to the HCF at the second peak for HS3 and HS4. The load directions varied between subjects at the first peak in HCF (Figure 2A) and, to a larger extent, at the second peak in HCF (Figure 2B).

FE model generation

Quantitative computed tomography (QCT) images were retrieved from the patients before they sustained a femoral fracture (Chapter 5). The following scan settings were used: 120 kVp, 220 mA, slice thickness 3 mm, pitch 1.5, spiral and standard reconstruction, in-plane resolution 0.9375 mm. The femoral bone tissue was segmented from the CT images and converted

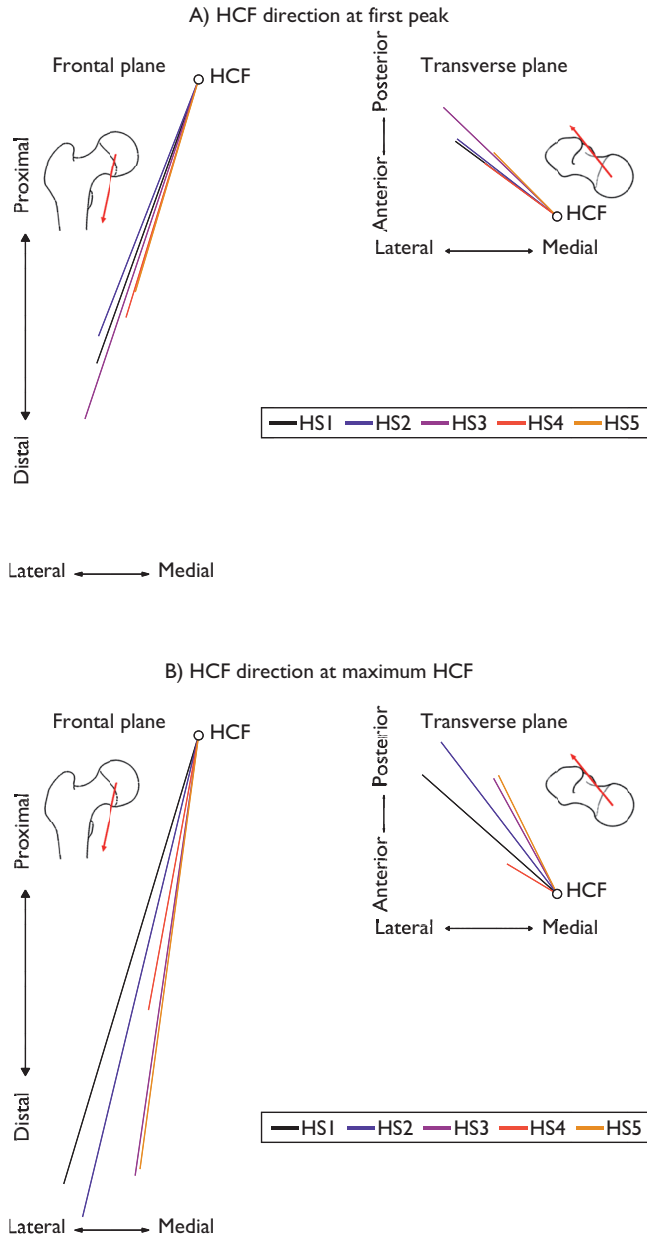


Figure 2. Direction of HCF at the instance of the first (A) and at the second peak in HCF (B) as applied to the FE models, based on musculoskeletal modelling results of 5 healthy subjects (HS1 to HS5). Schematic femur outlines and resultant HCF (red arrows) are given for interpretation of the results.

to a 3D surface (Mimics 11.0, Materialise, Leuven, Belgium) and solid mesh (Patran 2005 r2, MSC Software Corporation, Santa Ana, CA, USA). This solid mesh was translated and rotated to the neutral anatomical position, using the anatomical landmarks described above.

Patients were scanned on top of a calibration phantom, which was positioned at the level of the proximal femur (Image Analysis, Columbia, KY, USA). Using this phantom, the CT intensities of voxels representing bone tissue could be converted to calcium equivalent values. Based on the work by Keyak et al. (2005), these calcium equivalent values were converted to ash densities and linear elastic and non-linear elastic-plastic material properties, respectively. Muscle attachment sites at the proximal femur (50% of total length) were morphed from the musculoskeletal models of the healthy subjects to the patient femurs (Redert et al., 1999). Muscle forces were then applied to the node closest to the morphed attachment site (Figure 3).

For application of the HCF to the FE model a hemispherical cup was used. This cup was positioned such that it resembled the neutral anatomical position of the acetabulum; its size was adapted to the size of the femoral head of the patient. A node defined in the hip joint centre served as a control node for the cup. The HCF was applied to this control node, thereby loading the femoral head via the cup. In this way, we aimed to apply the HCF in a distributed

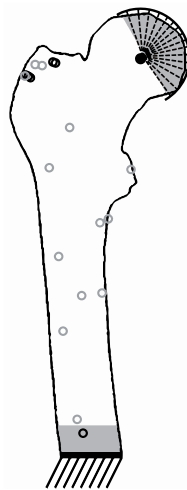


Figure 3. Schematic overview of the FE model. The HCF was applied on a control node, located in the hip joint centre, thereby moving a cup onto the femoral head. The FE model was fixated in all three directions at the distal end. Black circles indicate muscle attachment point on the anterior surface of the femur; grey circles indicate attachment points on the medial, lateral or posterior surface. Shaded areas represent elements in the model that were excluded from plastic analysis. Elements near attachment sites of the muscles were also excluded from plastic analysis (not indicated in figure).

and realistic manner (Figure 3). At the start of each simulation, a small load was applied to the control node in order to initialise contact between the cup and the femoral head. On the distal side, nodal points were fixated in three directions, thereby completely restraining rotations and translations. After running some simulations, it appeared that all P2 simulations had problems reaching stable contact, which was solved by gluing the contact between the cup and femoral head. In this way, all P2 simulations successfully converged up to ten gait cycles.

FE simulations

For every patient (P1, P2) and every load case obtained from the healthy subjects (HS1 to HS5) we ran two simulations, resulting in 20 simulations in total. In the first simulation we applied one gait cycle (i.e. 23 frames with different HCFs and muscle forces acting on the femur) while modelling linear elastic material behaviour (Keyak et al., 2005). In these simulations, failure was quantified by assessing the volume of elements with a safety factor (SF) < 1 , relative to the total bone volume. SFs were depending on calcium equivalent values and calculated by dividing the ultimate strength (Keyak et al., 2005) over the current Von Mises stress. In the second simulation, a series of 10 consecutive gait cycles was applied (i.e. 230 frames) while modelling non-linear elastic-plastic material behaviour as defined by Keyak et al. (2005). More specifically, when the yield stress was reached, plasticity was induced and further defined by an initial ideal plastic phase, subsequent softening, and a final ideal plastic

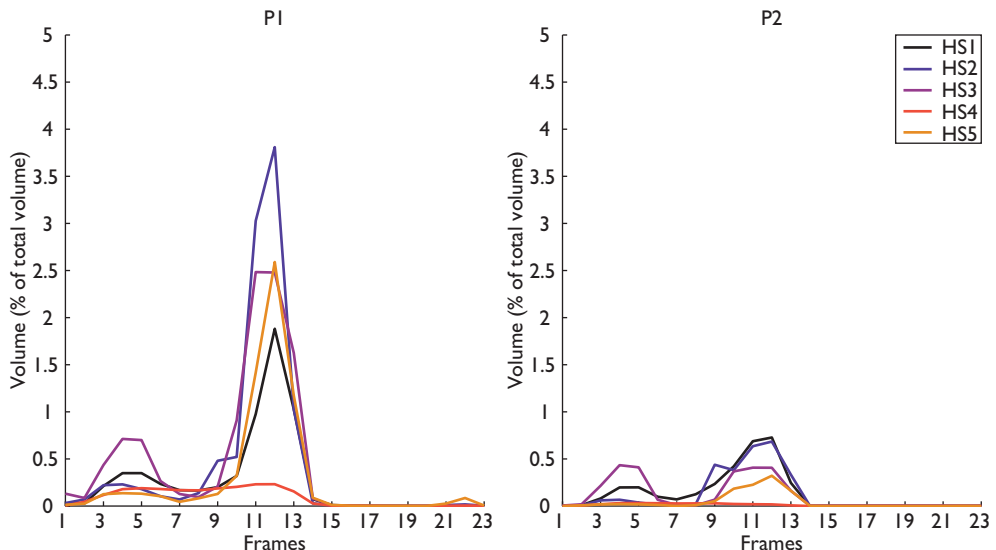


Figure 4. Failure of bone, defined as the relative volume of elements with $SF < 1$ during linear elastic analysis of a single gait cycle. Different lines represent load cases from different healthy subjects (HS1 to HS5).

phase. In these simulations, failure was defined as the summed volume of all elements with plasticity (i.e. elements that had reached the yield stress), divided over the total volume of the femur. It should be mentioned that elements underneath the cup and close to the bottom fixation (shaded areas in Figure 3), as well as elements close to the muscle attachment sites were assigned linear elastic material behaviour in all simulations to prevent failure as a result of stress artefacts caused by the definition of the boundary conditions. These elements were excluded from the calculation of SF volumes as well as plasticity volumes. In order to define a realistic end-point of the simulations, the displacement in z-direction of a reference node at the proximal surface of the femoral head was used. Force-displacement curves from previous work (Chapter 5) were used to determine the displacement of this same node at the moment of structural failure under axial loading. As such, the increment in which the z-displacement well exceeded the critical displacement in the axial loading simulations was the last increment of interest; the remaining increments were omitted.

Femoral failure from the linear elastic simulations and the non-linear elastic-plastic simulations was compared within and between patients, in terms of volume and ranking order. Failure locations were qualitatively compared to the actual fracture lines as determined by an experienced clinician on post-fracture X-rays of the patients.

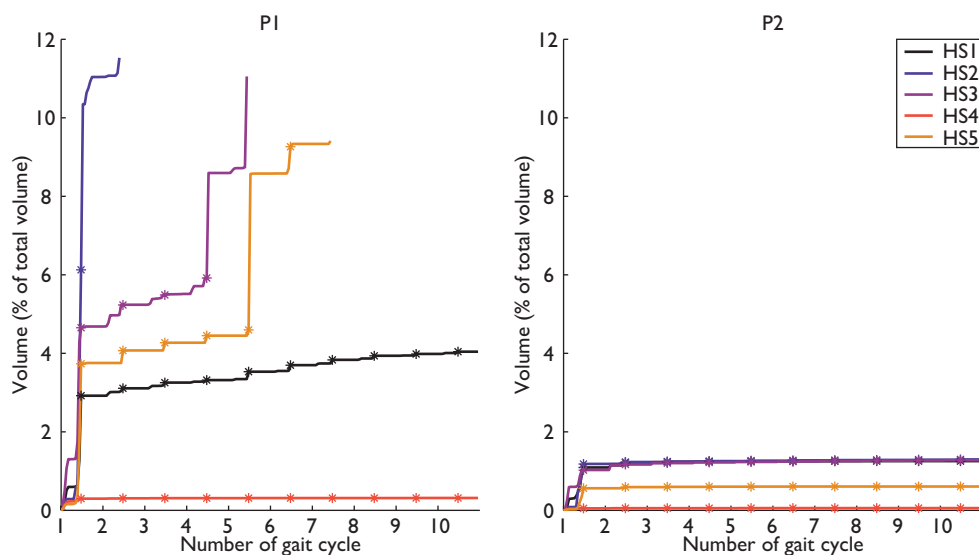


Figure 5. Failure of bone, defined as the relative volume of elements with plasticity during non-linear elastic-plastic analysis modelling cyclic walking. Different lines represent load cases from different healthy subjects (HS1 to HS5). Asterisks indicate instances of the second peak in HCF in the ten gait cycles.

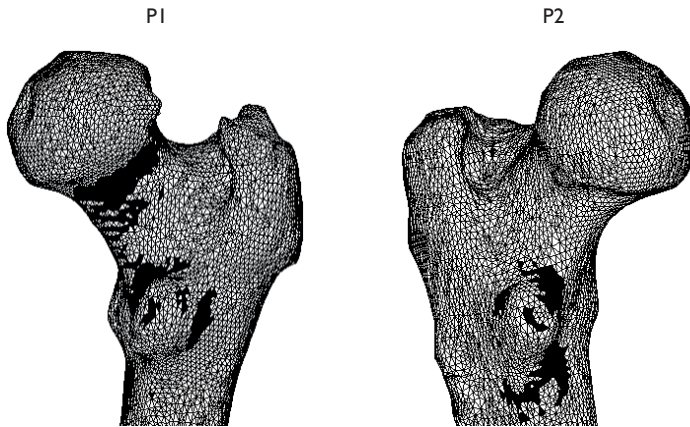


Figure 6. Distribution of elements with $SF < 1$ (in black) in linear elastic analysis at the second peak in HCF. For both patients, results for load case HS2 are shown, as the failure volume was largest in these simulations.

Results

Effects of modelling multiple physiological load cases on failure volumes

Relatively small differences between load cases showed to have considerable effects on failure. In P1, the HS2 load case resulted in the largest volume of failed elements (Figures 4 and 5). Failure as a result of the HS1 load case was much smaller, although the HCFs at the second peak as well as total HCF load over the gait cycle were quite comparable for HS1 and HS2. However, in HS1, the HCF is imposed in more anterolateral direction (i.e. more along the femoral neck) than in load case HS2 (and HS3 and HS5) (Figure 2B). Hence, the femur of P1 seemed to be sensitive to the angle under which the HCF is imposed. Apparently, subtle differences in the direction of the HCF, in combination with the femur's anteversion angle, can have a large impact on the failure in the femoral neck region. The failure as a result of load case HS4 resulted in the lowest failure at the second peak in HCF.

In P2, the volume of failed elements was low and always $< 1\%$ of total volume in the linear elastic analyses (Figure 4) and $< 2\%$ in the non-linear elastic-plastic analyses (Figure 5). The direction of the HCF seemed to be less critical in this femur, since load case HS1 (which in P1 was less detrimental than HS2 and HS3) in P2 ranks high in the calculated failure volume. Load case HS3 in P2 showed a sharp increase in plasticity volume after the first peak in HCF. Apparently, this first peak causes plasticity that further catalyses failure in subsequent frames. At the second peak in the first gait cycle, the failure in load case HS3 is much larger than the failure in HS5, while the magnitude and direction of HCF are comparable at this time instance for these two load cases. This effect was also seen in P1: in the linear analyses, the failure volume at the second peak HCF was comparable for HS3 and HS5, but in the non-linear

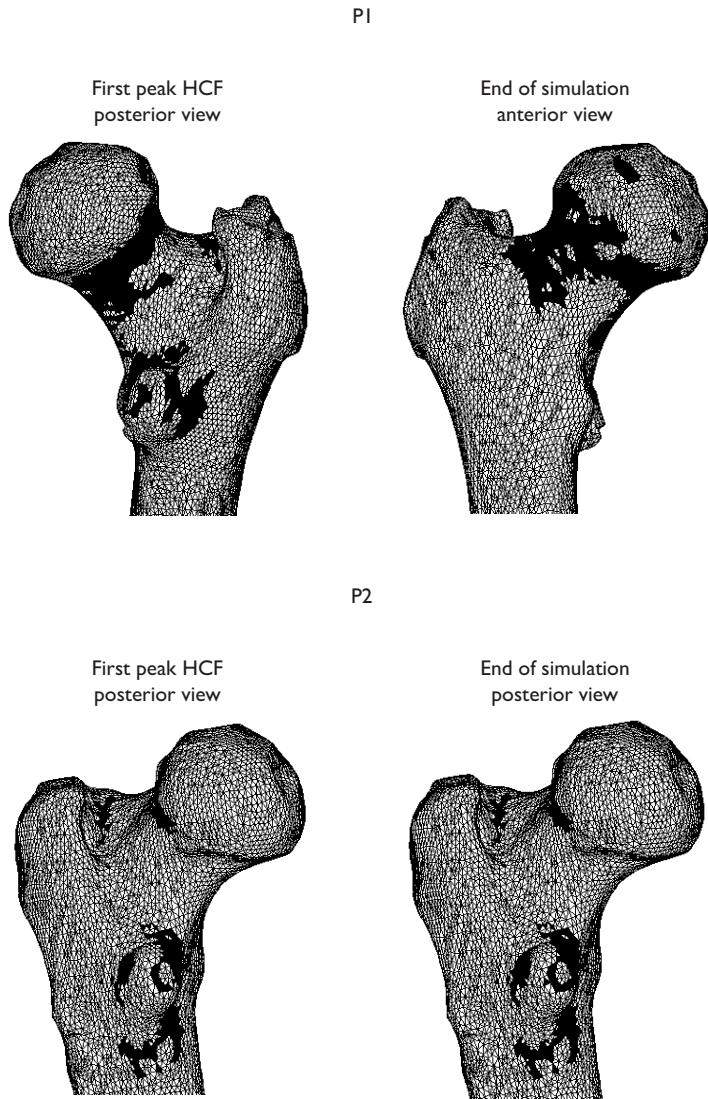


Figure 7. Distribution of elements with plasticity (in black) in non-linear elastic-plastic analysis at the second peak in HCF in the first gait cycle and at the end of the simulation. For both patients, results for load case HS2 are shown, as failure volume was largest in these simulations.

analyses failure was larger for HS3. Hence, in both patients, the failure was sensitive to the loading history.

Effect of modelling multiple physiological load cases on failure locations

The different load cases did not have a major effect on the failure locations (both the elements

with $SF < 1$ and the elements with plasticity) in the two bones. P1 suffered from multiple lytic lesions in the proximal femur, and eventually sustained a collum fracture. Accordingly, for all load cases, the largest failure areas were seen in the dorsal neck. In addition, failure areas were located at the proximal side of the lesser trochanter (around the attachment of the m. psoas) and around the attachment of the m. gluteus medius at the greater trochanter (Figure 6). P2 suffered from blastic and lytic lesions, with a lytic lesion at the level of the lesser trochanter through which a subtrochanteric fracture was sustained. In this patient the same failure locations were seen, albeit that the failure areas were smaller than those of P1. Furthermore, an additional failure location was found around the attachment site of the m. iliacus and m. pectineus, below the lesser trochanter. For P2, the different load cases resulted in subtle differences in failure locations. In load case HS2 the failure at the level of the lesser trochanter was more pronounced. In HS3 the failure area near the attachment of the m. gluteus medius was larger relative to the other load cases, while in HS5 this area was quite small.

Effect of modelling non-linear elastic-plastic material properties as compared to linear elastic material properties

Using a non-linear elastic-plastic material model induced accumulation of plasticity in the models, sometimes leading to numerical convergence problems. For P1, 9 out of 10 load cases were successfully simulated. The remaining simulation (load case HS5) did not converge during simulation of the second peak in HCF in the 9th gait cycle, probably due to gross failure. Moreover, after applying a few gait cycles, the simulations with load cases HS2, HS3 and HS5 showed extremely large and unrealistic deformations in the femoral neck. Hence, although the FE simulations still converged, structural failure of the femur was reached at these instances.

When qualitatively comparing the failure volumes in the non-linear elastic-plastic analyses (Figure 5) to those in the linear analyses (Figure 4) a number of similarities were found. For all load cases and for both material models, failure in P2 was far lower (always below 2% of total volume) than in P1. In addition, in P1, the ranking order of the failure volumes was comparable for the two material models: the plasticity in P1 was largest for load case HS2 and far smaller for load case HS1 at the second peak in HCF (and after 10 gait cycles, in the non-linear analyses).

Except for these similarities, the following differences were found between the different material models. The volume of plasticity at the second peak in HCF was always higher than the volume of elements with $SF < 1$ in linear elastic analyses. In addition, in both patients and for all load cases, plasticity accumulated over gait cycles; an effect that could obviously not be

detected in the linear elastic analyses. Accumulation was much larger for P1 than for P2, with the exception of load case HS4. Again, this finding would never be detectable with a linear elastic model. As mentioned above, especially in load case HS3 in P2, this effect seemed to be relevant as the accumulated plasticity volume for this load case was much higher than the volume of elements with a SF < 1 in the linear analyses. Apparently, the non-linear analyses rendered the femur sensitive to the loading history. Hence, the accumulation of plasticity revealed additional information on the failure process in both patients.

At the maximum HCF in the first gait cycle, the distribution of plasticity (Figure 7) largely resembled the distribution of failure in the linear analyses (Figure 6), with major failure locations at the insertion of the m. gluteus medius, m. psoas and in the distal neck. In P1, the failure areas enlarged over additional gait cycles. Especially the failure area in the neck expanded from dorsal to ventral, thereby covering a large part of the cross-sectional area of the neck. In contrast, in P2 no major changes in failure locations could be noticed over subsequent gait cycles, since the accumulation of plasticity over the additional loading cycles was small.

Discussion

The aim of this study was to assess whether the modelling of physiological load cases majorly affects failure predictions and to investigate whether the inclusion of non-linear elastic-plastic material properties is required to capture these differences. For this purpose, we applied muscle forces and hip contact forces of five healthy subjects to the femurs of two patients with metastatic bone disease who sustained a pathological femoral fracture. We compared the effect of these different load cases (HS1 to HS5) on the femoral failure in terms of failure volume and failure location, calculated by applying either linear elastic or non-linear elastic-plastic material behaviour.

The results in this study showed that subtle differences between load cases can have considerable effects on failure predictions in femurs with metastatic lesions. For example, in P1 but not P2, the predicted failure was lower for the HCF acting in more anterolateral direction, i.e. along the neck axis. This effect was seen in both linear elastic and non-linear elastic-plastic analyses. In both patients it was shown that a load case with a relatively high HCF at the first peak in the gait cycle already induced plasticity that rendered the model more vulnerable to the HCFs in the subsequent frames. This effect was not seen in the linear simulation for this particular load case. These results are in line with findings by Falcinelli et al. (2014) who found an increased association between calculated FE bone strength and fracture in osteoporotic/osteopenic patients when modelling multiple load cases. According to the authors, this effect can be explained by the fact that modelling multiple load cases increases chances

of imposing peak stresses and strains to affected regions in the femur, which may serve as the weakest link. This hypothesis may be even more plausible in the case of metastatic bone disease, as the bone tissue is most often very locally affected by metastatic lesions. Hence, it may be interesting to include additional physiological loading conditions (such as stair climbing or sit-to-stand) in the future FE simulations, thereby further increasing the variability in HCFs and muscle forces.

In addition to variable HCFs, the different load cases contained variable muscle forces. However, the direct effect of modelling muscle forces was difficult to interpret, at least in the two femurs modelled in this study. Some failure locations were femur-specific and located at a lesion site. Other failure areas, located around the attachment points of the m. gluteus medius and the m. psoas, however, were not involved in the actual clinical fracture and were approximately the same in both patients. Since muscles inserting at these particular locations exert relatively high forces during a gait cycle, it can be questioned whether these failure areas resulted from local bone weakness or rather from an artificial local stress peak caused by the applied point load. Furthermore, in the simulations applying simple axial loads and no muscle forces (Chapter 5), failure was also predicted at the clinical fracture lines. Thus, for these two femurs, the simulations with physiological loading conditions did not improve the predictions of fracture location over simulations applying only a load on the femoral head. Therefore, it should be noted that failure around the muscle attachment points may not have been simulated adequately and more research is required to obtain a realistic simulation of avulsion fractures around attachments of muscles and tendons. Nevertheless, the muscle forces have an additional indirect effect on the FE simulations, since the variations in HCF magnitudes and directions emerge from subject-specific variation in muscles forces. The results in this study show that the failure predictions are sensitive to these variations. Hence, indirectly, muscle forces did affect failure predictions in the femurs in this study.

Specific aspects in the results of the linear elastic simulations and non-linear elastic-plastic simulations were similar. First of all, the ranking order on bone failure for different load cases was comparable in P1. In addition, both linear elastic and non-linear elastic plastic models resulted in the highest failure for P1, and a far lower failure for P2. Moreover, the predicted fracture locations were also roughly the same, as discussed above. Nevertheless, there were also some discrepancies in the results of the two different material models. First, for all load cases, the plasticity volume was higher than the volume of elements with a SF < 1. In both femurs, but most pronounced in P2, one load case resulted in a much higher volume of plasticity than the volume of elements with SF < 1 in the linear analysis at the second peak in the gait cycle. These results show that the non-linear elastic-plastic material model may render

the FE model sensitive to the loading history. More specifically, due to the variable and local weakening of the bone strength by metastatic lesions, relatively small changes in magnitude or direction of loading may initiate local failure and may subsequently catalyse progressive failure in consecutive loading cycles.

This study investigated the effect of modelling physiological loading conditions obtained from five healthy subjects on the FE predicted femoral failure. The effect of applying physiological loading conditions on other FE predicted parameters models has been investigated before. For example, Jonkers et al. (2008) demonstrated that the implementation of physiological loads drastically influenced Von Mises stresses in the bone tissue along the stem of a hip prosthesis. Moreover, it was shown that these stresses were more sensitive to differences in muscle forces and HCFs, than to changes in femoral geometry. In addition, the effect of physiological loading conditions on the bone density distribution using a bone remodelling algorithm was investigated by Vahdati et al. (2014). They showed that FE predicted bone density distributions better resembled the CT bone density distribution when the bone remodelling algorithm applied patient-specific loading conditions rather than loading conditions from another subject under study. As a final example, the effect of applying physiological loading conditions on FE-predicted micromotions has been investigated (van der Ploeg et al., 2012). In that study, it was shown that peak micromotions were equally predicted under simple loading conditions and when modelling a full gait cycle, but that motions depended on the variable loading directions. Hence, the results in these and our study consistently show the relevance of applying physiological loading conditions to femoral FE predictions.

Some limitations should be mentioned when interpreting the results in this study. First of all, the coupling of HCFs and muscle forces from healthy subjects to FE models of patients with metastatic bone disease resulted in mechanically inconsistent models, since the anatomy and the gait pattern of the healthy subjects were obviously different from those of the patients. The overall goal of our work is to improve clinical fracture risk assessments in patients with cancer and femoral metastases at risk of fracturing. In the current study, we investigated the potential need for modelling complex loading conditions in FE models (as opposed to modelling single, simple loading conditions). By modelling gait cycles of five healthy subjects, we aimed to capture some of the biomechanical variation that exists in the human population. As explained before, gait analyses are unethical to perform in this patient population, therefore the use of motion data from healthy subjects will remain necessary in order to calculate muscle and hip contact forces to apply to the FE models of these patients. In future work, however, this workflow may be further personalised by adding more patient-specific details to the musculoskeletal model.

Secondly, the HCFs calculated using static optimisation techniques were relatively high, and exceeded HCFs measured in patients with instrumented hip prostheses (Bergmann et al., 2001). This overestimation is more generally seen in musculoskeletal modelling, and potential causes for these results are elaborately discussed in previous work (Wesseling et al., 2015b). However, the aim of the current study was to evaluate the potential need of complex loading conditions, which, despite these limitations, could be investigated in a qualitative manner. Further development of musculoskeletal modelling techniques should result in more physiological and personalised loading conditions, which then could be used to quantitatively analyse these FE results.

Thirdly, the patient femurs were positioned in the FE coordinate system using anatomical landmarks, which might lead to an orientation that differs from the orientation of the femur in the coordinate system of the musculoskeletal models. This could potentially lead to errors in transforming force vectors from the healthy subjects to the patient femora. As a result, specific anatomic features, such as the femoral anteversion angle, may incorrectly increase or decrease the moment arm, thereby inducing artificial sensitivity to the direction of the applied HCFs. This aspect is worthwhile to improve in future work, as it is suggested that higher reproducibility of generating FE models, of which the correct orientation is an important part, leads to a higher statistical (but not mechanical) association between FE and clinical output parameters (Keyak et al., 2013).

Finally, it should be stressed that the absolute volumes of failure should be interpreted with caution, for two reasons. First, failure calculated close to the cup or the muscle attachment points can result from a local decrease in bone strength caused by a metastatic lesion, but can also result from transmitted stress artefacts caused by these boundary conditions. As it is difficult to distinguish these two effects, the definition of the boundary conditions should be further investigated. That is, different definitions of boundary conditions should be modelled, and the resulting local stresses and strains should be compared to values as determined in cadaver experiments, or, ideally, *in vivo*, following for example the workflow of Philips et al. (2009). Secondly, it should be noted that the contact definitions of P1 and P2 were different, which, however, is unlikely to result in different answers to the research questions. As the gluing refrains the elements to lose contact, it may increase tensile stresses in the elements in and around the contact surface. Yet, the current failure volumes in P2 were small as compared to P1 and would probably have been even smaller if the glued contact definition would not have been necessary to apply.

In conclusion, the outcome of our study suggests that the FE predicted failure is rather sensitive to differences in load cases from multiple subjects. This indicates that a loading condition

for reliable fracture prediction should be as physiological and patient-specific as possible. Currently, this process is challenging, as personalised load cases cannot be established for patients with cancer suffering from metastatic bone disease. Furthermore, the direct effect of modelling muscle forces is currently difficult to interpret. The resulting failure locations did not better resemble clinical fracture lines than failure locations predicted in simulations applying a simple uniaxial loading condition, indicating that it is very difficult to correctly model such boundary conditions without causing artefacts. No major differences were found in the prediction of fracture location or the ranking order of bone failure (in P1) between linear elastic and non-linear elastic-plastic material models. Yet, the accumulation of plasticity rendered the model sensitive to the loading history of the femur. Hence, to capture this sensitivity, non-linear elastic-plastic material models may be preferred over linear elastic models for femoral fracture predictions.

Acknowledgements

The authors thank Jan Schepers, PhD (Materialise N.V.) for his help in morphing muscle attachment sites. This work was funded by Fonds NutsOhra and the Dutch Cancer Society.

References

- Anderson FC, Pandy MG. 2001. Static and dynamic optimization solutions for gait are practically equivalent. *J Biomech* 34(2): 153-161.
- Bergmann G, Deuretzbacher G, Heller M, Graichen F, Rohlmann A, Strauss J, Duda GN. 2001. Hip contact forces and gait patterns from routine activities. *J Biomech* 34(7): 859-871.
- Bessho M, Ohnishi I, Matsuyama J, Matsumoto T, Imai K, Nakamura K. 2007. Prediction of strength and strain of the proximal femur by a CT-based finite element method. *J Biomech* 40(8): 1745-1753.
- Delp SL, Anderson FC, Arnold AS, Loan P, Habib A, John CT, Guendelman E, Thelen DG. 2007. OpenSim: open-source software to create and analyze dynamic simulations of movement. *IEEE Trans Biomed Eng* 54(11): 1940-1950.
- Derikx LC, van Aken JB, Janssen D, Snyers A, van der Linden YM, Verdonck N, Tanck E. 2012. The assessment of the risk of fracture in femora with metastatic lesions: comparing case-specific finite element analyses with predictions by clinical experts. *J Bone Joint Surg Br* 94(8): 1135-1142.
- Falcinelli C, Schileo E, Balistreri L, Baruffaldi F, Bordini B, Viceconti M, Albinetti U, Ceccarelli F, Milandri L, Toni A, Taddei F. 2014. Multiple loading conditions analysis can improve the association between finite element bone strength estimates and proximal femur fractures: a preliminary study in elderly women. *Bone* 67: 71-80.
- Jonkers I, Sauwen N, Lenaerts G, Mulier M, Van der Perre G, Jaecques S. 2008. Relation between subject-specific hip joint loading, stress distribution in the proximal femur and bone mineral density changes after total hip replacement. *J Biomech* 41(16): 3405-3413.
- Keyak JH, Kaneko TS, Tehranzadeh J, Skinner HB. 2005. Predicting proximal femoral strength using structural engineering models. *Clin Orthop Relat Res* 437: 219-228.
- Keyak JH, Sigurdsson S, Karlsdottir GS, Oskarsdottir D, Sigmarsdottir A, Kornak J, Harris TB, Sigurdsson G, Jonsson BY, Siggeirsdottir K, Eiriksdottir G, Gudnason V, Lang TF. 2013. Effect of finite element model loading condition on fracture risk assessment in men and women: the AGES-Reykjavik study. *Bone* 57(1): 18-29.
- Mirels H. 1989. Metastatic disease in long bones. A proposed scoring system for diagnosing impending pathologic

- fractures. *Clin Orthop Relat Res* 249: 256-264.
- Phillips AT. 2009. The femur as a musculo-skeletal construct: a free boundary condition modelling approach. *Med Eng Phys* 31(6): 673-680.
- Redert A, Kaptein B, Reinders M, van den Eelaart I, Hendriks E. 1999. Extraction of semantic 3D models of human faces from stereoscopic image sequences. *Acta Stereologica* 18: 255-264.
- Schileo E, Balistreri L, Grassi L, Cristofolini L, Taddei F. 2014. To what extent can linear finite element models of human femora predict failure under stance and fall loading configurations? *J Biomech* 47(14): 3531-3538.
- Tanck E, van Aken JB, van der Linden YM, Schreuder HWB, Binkowski M, Huizenga H, Verdonshot N. 2009. Pathological fracture prediction in patients with metastatic lesions can be improved with quantitative computed tomography based computer models. *Bone* 45(4): 777-783.
- Vahdati A, Walscharts S, Jonkers I, Garcia-Aznar JM, Vander Sloten J, van Lenthe GH. 2014. Role of subject-specific musculoskeletal loading on the prediction of bone density distribution in the proximal femur. *J Mech Behav Biomed Mater* 30: 244-252.
- van der Linden YM, Dijkstra PD, Kroon HM, Lok JJ, Noordijk EM, Leer JW, Marijnen CA. 2004. Comparative analysis of risk factors for pathological fracture with femoral metastases. *J Bone Joint Surg Br* 86(4): 566-573.
- van der Linden YM, Kroon HM, Dijkstra SP, Lok JJ, Noordijk EM, Leer JW, Marijnen CA, Dutch Bone Metastasis Study G. 2003. Simple radiographic parameter predicts fracturing in metastatic femoral bone lesions: results from a randomised trial. *Radiother Oncol* 69(1): 21-31.
- van der Ploeg B, Tarala M, Homminga J, Janssen D, Buma P, Verdonshot N. 2012. Toward a more realistic prediction of peri-prosthetic micromotions. *J Orthop Res* 30(7): 1147-1154.
- van der Zijden AM, Janssen D, Verdonshot N, Groen BE, Nienhuis B, Weerdesteijn V, Tanck E. 2015. Incorporating in vivo fall assessments in the simulation of femoral fractures with finite element models. *Med Eng Phys* 37(6): 593-598.
- Wesseling M, De Groote F, Bosmans L, Bartels W, Meyer C, Desloovere K, Jonkers I. 2015a. MRI-based geometrical detail affects hip contact forces more than cost function formulation. 25th Congress of the International Society of Biomechanics. Glasgow.
- Wesseling M, Derikx LC, de Groote F, Bartels W, Meyer C, Verdonshot N, Jonkers I. 2015b. Muscle optimization techniques impact the magnitude of calculated hip joint contact forces. *J Orthop Res* 33(3): 430-438.

8

General discussion and future perspectives

Parts of this chapter have been published in *Loes C. Derikx, Nico Verdonschot, Esther Tanck. Towards clinical application of biomechanical tools for the prediction of fracture risk in metastatic bone disease. J Biomech 2015; 48(5), 761-766.*



This chapter reflects on the work described in this thesis, including a discussion about the challenges and future perspectives of the application of finite element (FE) modelling in the treatment of patients with metastatic bone disease.

The goal of this thesis was to develop and validate a patient-specific finite element model to assess the femoral fracture risk in patients with metastatic bone disease. The validation of the FE model started with an experimental study, in which ten paired cadaver femurs were axially loaded until failure (Chapter 2). The experiments were simulated in FE models and the results showed that the FE models accurately predicted the experimental failure load. Under these simple loading conditions, a ranking on FE failure load better resembled the experimental results than a ranking by clinical experts who commonly treat these patients, such as orthopaedic surgeons and radiation oncologists. By implementing more realistic material behaviour (using the asymmetrical Drucker-Prager yield criterion), we were able to further improve the FE predictions (Chapter 3), although a more extensive sensitivity analysis is needed before the Drucker-Prager yield criterion can be reliably implemented.

Although these initial simulation results were promising, the predictive capacity of these models could probably be further improved, e.g. by implementing modelling anisotropic material properties. However, since bone anisotropy cannot be quantified using a clinical CT resolution, considerable work on multi-level modelling should be done in order to enable the implementation of these mechanical properties in a patient-specific manner. The first steps in that direction have been taken by Hazrati Marangalou et al. (2013). They determined the fabric tensors and bone mineral density from micro-CT images for 33 femurs, and used them as input for an FE model implementing elastic-plastic damage behaviour. Subsequently they randomly selected ten femurs from their database. Each of these ten femurs was matched to another femur in the database with the most similar bone mineral density distribution. The fabric tensor of that matching femur was then applied to the test femur. The results were compared to the simulations with the original fabric tensor and to simulations with isotropic material properties. The implementation of anisotropy based on the database-matched fabric closely resembled the simulation using the original femur-specific fabric tensor, in terms of stiffness, damage, Von Mises stress and strain energy distribution. Although their findings have not yet been confirmed using clinical CT images, the results were promising and suggest that extrapolating anisotropic material properties from micro-level CT data to macro-level FE models is possible. In addition, imaging techniques are vastly improving, and it is only a matter of time before this micro-level information can be gleaned from clinical CT images with a radiation dose acceptable for *in vivo* scanning. Alternatively, recent pre-clinical re-

search on bone specimens showed that ultrasound can be used to determine the structural properties of bone (Lin et al., 2012). However, whether this new technique is applicable *in vivo* as well, remains to be seen.

The implementation of anisotropy would better approach the actual mechanical behaviour of bone, potentially leading to better FE strength predictions. This would particularly be the case in fracture risk assessments for patients suffering from osteoporosis. More specifically, previous studies have shown an increase in the degree of anisotropy in human osteopenic bone (Newitt et al., 2002) or osteoporotic animal models (Kreipke et al., 2014). Hence, accounting for it may improve the association between FE predicted bone strength and fracture in osteoporosis. In metastatic bone disease, however, the bone tissue is more locally destroyed so that the effect of implementing anisotropy in FE simulations may be limited. Alternatively, developing realistic material models for metastatic tissue could further improve the FE simulations. This issue is further addressed in the discussion on Chapter 5.

The results from the FE simulations in Chapter 2 were additionally compared against results from computed tomography based rigidity analysis (CTRA) applied to the same femurs (Chapter 4). It was shown that both methods are equally able to predict experimentally measured failure loads. However, compared to patient-specific FE modelling, CTRA is a faster and cheaper method to quantify bone strength (i.e. about 30 minutes for CTRA as compared to approximately one day for FE modelling). Hence, CTRA may be easier to implement in clinical practice, especially in cases where treatment decision is urgent. However, the implementation of more physiological loading conditions is easier in FE modelling, since CTRA is not suited to assess effects of different external loading modes and is therefore difficult to use in a clinical setting where clinicians would like to advise the patient as to which daily activities can be safely performed and which may lead to bone fracture. Moreover, the outcome measures (axial, bending or torsional rigidities) are difficult to interpret in clinical practice. In future research, the comparison of the two methods on their accuracy to predict bone strength *in vivo* should reveal the better performance of the one method over the other.

In Chapter 5, we described a prospective patient study which was conducted in three different institutes to test if FE models can improve upon standard clinical guidelines in predicting femoral bone fractures in patients with disseminated cancer and bone metastases. The patients in this study received single or multiple fraction radiotherapy to treat pain. Before and after radiotherapy the patients underwent quantitative CT scans and filled out questionnaires on physical activity, pain and quality of life. Through their hospital records, they were

followed for six months. The three institutes in this study used two different scanners from the same manufacturer. The CT images were reconstructed using different algorithms, and analysis of the CT data revealed that the images from two of the institutes seemed to be affected by air artefacts. This hampered the patient-specific calibration and subsequent material property assignment. Hence, further research is needed to develop a more robust calibration procedure to correct for such artefacts. Therefore, results from patients accrued at the Radboud university medical center ($n = 23$) were presented first in Chapter 5, as they were scanned using the same equipment as during the validation against experiments. The results for this subgroup of patients, with five femoral fractures in three patients, showed that the median failure load in the fracture group was significantly lower than in the non-fracture group. In line with the findings in Chapter 2, the results in this study showed a tendency towards more accurate fracture risk predictions by FE models than by experienced clinicians. However, due to the small number of patients in this study, the results have to be confirmed in the full data set of 66 patients (after correcting for the air artefact and potential interscanner artefacts) and its robustness should be further established by cross-validation in large patient cohorts from other institutes.

Chapter 5 additionally revealed a number of challenges related to the transition from modelling cadaver experiments to *in vivo* fracture risk assessments using FE models. In general, the validation of engineering models simulating biological processes is difficult (Henninger et al., 2010; Lund et al., 2012). *Ex vivo*, these processes can be simplified to a certain extent, but *in vivo* numerous additional factors and interactions should be accounted for. In the cadaver experiment, for example, artificial lesions were created by drilling defects in the femoral cortex. *In vivo*, however, these metastatic lesions contain lytic or blastic metastatic tissue (or both). In Chapter 5, the FE model predicted very high failure loads for some of the femurs with extensive blastic lesions, which may have resulted from the high CT intensities that these lesions present with. However, the composition and mechanical behaviour of metastatic bone tissue may be rather aberrant and, consequently, may need adapted material models. Sone et al. (2004) compared the microarchitecture of blastic metastases and normal tissue and found distinct differences between the two tissue types. The metastatic bony tissue showed more (but not thicker) trabeculae, leading to an increased bone volume fraction. Furthermore, the tissue was more isotropic and irregularly formed, and the degree of mineralization was lower than in healthy tissue. Unfortunately, the subsequent effect on bone mechanics was not included in the work of Sone et al.. Kaneko et al. studied the mechanical behaviour of blastic, lytic and mixed metastatic tissue, and found different material properties for cortical (Kaneko et al., 2003) but not trabecular (Kaneko et al., 2004) metastatic bone tissue. However, the sub-

sequent application of these adapted material properties in FE models of femoral shafts did not result in additional predictive power of the FE models (Keyak et al., 2005). However, in the work of Kaneko et al., blastic, lytic and mixed metastatic tissue samples were combined, which could have averaged out peculiar material behaviour in either of the tissue types. Thus, further research is required to reliably determine the mechanical behaviour of different types of metastatic tissue before the failure load in femurs with blastic lesions can be accurately predicted.

Another major difference between *ex vivo* and *in vivo* FE modelling lies in their input, i.e. the QCT scans. The cadaver femurs were separately scanned in a water basin, whereas in patients surrounding bony structures and soft tissues affect the CT attenuation in the femur. These effects are obviously dependent on anatomy and are therefore patient-specific. In order to minimise these beam hardening effects, a calibration phantom was used to establish patient-specific or even image-specific calibration lines for converting CT intensities to calcium equivalent values. However, the size of beam hardening effects and other factors influencing CT intensities may additionally be dependent on the type of scanner and scanner software used, which complicates the design and analysis of multicentre studies. This is especially important for the prospective patient study (Chapter 5) that included 66 patients from three institutes, which used two different scanners from the same manufacturer. Recent work by Carpenter et al. (2014) showed large differences in calculated femoral bone strength based on QCT images retrieved from two different scanners, especially under single leg stance loading (mean difference -1100 N, 95% CI between 390 and -2526 N, approximately; independent of femoral strength). The use of hydroxyapatite calibration phantoms could not sufficiently correct for these differences between scanners. Obviously, such measurement errors are unacceptable when using FE predictions for clinical decision making on a patient-specific basis, and rigorous alternative calibration protocols should be developed for future multicentre studies.

Chapters 6 and 7 aimed at the development of more physiological loading conditions to apply to the FE models. For that purpose, four different optimisation techniques were selected and their effect on the calculated muscle forces and subsequent hip contact forces was investigated in five healthy subjects. It was shown that static optimisation techniques best approached hip contact forces as measured *in vivo*, although they still overestimated these forces. Based on these static optimisation results, we generated physiological load cases that resembled cyclic walking and subsequently applied them to the FE models of two patients with metastatic bone disease using linear elastic or non-linear elastic-plastic material models (Chapter 7). The results in this chapter revealed that subtle differences in physiological load cases can have

major effects on failure predictions, and hence, are required to perform reliable fracture risk assessments. In addition, when comparing the results of the two material models, we found no differences in the predicted fracture location. In addition, the ranking order on bone failure was comparable in one patient. However, plasticity accumulated over multiple gait cycles, which showed that modelling physiological loading conditions needs non-linear elastic-plastic material models.

The work in Chapters 6 and 7 revealed that different modelling techniques, i.e. FE-modelling and musculoskeletal modelling, come with strengths and weaknesses that should be borne in mind when combining them into multiscale models. As discussed by Lund et al. (2012), the validation of such models is difficult, as unknown interactions between different levels may lead to unexpected modelling errors. For example, the subject-specific contact forces calculated in Chapter 6 were used as loading conditions for patient-specific FE-models. However, gait patterns are subject-specific and thus differ within and between healthy subjects and patients. Using muscle forces and hip contact forces from healthy subjects to load FE models of patients will thus result in mechanical inconsistency, which may lead to erroneous fracture predictions. The extent of these errors is unknown, and hence, the results from these multiscale models should be interpreted carefully.

Future applications of FE models in the clinical practice of patients with metastatic bone disease

Future applications of femoral FE models in clinical practice

The work described in this thesis applied FE models to determine bone strength in femurs with metastatic lesions, thereby ignoring any potential temporal changes to bone mineral density. However, different treatment options such as hormone therapy, chemotherapy (Gralow et al., 2013; Rizzoli et al., 2013) and radiotherapy (short term) (Koswig et al., 1999; Gralow et al., 2013) can decrease the patients' bone quality over time, as does general disease progression. In contrast, radiotherapy (Koswig et al., 1999; Foerster et al., 2015) as well as the (additional) administration of bisphosphonates (Rizzoli et al., 2013; Foerster et al., 2015) can result in bone remineralisation on the long term. Currently, such treatment effects can be evaluated in terms of bone mineral density, generally determined using specific imaging techniques (dual-energy X-ray absorptiometry, DXA). In addition, FE models could be used to further translate these findings to patient-specific bone strength. Previous work on bone strength in patients with osteoporosis (Keaveny et al., 2008; Keaveny et al., 2010) has shown that FE models can provide additional information on the pathological process. More specifically, changes in areal bone mineral density (aBMD, the standard measure for fracture risk

assessment in osteoporosis) and femoral FE bone strength as a result of aging (Keaveny et al., 2010) or after drug administration (Keaveny et al., 2008) were investigated. In both studies, FE bone strength was affected to a larger degree than bone mineral density. According to the authors, one of the underlying mechanisms may be that FE models are sensitive to local changes in bone compartments (i.e. trabecular and cortical bone), whereas these changes may be cancelled out in the 2D projections of bone mineral densities in a DXA measurement. Hence, studying FE bone strength may enable further differentiation of treatment effects and disease progression on bone mineral density.

Moreover, the work in this thesis showed that clinical experts who regularly treat these patients experience difficulties in estimating structural strength when the bone density is locally affected. In contrast, FE models are better able to comprehend this information. Hence, future FE models may also be able to better account for (adverse) treatment effects in these complex clinical assessments. The following virtual case may illustrate future clinical practice. A patient with widespread disseminated cancer is treated with radiotherapy to treat a painful femoral metastasis. The lesion shows moderate cortical involvement but the pre-treatment FE-based fracture risk assessment reveals that the patient does not need prophylactic surgery to the femur and is referred for radiotherapy. However, the latter may decrease the bone quality on the short term. By implementing such potential changes in bone quality and rerunning the FE analyses, the patient-specific bone strength after irradiation can be estimated, and a safety factor for performing specific daily life activities can be calculated. In this way, the patient can be advised for example to use a walking aid in the first weeks after treatment to prevent pathological fracturing of the (temporarily) weakened bone. In this way, the predictions of the FE models can be used to further personalise the patient's treatment.

Alternative sites for application of FE fracture risk predictions in metastatic bone disease

Pathological fracturing of the femur severely jeopardises the quality of life of patients, as mobility can be fully lost. However, impending pathologic fractures at other localisations such as the spinal column or the pelvis are also very common in clinical practice, and assessment of these fracture risks is at least as difficult. Hence, developing FE models to improve fracture risk assessments at these sites may form an important future perspective. In general, bone metastases mostly develop in ribs, the skull, the spine and the axial skeleton (Johnson et al., 2008; Laitinen et al., 2012; Mavrogenis et al., 2012). The second most common site of pathological fractures in the peripheral skeleton are the humeri (Laitinen et al., 2012). Pathological humerus fractures obviously decrease the quality of life by disabling arm function, but, additionally, can greatly affect mobility if patients are already dependent on supportive walking

aids. The axial skeleton, however, is more often affected by metastatic lesions than peripheral bones (spine (37%), pelvis (29%) and ribs (5%) versus femur (16%) and humerus (4%)) (van der Linden et al., 2002). Hence, spinal metastases seem to be the most important future perspective for applying FE models. These lesions are most common in metastatic bone disease (van der Linden et al., 2002) and entail an additional clinical problem. More specifically, impending vertebral fractures do not require surgical treatment per se; stable fractures can be treated conservatively, e.g. with radiation therapy. In the case of unstable fractures, however, the different bone parts may move, thereby narrowing the spinal canal and potentially compressing the spinal cord or nerve roots. This compression should be prevented or urgently released by means of spinal surgery. Thus, FE models for spinal fracture risk assessment should be able to predict both vertebral bone strength and post-fracture mechanical stability in order to serve as a useful clinical tool when deciding on treatment, e.g. surgery and/or radiotherapy.

Requirements from clinical practice

From a more practical point of view, the workflow for fracture risk assessment using QCT based FE models for daily use in clinical practice should be accelerated towards a clinically acceptable limit. Implementation in the hospital is currently hampered by the fact that the procedure to calculate the fracture risk takes about a day and requires specific modelling software and engineering knowledge. In order to make these mechanical tools available for clinicians, the workflow should be further automated. A promising method to do so is probabilistic modelling (Taylor et al., 2013), which would use principal component analysis to select characteristics from the FE models that are statistically predictive for the fracture risk. If these significant components are determined for every patient, a statistical model can be used to calculate the individual fracture risk. In this way, the extensive patient-specific modelling becomes redundant and the fracture risk assessment will be accelerated. By further implementing this statistical model in the PACS software or in a more general software application, the clinical expert can perform the fracture risk assessment instantly. We have recently started a research project that aims at the development of such a biomechanically-based statistical model (funded by the Dutch Cancer Society (KUN 2012-5591)).

It should be noted that the value of probabilistic models based on FE analysis will most likely increase after its introduction into clinical practice. More specifically, a growing database of clinical follow-up data comprises valuable feedback to validate previous and improve future model predictions. Moreover, it allows for investigating additional disease-related factors that may be associated with pathological fracturing, such as the primary tumour type, earlier sys-

temic or local treatments or the general condition of the patient. In this way, different sources of information on the patient are combined and integrated, thereby allowing for more personalised healthcare (Panahiazar et al., 2014).

To further define requirements from clinical practice, we have interviewed a large group of national and international clinical experts from different disciplines involved in the treatment of patients with metastatic bone disease. Based on their answers an inventory of additional clinical requirements was established to guide future research, which is shortly addressed here.

First of all, clinicians obviously require extensive validation before they accept a new technology in their clinical practice. Secondly, the tool should be simple and very easy to use, as the limited time available for consulting is better spent to the patient than to handling such a tool. The waiting time for the result of a fracture risk assessment, however, can be much longer as clinicians find it acceptable to wait for the results up to a few days (comparable to e.g. waiting for lab results of blood samples). Finally, a potential clinical tool for fracture risk assessment should preferably include temporal aspects, as clinicians like to know the term of validity of the predictions. In this way, they can plan multiple fracture risk assessments over time, which would enable to better monitor their patients and align lesion-specific treatment plans with other local or systemic cancer-related treatment plans. Moreover, it could lead to more shared-decision making between the treating clinicians and the patient.

These clinical requirements should be used to prioritise the next steps in developing bio-mechanical tools for effectively improving fracture risk assessment. Such a vision should be developed in an interdisciplinary manner, i.e. in a concerted effort with patients, clinicians, engineers and policymakers. This can be fostered by a continuous discussion on the current performance and concomitant costs on the one hand, and remaining clinical needs and technical challenges on the other hand. In this way, improvement of clinical fracture risk assessments can be reached as time- and cost-efficiently as possible.

Concluding remarks

This thesis described the development and validation of an FE model to improve clinical fracture risk assessments in patients with metastatic bone disease. Current clinical guidelines omit mechanical parameters, such as initial bone strength, that are crucial for accurate fracture risk assessments. As a result, relatively high numbers of patients are over- or undertreated: patients undergo surgery for low risk lesions or sustain pathological fractures that were not anticipated. Experimental as well as *in vivo* studies demonstrate that patient-specific FE models are a promising tool to further improve the sensitivity and specificity of fracture risk

assessments, and to outperform clinicians that rely on their own experience.

Obviously, the superior performance of this approach needs to be confirmed in clinical trials before this technology can be made available for clinicians treating patients with metastatic bone disease. The transition to *in vivo* fracture risk assessment is challenging, but there are a number of modelling and imaging developments that may further improve the predictive capacity of these models. With such improvements ahead, these models may become of great added value for the fracture risk assessment in patients with metastatic bone disease. Namely, FE models may serve as a basis for statistical prediction models, which can be developed into simple and accessible clinical tools. In this way, FE models will indirectly find their way into clinical practice and help both patients and their treating clinicians to choose appropriate treatment modalities that result in more optimal and individualised care, and, subsequently, in fewer unexpected fractures and unnecessary surgeries. This can lead to an improvement in the quality of life and potentially better survival of patients with metastatic bone disease.

References

- Carpenter RD, Saeed I, Bonaretti S, Schreck C, Keyak JH, Streeper T, Harris TB, Lang TF. 2014. Inter-scanner differences in *in vivo* QCT measurements of the density and strength of the proximal femur remain after correction with anthropomorphic standardization phantoms. *Med Eng Phys* 36(10): 1225-1232.
- Foerster R, Eisele C, Bruckner T, Bostel T, Schlampp I, Wolf R, Debus J, Rief H. 2015. Bone density as a marker for local response to radiotherapy of spinal bone metastases in women with breast cancer: a retrospective analysis. *Radiat Oncol* 10(1): 368.
- Gralow JR, Biermann JS, Farooki A, Fornier MN, Gagel RF, Kumar R, Litsas G, McKay R, Podoloff DA, Srinivas S, Van Poznak CH. 2013. NCCN Task Force Report: Bone Health In Cancer Care. *J Natl Compr Canc Netw* 11 Suppl 3: S1-50; quiz S51.
- Hazrati Marangalou J, Ito K, Cataldi M, Taddei F, van Rietbergen B. 2013. A novel approach to estimate trabecular bone anisotropy using a database approach. *J Biomech* 46(14): 2356-2362.
- Henninger HB, Reese SP, Anderson AE, Weiss JA. 2010. Validation of computational models in biomechanics. *Proc Inst Mech Eng H* 224(7): 801-812.
- Johnson SK, Knobf MT. 2008. Surgical interventions for cancer patients with impending or actual pathologic fractures. *Orthop Nurs* 27(3): 160-171; quiz 172-173.
- Kaneko TS, Bell JS, Pejcić MR, Tehranzadeh J, Keyak JH. 2004. Mechanical properties, density and quantitative CT scan data of trabecular bone with and without metastases. *J Biomech* 37(4): 523-530.
- Kaneko TS, Pejcić MR, Tehranzadeh J, Keyak JH. 2003. Relationships between material properties and CT scan data of cortical bone with and without metastatic lesions. *Med Eng Phys* 25(6): 445-454.
- Keaveny TM, Hoffmann PF, Singh M, Palermo L, Bilezikian JP, Greenspan SL, Black DM. 2008. Femoral Bone Strength and Its Relation to Cortical and Trabecular Changes After Treatment With PTH, Alendronate, and Their Combination as Assessed by Finite Element Analysis of Quantitative CT Scans. *J Bone Miner Res* 23(12): 1974-1982.
- Keaveny TM, Kopperdahl DL, Melton LJ, 3rd, Hoffmann PF, Amin S, Riggs BL, Khosla S. 2010. Age-dependence of femoral strength in white women and men. *J Bone Miner Res* 25(5): 994-1001.
- Keyak JH, Kaneko TS, Rossi SA, Pejcić MR, Tehranzadeh J, Skinner HB. 2005. Predicting the strength of femoral shafts with and without metastatic lesions. *Clin Orthop Relat Res* 439: 161-170.
- Koswig S, Budach V. 1999. [Remineralization and pain relief in bone metastases after after different radiotherapy

- fractions (10 times 3 Gy vs. 1 time 8 Gy). A prospective study]. *Strahlenther Onkol* 175(10): 500-508.
- Kreipke TC, Rivera NC, Garrison JG, Easley JT, Turner AS, Niebur GL. 2014. Alterations in trabecular bone microarchitecture in the ovine spine and distal femur following ovariectomy. *J Biomech* 47(8): 1918-1921.
- Laitinen M, Ratasvuori M, Pakarinen TK. 2012. The multi-model approach to metastatic disease, in: *European Instructional Lectures*. Springer Berlin Heidelberg, Berlin, pp. 35-44.
- Lin L, Cheng J, Lin W, Qin YX. 2012. Prediction of trabecular bone principal structural orientation using quantitative ultrasound scanning. *J Biomech* 45(10): 1790-1795.
- Lund ME, de Zee M, Andersen MS, Rasmussen J. 2012. On validation of multibody musculoskeletal models. *Proc Inst Mech Eng H* 226(2): 82-94.
- Mavrogenis AF, Pala E, Romagnoli C, Romantini M, Calabro T, Ruggieri P. 2012. Survival analysis of patients with femoral metastases. *J Surg Oncol* 105(2): 135-141.
- Newitt DC, Majumdar S, van Rietbergen B, von Ingersleben G, Harris ST, Genant HK, Chesnut C, Garnero P, MacDonald B. 2002. In vivo assessment of architecture and micro-finite element analysis derived indices of mechanical properties of trabecular bone in the radius. *Osteoporos Int* 13(1): 6-17.
- Panahiazar M, Taslimitehrani V, Jadhav A, Pathak J. 2014. Empowering Personalized Medicine with Big Data and Semantic Web Technology: Promises, Challenges, and Use Cases. *Proc IEEE Int Conf Big Data 2014*: 790-795.
- Rizzoli R, Body JJ, Brandi ML, Cannata-Andia J, Chappard D, El Maghraoui A, Gluer CC, Kendler D, Napoli N, Papaioannou A, Pierroz DD, Rahme M, Van Poznak CH, de Villiers TJ, El Hajj Fuleihan G, International Osteoporosis Foundation Committee of Scientific Advisors Working Group on Cancer-Induced Bone D. 2013. Cancer-associated bone disease. *Osteoporos Int* 24(12): 2929-2953.
- Sone T, Tamada T, Jo Y, Miyoshi H, Fukunaga M. 2004. Analysis of three-dimensional microarchitecture and degree of mineralization in bone metastases from prostate cancer using synchrotron microcomputed tomography. *Bone* 35(2): 432-438.
- Taylor M, Bryan R, Galloway F. 2013. Accounting for patient variability in finite element analysis of the intact and implanted hip and knee: a review. *Int J Numer Method Biomed Eng* 29(2): 273-292.
- van der Linden YM, Steenland E, Post WJ, van den Hout WB. 2002. Eenmalige bestraling van pijnlijke botmetastasen even effectief als meervoudige bestraling. Uitkomsten van de 'Nederlandse botmetastasenstudie'. *Ned Tijdschr Geneesk* 146: 1645-1650.

9

Summary



The aim of this thesis was to develop and validate a patient-specific finite element model to improve clinical fracture risk assessments in patients suffering from metastatic bone disease. This chapter summarises the key findings of this thesis.

In Chapter 1, the clinical problem of metastatic bone disease was introduced. The number of patients suffering from metastatic bone disease will grow over the next decades due to a combined effect of increasingly effective treatment options and a higher cancer incidence. Current clinical practice lacks accurate predictors for fracture risk assessment needed to choose appropriate treatment modalities and prevent pathological fractures. Over the last decades, finite element (FE) models have shown to serve as a potential tool to calculate *in vivo* bone strength, both in healthy and diseased subjects, as this method is able to incorporate multiple biomechanical parameters. The work described in this thesis aimed at the development and validation of an FE model to improve clinical fracture risk predictions in patients suffering from metastatic bone disease.

Validation of a subject-specific finite element model against mechanical experiments

In Chapter 2, we validated the FE model against mechanical cadaver experiments. For that purpose, artificial lytic lesions were drilled in paired cadaver femurs. The femurs were immersed in a water basin, CT scanned and subsequently loaded under compression until failure. This experimental setup was mimicked in the FE models, and the calculated failure loads were compared to the failure loads registered in the mechanical experiments. In addition, six clinicians (three orthopaedic surgeons, two radiation oncologists and one radiologist) were asked to rank the femora on failure load and to report on their ranking strategies. The failure load for intact and metastatic femora calculated by the FE models well resembled the results of the mechanical experiments. For the clinicians, however, ranking metastatic femora on failure load appeared to be difficult. Both the FE models and the clinicians incorporated the lesion characteristics, but the initial bone strength, which is essential for accurately predicting the risk of fracture, was only accounted for in the FE models. We concluded that FE models are promising for predicting bone strength in femurs with metastatic lesions; they should be further developed in order to yield a method for accurate fracture prediction to help clinicians in their every day practice.

In the FE models described in Chapter 2, non-linear material behaviour using the Von Mises yield criterion (VMYC) was implemented, assuming equal bone strength in tension

and compression. However, it is widely shown in experimental studies that bone is stronger under compressive loading than under tensile loading. Therefore, in Chapter 3, it was investigated if this so called asymmetric yielding in FE models can be captured using the Drucker-Prager yield criterion (DPYC), and can provide better results than simulations using the VMYC. A sensitivity analysis on parameters defining the DPYC, i.e. the degree of yield asymmetry and the yield stress settings, was performed, focusing on the effect on bone failure. The implementation of a larger degree of yield asymmetry improved the prediction of the fracture location, whereas variations in the yield stress mainly affected the predicted failure load. We concluded that the implementation of asymmetric yielding in subject-specific finite element models improves the prediction of femoral bone strength. However, a more extensive sensitivity analysis is needed before the DPYC can be reliably implemented.

Comparing the performance of FE models and an alternative state of the art biomechanical tool

Subsequently, the prediction accuracy of FE models was compared to an alternative, state-of-the-art biomechanical tool (Chapter 4). By means of computed tomography rigidity analysis (CTRA), axial and bending rigidity measurements were obtained. The FE models and CTRA were compared based on their capacity to assess femoral failure load. The two techniques showed good correlation with values obtained from the experimental mechanical testing. Kendall rank correlation coefficients between the FE rankings and the CTRA rankings showed moderate to good correlations, and no significant differences in prediction accuracy were found between the two methods. The slight differences that were found between the methods should be further investigated in prospective patient studies in order to prove surplus value of the one method over the other. We concluded that both non-invasive fracture risk assessment techniques could be developed into a practical tool that can be used in clinical practice.

***In vivo* validation of FE models**

To investigate the clinical value of FE models in femoral fracture risk assessments, we performed a prospective cohort study. Between August 2006 and September 2009, we included 66 patients with painful femoral bone metastases from three different institutes. These patients received single or multiple fraction radiotherapy to treat pain. They underwent quantitative CT-scans before and after radiotherapy and filled out questionnaires on physical activity, pain and quality of life. Through their hospital records, patients were followed for six months. A setback in this prospective study was the fact that we found indications for an air artefact and interscanner differences in CT images (i.e. as a result of scanning patients on CT-equipment

from different vendors). This finding required further calibration analyses before pooling the data from different institutes was deemed valid. Therefore, only the results from patients accrued at the Radboud university medical center ($n = 23$) were presented first in Chapter 5, as they were scanned using the same equipment as during the validation against experiments. During follow-up, five pathological fractures occurred in three patients. Using FE models, femoral failure load was calculated and compared between fractured and non-fractured femurs. In addition, the FE predictions were compared against fracture risk assessments by experienced clinicians. We found lower median failure loads in the patients that sustained a fracture than in the patients with no fractures. In addition, fracture locations were well predicted, when compared to post-fracture radiographs. Finally, the FE model tended to more accurately identify patients with a high fracture risk than experienced clinicians. These findings indicate that FE models are a high-potential tool to improve fracture risk predictions in clinical practice. Future work in the full patient population ($n = 66$) should confirm the higher predictive power of the FE models over current clinical guidelines.

Implementation of physiological loading conditions

In the next study, we aimed to apply more physiological loading conditions to the FE models, as it was hypothesised that such extended FE models may better capture the local balance between applied load and load bearing capacity. For that purpose, muscle forces and hip contact forces (HCF) were calculated using musculoskeletal modelling techniques. However, several optimisation techniques can be used to calculate muscle forces, which subsequently affect the calculated HCFs. Therefore, in Chapter 6 four different optimisation techniques were used for calculating muscle forces, i.e. two different static optimisation techniques, computed muscle control (CMC) and the physiological inverse approach (PIA). We investigated their subsequent effects on calculated HCFs during gait and sit to stand and found that the use of different optimisation techniques considerably affected calculated HCFs. Muscle forces and HCFs calculated using static optimisation approached experimental values best. Hence, the latter were used to design more physiological loading conditions for the FE models. More specifically, in Chapter 7, the HCFs and muscle forces calculated for five healthy subjects were applied to the FE models of the femur of two patients suffering from metastatic bone disease. Two simulations were run for each patient and each loading case: a simulation modelling a single gait cycle and implementing linear elastic material behaviour, and a simulation modelling cyclic walking and applying non-linear elastic-plastic material behaviour. Results showed that the simulations predicting fracture risk of metastatic bones are rather sensitive to the differences between load cases from multiple healthy subjects. This indicates

that a true representation of the actual loading conditions within the patient is required in order to perform a reliable patient-specific fracture prediction. However, this is difficult for patients with metastatic bone disease. In addition, the accumulation of plasticity rendered the model sensitive to the loading history of the femur. Therefore, non-linear elastic-plastic material models may be preferred over linear elastic models for predictions of femoral fracture in patients with disseminated cancer.

Discussion and future perspectives of FE modelling for fracture risk assessment in metastatic bone disease

In **Chapter 8** we reflected on the work described in this thesis and on the future challenges to further improve the FE models. Some of these challenges, e.g. correcting for interscanner differences, should be conquered before the FE models are deemed safe for widespread clinical implementation. Others, such as for example defining a material model for metastatic tissue, may take a longer time to establish.

Current clinical guidelines poorly predict the patient-specific fracture risk, but the results in this thesis, for example, suggest that the predictive capacity of current FE simulations is better than the assessment applied in clinical practice. The further development and implementation of a biomechanical tool should be done in a multidisciplinary manner, in which future studies on further development of the model are guided by clinical needs. These needs have already been formulated by the future users; the clinical tool should be easily applicable, includes temporal aspects, does not need additional time of the clinician and has proven effectiveness (with excellent sensitivity and specificity). In this way, improvement of clinical fracture risk assessments can be reached as time and cost-efficiently as possible.

With such clear needs and opportunities for further improvement ahead, FE models may become of great added value for the fracture risk assessment in metastatic bone disease. Namely, FE models may serve as a basis for statistical prediction models, which can be developed into simple and accessible clinical tools. Hence, we recently started a research project (funded by the Dutch Cancer Society (KUN 2012-5591)) aiming at the development of such a statistical model. In this way, FE models will indirectly find their way to clinical practice and help both patients and their treating clinicians choosing appropriate treatment modalities that result in more optimal and individualised care, and, subsequently, in fewer unexpected fractures and unnecessary surgeries. This would probably lead to an improved quality of life and potentially better survival rates in patients with metastatic bone disease.

10

Samenvatting



Dit proefschrift beschrijft de ontwikkeling en validatie van een patiënt-specifiek eindige elementen (EE) model met als doel klinische fractuurvoorspellingen bij patiënten met botmetastasen te verbeteren. In dit hoofdstuk worden de belangrijkste bevindingen uit dit proefschrift samengevat.

In hoofdstuk 1 wordt de klinische probleemstelling uiteengezet. Door verbeterde behandelingen en een toenemende incidentie van kanker zal het aantal patiënten met botmetastasen blijven stijgen de komende jaren. Botmetastasen kunnen verschillende klachten veroorzaken, bijvoorbeeld pijn, maar kunnen ook leiden tot een pathologische fractuur. Enerzijds wordt ingezet op een minimaal belastende behandeling, bijvoorbeeld met radiotherapie, om de pijn te bestrijden, anderzijds moeten pathologische fracturen bij deze patiënten voorkomen worden, bijvoorbeeld door het electief stabiliseren middels preventieve chirurgie. Om een optimale behandeling te kiezen zijn daarom correcte fractuurvoorspellingen nodig. De fractuurvoorspellers die in de huidige klinische praktijk gebruikt worden zijn echter onvoldoende nauwkeurig. Recent onderzoek naar het berekenen van botsterkte met behulp van EE-modellen toont veelbelovende resultaten. Omdat deze methode meerdere biomechanische parameters gebruikt om de sterkte van pathologisch en gezond bot te berekenen, heeft zij potentie als instrument voor klinische fractuurvoorspellingen. Het werk in dit proefschrift beschrijft de ontwikkeling en validatie van een EE-model om de klinische fractuurvoorspellingen bij patiënten met kanker en botmetastasen te verbeteren.

Validatie van een femur-specifiek eindige elementenmodel aan de hand van mechanische experimenten

Hoofdstuk 2 beschrijft de validatie van de EE-modellen aan de hand van mechanische experimenten met donorbotten. In deze gepaarde femora werden gaten geboord die qua grootte en locatie vergelijkbaar waren met osteolytische uitzaaiingen in het bot van patiënten met kanker. De botten werden in een waterbak geplaatst om vervolgens CT-scans te maken. Daarna werden ze in een trekbank onder compressie belast totdat ze braken. Deze experimentele opzet werd nagebootst in de EE-modellen en de berekende faalkracht werd vergeleken met de resultaten uit de mechanische experimenten. Bovendien werd aan zes ervaren artsen (drie orthopedisch chirurgen, twee radiotherapeuten en een radioloog) gevraagd deze femora te rangschikken op botsterkte en daarbij hun overwegingen te rapporteren. Hun rangschikking en die op basis van EE-modellen werden vergeleken met de experimentele resultaten. De faalkracht berekend door de EE-modellen kwam goed overeen met de faalkrachten gemeten tijdens de experimenten, maar de ervaren artsen hadden moeite de femora correct te rang-

schikken op botsterkte. De artsen bleken met name te letten op eigenschappen van de uitzaaiing, zoals bijvoorbeeld de grootte of de locatie, terwijl het EE-model ook de botkwaliteit, essentieel voor correcte fractuurvoorspellingen, mee kan nemen in de botsterkteberekeningen. Hieruit concludeerden we dat het EE-model dus potentieel toegevoegde waarde kan hebben bij de voorspelling van pathologische fracturen bij patiënten met kanker en botmetastasen. De verdere ontwikkeling van deze modellen is belangrijk om artsen in de toekomst een instrument te kunnen bieden waarmee fractuurrisico's nauwkeurig voorspeld kunnen worden.

In de modellen beschreven in hoofdstuk 2 werd gebruik gemaakt van een materiaalmodel met een symmetrisch vloeicriterium (Von Mises vloeicriterium, VMVC), onder de aanname dat botweefsel onder trekbelasting even sterk is als onder drukbelasting. Voorgaande studies hebben echter meermaals aangetoond dat bot sterker is onder druk dan onder trek. In hoofdstuk 3 werd daarom onderzocht of dit zogenoemde asymmetrisch vloeigedrag gemodelleerd kan worden met behulp van het Drucker-Prager vloeicriterium (DPVC) en of het gebruik van dit criterium de EE-voorspellingen verbetert ten opzichte van simulaties met het VMVC. Er werd een sensitiviteitsanalyse uitgevoerd waarbij het effect van variaties in de parameters die het vloeicriterium definiëren, te weten de mate van asymmetrie en de vloeispanning, op botfalen onderzocht werden. Het gebruik van een grotere asymmetrie in het vloeigedrag leidde tot een betere voorspelling van de fractuurlocatie, terwijl de variaties in vloeispanning met name invloed hadden op de voorspelde faalkracht. We concludeerden dat de implementatie van een asymmetrisch vloeicriterium de fractuurvoorspellingen kan verbeteren, maar dat een uitgebreidere sensitiviteitsstudie nodig is voordat het DPVC betrouwbaar gebruikt kan worden.

Vergelijking van de prestaties van EE-modellen en een alternatief, state-of-the-art biomechanisch model

In hoofdstuk 4 vergeleken we de nauwkeurigheid van de voorspellingen van het EE-model met die van een alternatief biomechanisch model. Op basis van CT-scans berekent dit model de axiale stijfheid en buigstijfheid van de femora (computed tomography rigidity analysis (CTRA)). Aan de hand van meerdere statistische technieken werden de voorspellingen van de EE-modellen en de CTRA analyses vergeleken. Beide methoden vertoonden een goede correlatie met de faalkrachten zoals gemeten in de experimenten. Kendall rank correlatiecoëfficiënten tussen EE-rankings en CTRA rankings waren matig tot goed en er waren geen significante verschillen in de nauwkeurigheid waarmee de twee methoden de faalkracht voorspelden. De minimale verschillen tussen de methoden moeten verder uitgediept worden in een

grotere, prospectieve patiëntenstudie om te kunnen concluderen welke methode het meest geschikt is voor de klinische implementatie. Voor nu bieden beide niet-invasieve methoden veel perspectief voor doorontwikkeling tot een bruikbaar instrument dat gebruikt kan worden in de klinische praktijk.

Validatie van de eindige elementenmodellen *in vivo*.

Om vervolgens de klinische relevantie van de EE-modellen te onderzoeken, werd een prospectieve cohortstudie uitgevoerd (hoofdstuk 5). Tussen augustus 2006 en september 2009 werden 66 patiënten met kanker en pijnlijke botmetastasen vanuit drie radiotherapeutische instituten geïncludeerd. Deze patiënten werden behandeld voor pijn met een eenmalige of gefractioneerde dosis radiotherapie. Ze ondergingen een kwantitatieve CT-scan voor en na radiotherapie, en vulden vragenlijsten in met betrekking tot fysieke activiteit, pijn en kwaliteit van leven. Middels hun medische status werden de patiënten zes maanden gevolgd. Tijdens de studie werden indicaties voor een luchtartefact en interscannerverschillen (d.w.z. als gevolg van het gebruik van CT-scanners van verschillende leveranciers) gevonden in de CT-beelden uit de verschillende instituten. Om die reden konden de data in deze studie niet zonder meer gegroepeerd worden en zijn verdere kalibratieanalyses nodig om te corrigeren voor deze effecten. Daarom werden in dit hoofdstuk alleen patiënten uit het Radboudumc (n=23) opgenomen, omdat zij werden gescand in de scanner die gebruikt is in de validatiestudie. Tijdens follow-up liepen drie patiënten vijf femorale fracturen op. Aan de hand van EE-modellen werd de faalkracht berekend en vergeleken tussen femora met en zonder fractuur. Bovendien werden de EE-voorspellingen vergeleken met de fractuurvoorspellingen van ervaren artsen. Het bleek dat de mediane faalkracht van de femora die gebroken waren significant lager was dan de mediane faalkracht van de femora die niet gebroken waren. Verder kwamen de voorspelde fractuurlocaties vrij goed overeen met de fracturen die te zien waren op de röntgenbeelden van de patiënten die een breuk hadden opgelopen. Tenslotte leken de resultaten aan te tonen dat de EE-modellen beter in staat waren de femora met een hoog fractuurrisico te identificeren dan de ervaren artsen. De bevindingen in deze studie laten opnieuw zien dat EE-modellen perspectief bieden om fractuurvoorspellingen in de klinische praktijk te verbeteren. Toekomstige resultaten van de totale patiëntenstudie (n=66) moeten deze resultaten echter nog bevestigen.

Implementatie van fysiologische belastingscondities

Het doel van de volgende stap in het onderzoek was om meer fysiologische belastingscondities op te leggen aan het EE-model. Op die manier simuleren de EE-modellen mogelijk

beter de balans tussen de lokale belasting en belastbaarheid. Daarom werden spierkrachten en heupcontactkrachten berekend aan de hand van spierskeletmodellen. Er zijn echter meerdere optimalisatietechnieken beschikbaar om spierkrachten te berekenen, waaruit vervolgens de heupcontactkracht berekend kan worden. Daarom werden in hoofdstuk 6 vier verschillende optimalisatietechnieken (twee statische optimalisatietechnieken, computed muscle control (CMC), en de physiological inverse approach (PIA)) gebruikt om spierkrachten te berekenen in het bovenbeensegment. We onderzochten vervolgens het effect op de berekende heupcontactkracht tijdens het gaan en opstaan uit een stoel. De resultaten lieten zien dat de verschillende optimalisatietechnieken leiden tot aanzienlijke verschillen in de berekende contactkracht. Spierkrachten en heupcontactkrachten die berekend waren met behulp van statische optimalisatie benaderden *in vivo* gemeten heupcontactkrachten het beste. Daarom werd deze laatste techniek gebruikt voor het berekenen van fysiologische belastingscondities voor het EE-model.

In hoofdstuk 7 werden heupcontactkrachten en spierkrachten, berekend voor vijf gezonde proefpersonen, opgelegd aan het EE-model van het femur van twee patiënten met kanker en botmetastasen. Voor elk femur en elke belastingsconditie werden twee simulaties gedraaid. In de eerste simulatie werd een enkele loopcyclus in combinatie met lineair elastisch materiaalgedrag gemodelleerd; in de tweede simulatie werden tien loopcycli in combinatie met niet-lineair elastisch-plastisch materiaalgedrag gesimuleerd. De resultaten lieten zien dat de simulaties die fractuurrisico's bij patiënten met kanker en botmetastasen voorspellen behoorlijk gevoelig zijn voor verschillen in belastingscondities tussen de vijf gezonde proefpersonen. Dit suggereert dat een belastingspatroon een ware afspiegeling dient te zijn van de werkelijke belasting van het femur van de patiënt alvorens een betrouwbare fractuurvoorspelling gedaan kan worden. Dit is echter moeilijk in het geval van patiënten met kanker en botmetastasen. Bovendien bleek dat het model gevoelig is voor de voorafgaande belastingen als de plasticiteit kan accumuleren. Daarom is er een voorkeur voor niet-lineair elastisch-plastisch materiaalgedrag in modellen die gebruikt worden voor het voorspellen van fracturen bij patiënten met botmetastasen.

Discussie en toekomstperspectieven voor het gebruik van EE-modellen bij fractuurvoorspellingen bij patiënten met kanker en botmetastasen

In hoofdstuk 8 reflecteerden we op het werk beschreven in dit proefschrift, en op de toekomstige uitdagingen om de EE-modellen verder te verbeteren. Sommige uitdagingen, zoals het corrigeren van verschillen tussen CT-scans, moeten opgelost worden voordat de EE-modellen veilig en breed uitgezet kunnen worden in de klinische praktijk. Voor andere uitdagingen,

zoals het definiëren van een materiaalmodel voor metastaseweefsel, is nog een lange weg te gaan.

Aan de hand van de huidige klinische richtlijnen kunnen patiëntspecifieke fractuurrisico's onvoldoende voorspeld worden door artsen. De resultaten in dit proefschrift laten zien dat de voorspellingen van de huidige EE-modellen beter zijn dan de klinische voorspellingen. De verdere ontwikkeling van deze modellen moet multidisciplinair van aard zijn, waarbij de doelen voor vervolgstudies mede vastgesteld worden door wensen en eisen uit de klinische praktijk. Zulke eisen zijn reeds geformuleerd door toekomstige gebruikers (zoals de artsen die deze patiënten behandelen): het instrument moet eenvoudig toepasbaar zijn, geschikt zijn voor herhaalde metingen in de tijd, weinig tijdrovend en bewezen accuraat zijn (d.w.z. een excellente sensitiviteit en specificiteit laten zien). Op die manier kan de verbetering van klinische fractuurvoorspellingen zo veel mogelijk tijds- en kostenefficiënt bereikt worden.

Met zulke duidelijke behoeften en kansen in het vizier, kunnen EE-modellen een grote toegevoegde waarde hebben voor fractuurvoorspellingen bij patiënten met kanker en botmetastasen. De EE-modellen kunnen als basis gaan dienen voor statistische predictiemodellen, welke doorontwikkeld kunnen worden tot eenvoudige en toegankelijke klinische instrumenten. Recentelijk zijn we een onderzoeksproject gestart (gesubsidieerd door KWF Kankerbestrijding (KUN 2012-5591)) om een dergelijk predictiemodel te ontwikkelen. Op die manier kunnen EE-modellen hun weg naar de klinische praktijk vinden om patiënten met kanker en hun artsen gezamenlijk een keuze te laten maken voor de beste behandeling. Dit resulteert in optimalere en meer gepersonaliseerde zorg en in minder onverwachte fracturen en overbodige operaties. Dit kan dan leiden tot een hogere kwaliteit van leven, betere mobiliteit, en hopelijk ook een betere overleving bij patiënten met kanker en botmetastasen.

||

Dankwoord
Curriculum Vitae
PhD Portfolio



Curriculum Vitae

Loes Derikx was born in Neer on April 12th, 1984. In 2002, she obtained her gymnasium diploma from Scholengemeenschap Sint Ursula in Horn, after which she started studying Biomedical Sciences at the Radboud University in Nijmegen. In 2005, she obtained her Bachelor's degree, followed by a Master's degree in 2007. Loes performed her Master's internship at the Orthopaedic Research Laboratory, under supervision of Dennis Janssen and Nico Verdonshot, and completed her Master's thesis at the Donders Institute for Brain, Cognition and Behaviour, Centre for Cognitive Neuroimaging, under supervision of Rick Helmich and Ivan Toni. After graduating, she worked as a research assistant at this institute. Subsequently, she spent three months at Utrecht University to follow courses on Science and Business Management. In December 2008, she started her PhD at the Orthopaedic Research Lab. In addition, in 2011, she formally enrolled the Katholieke Universiteit Leuven, as part of her joint doctoral PhD program. During her studies, she published the undermentioned publications and conference abstracts.

In addition to her research activities, Loes has been a member and secretary of the PhD Council of the NCEBP (currently known as the Radboud Institute for Health Sciences). Furthermore, she has been working on the valorisation of her research. For this purpose she presented her work to potential investors and was involved in product development analyses. Loes is currently appointed as a postdoctoral researcher at the Orthopaedic Research Lab to develop a biomechanically based statistical model to improve clinical decision making in patients with cancer and femoral bone metastases.

List of publications

- Derikx LC**, Verdonschot N, Tanck E. 2015. Towards clinical application of biomechanical tools for the prediction of fracture risk in metastatic bone disease. *J Biomech* 48(5): 761-766.
- Wesseling M*, **Derikx LC***, de Groot F, Bartels W, Meyer C, Verdonschot N, Jonkers I. 2015. Muscle optimization techniques impact the magnitude of calculated hip joint contact forces. *J Orthop Res* 33(3): 430-438. * *joint first authorship*
- Anez-Bustillos L, **Derikx LC**, Verdonschot N, Calderon N, Zurakowski D, Snyder BD, Nazarian A, Tanck E. 2014. Finite element analysis and CT-based structural rigidity analysis to assess failure load in bones with simulated lytic defects. *Bone* 58: 160-167.
- Derikx LC**, van Aken JB, Janssen D, Snyers A, van der Linden YM, Verdonschot N, Tanck E. 2012. The assessment of the risk of fracture in femora with metastatic lesions: comparing case-specific finite element analyses with predictions by clinical experts. *J Bone Joint Surg Br* 94(8): 1135-1142.
- Derikx LC**, Vis R, Meinders T, Verdonschot N, Tanck E. 2011. Implementation of asymmetric yielding in case-specific finite element models improves the prediction of femoral fractures. *Comput Methods Biomech Biomed Engin* 14(2): 183-193.
- Helmich RC, **Derikx LC**, Bakker M, Scheeringa R, Bloem BR, Toni I. 2010. Spatial remapping of cortico-striatal connectivity in Parkinson's disease. *Cereb Cortex* 20(5): 1175-1186.

Conference abstracts

- Derikx LC**, Janssen D, Schepers J, Wesseling M, Verdonschot N, Jonkers I, Tanck E. Modelling cyclic walking in femurs with metastatic lesions: femur-specific accumulation of plasticity. Congress of the European Society of Biomechanics, 2015, Prague, Czech Republic.
- Knoop TH, **Derikx LC**, Verdonschot N, Slump CH. A novel framework for the temporal analysis of bone mineral density in metastatic lesions using CT images of the femur. SPIE Medical Imaging, 2015, Orlando, USA.
- Derikx LC**, van der Linden YM, Snyers A, Rozema T, Janssen D, Schreuder HB, Kaatee R, Verdonschot N, Tanck E. Finite element analysis in metastatic bone disease: an in vivo sensitivity analysis on yield definitions. World Congress of Biomechanics, 2014, Boston, USA.
- Wesseling M, **Derikx LC**, Meyer C, de Groot F, Desloovere K, Verdonschot N, Jonkers I. Variation in estimated contact and muscle forces. 5th International Conference on Computational Bioengineering, 2013, Leuven, Belgium.
- Wesseling M, **Derikx LC**, de Groot F, Bartels W, Meyer C, Verdonschot N, Jonkers I. Hip joint contact forces calculated using different muscle optimization techniques. XXIV Congress of the International Society of Biomechanics, 2013, Natal, Brazil.
- Derikx LC**, Janssen D, van der Linden YM, Snyers A, Verdonschot N, Tanck E. Patient-specific finite element models differentiate between patients with and without a pathological fracture in metastatic bone disease. 4th Dutch Bio-Medical Engineering Conference 2013, Egmond aan Zee, The Netherlands.

Derikx LC, van der Linden YM, Snyers A, Verdonschot N, Tanck E. Patient-specific finite element models differentiate between patients with and without a pathological fracture in metastatic bone disease. Congress of the European Society of Biomechanics, 2012, Lisbon, Portugal.

Anez-Bustillos L, **Derikx LC**, Verdonschot N, Snyder BD, Nazarian A, Tanck E. CT-based finite-element analysis and structural rigidity analysis to assess failure load in bones with simulated lytic defects. Annual meeting of the Orthopaedic Research Society, 2012, San Francisco, USA.

Derikx LC, Groenen K, van Bon GA, van der Linden YM, Snyers A, Verdonschot N, Tanck E. Patient-specific finite element models discriminate between patients with and without a pathological fracture in metastatic bone disease. Congress of the International Society of Biomechanics, 2011, Brussels, Belgium.

Derikx LC, Groenen K, van Bon GA, van der Linden YM, Snyers A, Verdonschot N, Tanck E. Patient-specific Finite Element Models Discriminate between Patients with and without a Pathological Fracture in Metastatic Bone Disease. Annual meeting of the Orthopaedic Research Society, Long Beach, USA.

Derikx LC, Vis R, Meinders T, Verdonschot N, Tanck E. Implementation of Asymmetric Yielding in Case Specific Finite Element Models improves the Prediction of Femoral Fracture Risk. Congress of the European Society of Biomechanics, 2010, Edinburgh, UK.

Derikx LC, Vis R, Meinders T, Verdonschot N, Tanck E. Implementation of Asymmetric Yielding in Case Specific Finite Element Models improves the Prediction of Femoral Fracture Risk. Pre-ORS, 2010, New Orleans, USA.



PhD Portfolio

Name PhD student:	LCEM Derikx, MSc	PhD period:	15-12-2008 / 19-11-2015
Department:	Orthopaedic Research Lab	Promotors:	Prof. dr. ir. N. Verdonschot Prof. dr. I. Jonkers
Graduate School:	Radboud Institute for Health Sciences	Copromotors:	Dr. E. Tanck Dr. Y.M. van der Linden

TRAINING ACTIVITIES

	Year(s)	ECTS
a) Courses & Workshops		
Basiscursus begeleiden van onderzoeksstages	2010	0,4
Certificate in Advanced English	2010	5,1
NCEBP Introduction Course for PhD students	2011	1,8
Certificate of Proficiency in English	2011	5,1
Cursus loopbaanmanagement voor promovendi	2012	0,8
b) Seminars & lectures		
ESB Tutorial "Innovative methods for the generation and validation of musculoskeletal models" and "medical image analysis"	2010	0,2
OpenSim Workshop	2011	0,1
NVVO-Oncologiedag – Imaging in Oncology, Utrecht, NL	2014	0,3
Spinoza Lecture Prof. Hoskin	2014	0,1
c) Symposia & congresses: (OP/PP indicates oral or poster presentation)		
Pre-ORS, New Orleans, USA. (OP).	2010	0,8
Annual meeting of the Orthopaedic Research Society, New Orleans, USA.	2010	1,0
IUTAM Symposium Analysis and Simulation of Human Motion, Leuven, BE.	2010	0,8
Congress of the European Society of Biomechanics, Edinburgh, UK. (PP).	2010	1,5
ISB Technical Group on Computer Simulation, Leuven, Belgium.	2011	0,5
Congress of the International Society of Biomechanics, Brussels, BE. (PP).	2011	1,8
NCEBP PhD Retreat, Wageningen, NL. Organising Committee.	2011	0,5
Pre-ORS, San Francisco, USA.	2012	0,3
Annual meeting of the Orthopaedic Research Society, San Francisco, USA. (PP).	2012	1,0
Congress of the European Society of Biomechanics, Lisbon, PT. (OP).	2012	1,5
NCEBP PhD Retreat, Wageningen, NL. (OP).	2012	0,8
4th Dutch Bio-Medical Engineering Conference 2013, Egmond aan Zee, NL. (OP).	2013	0,8
Health Valley Event, Nijmegen, NL. (OP).	2013	0,5
NCEBP Science Day, Nijmegen, NL. Laptop presentation.	2013	0,5
World Congress of Biomechanics, Boston, USA. (PP).	2014	1,8
Botmetastasensymposium UMC Utrecht. Utrecht, NL	2015	0,3
Congress of the European Society of Biomechanics, Prague, CZ. (PP).	2015	1,0
d) Other		
Journal club Orthopaedic Research Lab	'11-'15	3,4
Lablunches Orthopaedic Research Lab	'11-'15	3,4

Continued

TEACHING ACTIVITIES		
	Year(s)	ECTS
e) Lecturing		
BSc course 5DT03 – Determinanten 3: Fysische factoren	'09-'15	5,2
MSc course 5HM02 – Tissue: Biomechanics and engineering	'09-'15	8,3
BSc course 5HM01 - Introduction to clinical human movement sciences	2011	0,1
Onderzoeker in de klas, Wetenschapsknooppunt, RU Nijmegen	2012	1,2
BSc course OMB2 – Oriënterende Onderzoeksstage	2013	1,0
Onderwijsdag orthopeden in opleiding: Pathologische fracturen	2015	0,1
Onderwijsdag palliatieve zorg voor radiotherapeuten in opleiding	2015	0,1
f) Supervision of internships / other		
BSc internships		
Geert van Bon, RU Nijmegen.	2009	1,0
Karlijn Groenen, RU Nijmegen.	2010	1,0
Dieuwke Strijker, RU Nijmegen.	2014	1,0
MSc internships		
Hanna Coes, RU Nijmegen.	2012	2,0
Lonneke Wijnhoven, RU Nijmegen.	2012	1,3
Tom Knoop, UT Enschede.	2014	3,0
Anne Luchtenberg, UT Enschede.	2015	3,0
TOTAL		64,0